*Copy* 3

# INHOMOGENEOUS TWO-STREAM TURBULENT MIXING USING THE TURBULENT KINETIC ENERGY EQUATION

M. L. Laster

Headquarters, Arnold Engineering Development Center

## May 1970

TECHNICAL REPORTS
FILE COPY

## ARNOLD ENGINEERING DEVELOPMENT CENTER
## AIR FORCE SYSTEMS COMMAND
## ARNOLD AIR FORCE STATION, TENNESSEE

# NOTICES

# INHOMOGENEOUS TWO-STREAM TURBULENT MIXING USING THE TURBULENT KINETIC ENERGY EQUATION

M. L. Laster

Headquarters, Arnold Engineering Development Center

# FOREWORD

This technical report has been reviewed and is approved.

M. L. Laster  
Research Division  
Directorate of Plans  
   and Technology

Harry L. Maynard  
Colonel, USAF  
Director of Plans  
   and Technology

# ABSTRACT

A study is made on applying the turbulent kinetic energy approach to inhomogeneous two-stream turbulent mixing calculations and to calculations of a two-dimensional symmetric wake. Mixing calculations are made and compared with experimental data for coaxial hydrogen-air and air-air mixing flows. The turbulent kinetic energy equation is transformed into a transport equation for the turbulent shear stress by assuming that the turbulent shear stress is directly proportional to the turbulent kinetic energy. A flux model is assumed for the lateral diffusion of turbulent kinetic energy. The energy dissipation is modeled to a form similar to that derived for isotropic turbulence. Mass and energy transport are incorporated in the analysis by assuming the Prandtl and Lewis numbers to be unity. The resulting set of partial differential equations is hyperbolic and the method of characteristics was chosen for their solution. The theoretical method inherently incorporates history of the turbulent structure in the calculations which is physically more acceptable than turbulent structure models based on local flow properties. The results show that the turbulent kinetic energy approach is quite applicable to two-stream mixing problems, although the method requires further development before it is useful for routine engineering calculations. Calculations for a wake behind a flat plate are made and found to compare well with experimental data. The flux model for the diffusion of turbulent kinetic energy and the energy dissipation model were found to produce results which agree well with experimental data for both the mixing jet and the wake.

TABLE OF CONTENTS

## LIST OF FIGURES

FIGURE                                                                PAGE

## NOMENCLATURE

A      Random variable; or square matrix coefficient of vector equation

$a_1$      Turbulent kinetic energy-shear stress parameter, $\tau/\overline{q}^{\,\prime\,2}$

$|a_1|_m$      Maximum absolute value of $a_1$

B      Random variable; or square matrix coefficient of vector equation

b      Width of the mixing zone, $r_o - r_i$

C      Species mass fraction; or vector

$C_p$      Molar specific heat

D      Density fluctuation parameter in the turbulent kinetic energy equation; or vector

$F_1$      Molar specific heat parameter

$F_2$      Static enthalpy parameter

$f_1$      First-regime diffusion function

$f_2$      Second-regime diffusion function

G      Parameter defined by Equation 63

H      Total enthalpy

h      Static enthalpy

K      Dissipation length proportionality constant

k      For plane two-dimensional flow equals zero, for axisymmetric flow equals one

L      Dissipation length

M      Mach number; or molecular weight

$n_\alpha$      Moles of gas specie $\alpha$

| | |
|---|---|
| P | Static pressure |
| Q | Mass entrainment flux |
| $\overline{q}'^2$ | Turbulent kinetic energy, $\overline{U}'^2 + \overline{V}'^2 + \overline{W}'^2$ |
| $R_o$ | Universal gas constant |
| $R_q$ | Continuity conservation parameter |
| $R_m$ | Momentum conservation parameter |
| r | Radial coordinate in axisymmetric flow |
| $r_j$ | Central jet radius |
| T | Parameter defined by Equation 83; or static temperature |
| t | Time |
| U | Component of velocity in the X-direction |
| $U_i$ | Component of velocity in the $X_i$-direction |
| $U_c$ | Centerline velocity |
| $U_{ch}$ | Characteristic velocity, $U_j - U_o$ |
| V | Component of velocity in the R-direction or Y-direction |
| $V_d$ | Turbulent kinetic energy diffusion velocity |
| $V_D$ | Entrainment velocity |
| W | Arbitrary vector |
| $x_i$ | Cartesian coordinates, $x_1 = x$ in the longitudinal coordinate; $x_2 = y$ in the lateral coordinate; or $x_2 = r$ in axisymmetric coordinates |
| $y_\alpha$ | Mole fraction of specie $\alpha$ |
| z | $(r - r_i)/(r_o - r_i)$ |
| $z_o$ | z at $|a_1|_m$ |
| $\overline{\phantom{x}}$ | Time averaged conditions |

Instantaneous conditions

Greek

| | |
|---|---|
| $\gamma$ | Ratio of specific heat |
| $\delta$ | Boundary layer thickness |
| $\eta$ | Similarity parameter defined as $\sigma r/x$ |
| $\theta_o$ | Momentum thickness |
| $\lambda$ | Characteristic direction |
| $\rho$ | Density |
| $\sigma$ | Similarity constant |
| $\sigma_{ij}$ | Viscous stress tensor |
| $\tau$ | Turbulent shear stress |
| $\phi_u$ | Dimensionless velocity, $(U - U_o)/(U_j - U_o)$ |
| $\phi_{uc}$ | Dimensionless centerline velocity, $(U_c - U_o)/$ $(U_j - U_o)$ |
| $\Omega$ | Stability parameter defined by Equation 93 |

Subscripts

| | |
|---|---|
| $\alpha$ | 1,2 for two different gas species |
| hv | High velocity boundary |
| i | Coordinate indices; or inner boundary conditions |
| j | Coordinate indices; or central jet conditions |
| L | Left characteristic |
| Lv | Low velocity boundary |
| o | Outer boundary conditions |
| R | Right characteristic |
| s | Starting line |

Superscripts

| | |
|---|---|
| b | Boundary |

bi          Inner boundary

bo          Outer boundary

CHAPTER I

INTRODUCTION

Turbulent mixing in jets and wakes has been studied
for several decades.  Interest in inhomogeneous two-stream
turbulent mixing has increased significantly in the last
several years as the result of increased interest in super-
sonic combustion, gas ejectors, and exhaust jets.  At best
only a qualitative understanding of the physical processes
occurring in the most simple turbulent shear flows is exis-
tent.  Both analytical and experimental progress are still
not satisfactory.

Until recently the analytical approaches on turbulent
jet mixing could be classified [1] as follows:

1.  Point source diffusion of momentum, material, or
temperature using equations and solutions well known from
the study of heat flow.

2.  Boundary-layer form of the Navier-Stokes equation,
into which are inserted various transport theories such as

   a.  Momentum transport, using the mixing length
       concept

   b.  Vorticity transport, using the mixing length
       concept

   c.  Constant exchange coefficient

---

[1]Numbers in brackets refer to similarly numbered
references in the bibliography.

d.  Karman similarity theory

e.  Statistical theory

3.  Integral equations of motion.

Also, Forstall and Shapiro [1] have compiled a very extensive
list of references covering experimental and analytical work
on jet mixing prior to 1950.  Some of the more recent work
is reported in References 2 through 21.  Most analytical
approaches have dealt with method 2 choosing various trans-
port theories.  Perhaps the most widely used and successful
transport theories are those proposed by Prandtl, i.e., his
mixing length theory and constant exchange coefficient
hypothesis discussed in Reference 22.  Both the mixing
length theory and constant exchange coefficient hypothesis
relate the structure of turbulence through the shear stress
to local mean flow properties which in effect relate the
turbulence structure to local flow properties.  These
approaches, however, are used successfully in many jet mix-
ing problems.  Since they do not include the physics of past
history of the turbulent structure, they do not account for
the characteristics of the experimental apparatus which
induces turbulent history into the flow.  Ferri [23] dis-
cusses this problem in detail particularly as related to the
two-stream mixing problem.  The characteristics of the
experimental apparatus upstream of the mixing region
(initial boundary layers) have important effects on the
mixing phenomena near the origin of mixing.  Oftentimes
this point is neglected in presenting and comparing

2

experimental results. Thus, because the character of the
initial conditions does significantly contribute to the
mixing phenomena and turbulence structure in the vicinity of
the origin of mixing, it seems reasonable that the analytical
solution of the jet mixing problem should be an initial
valued problem for both the turbulent and mean flow fields.
Such an analytical approach will be discussed in detail in
this dissertation.

The basic idea was derived from Bradshaw, Ferriss, and
Atwell's analytical treatment of the equilibrium turbulent
boundary-layer problem [24 and 25]. They used Townsend's
suggestion [26] that the turbulent shear stress was propor-
tional to the turbulent kinetic energy and then rewrote the
turbulent kinetic energy equation as a transport equation
for the turbulent shear stress. They also assumed that the
diffusion of turbulence was purely convective and dominated
by the large-scale flow eddies as opposed to small-scale
high-intensity turbulent motion. Customarily [27] it is
assumed that the small-scale high-intensity turbulence dif-
fuses according to a gradient model; i.e.,

$$\text{Diffusion} \sim \frac{\partial \overline{q}^2}{\partial y}$$

and large-scale eddies diffuse according to

$$\text{Diffusion} \sim V_d \overline{q}^2$$

where $V_d$ is the effective rate at which the turbulence

3

diffuses or is convected in the lateral direction. Bradshaw
et al. [28] further emphasizes that large eddies entirely
dominate the free mixing layer. If this is correct, a con-
vective model for the lateral diffusion appears more suited
to the free-jet mixing problem than a gradient model.

However, Patankar and Spaulding [29] have formulated
the problem by assuming a gradient model for the diffusion
of turbulent kinetic energy. Along with this assumption
they have also assumed a gradient model for the turbulent
shear stress. These two assumptions result in the momentum
and turbulent kinetic energy equations both being parabolic.
Lee and Harsha [30] have studied the two-dimensional wake
and the two-stream mixing problems utilizing Bradshaw's
assumption [24] that the turbulent shear stress is linearly
proportional to the turbulent kinetic energy and a gradient
model for the diffusion of turbulent kinetic energy. They
used the Patankar and Spaulding method for solving the
resulting general set of parabolic equations. The method is
reasonably successful. In the Bradshaw et al. approach [24]
the shear stress is not modeled in the momentum equation,
but left as a dependent variable. With the convective
lateral diffusion formulation, the continuity, momentum, and
turbulent kinetic energy equations form a first-order quasi-
linear hyperbolic set of partial differential equations. In
fact, the equations are still hyperbolic if diffusion is
neglected. Using either the Lee and Harsha approach [30] or
Bradshaw's approach [24] with the turbulent kinetic energy

4

equation achieves the objective of formulating the jet mixing problem as an initial valued problem with respect to the turbulent structure. The approach in this dissertation is to use the Bradshaw method for the two-stream mixing problem and incorporate the density variation by use of the Crocco law. Comparisons with air-air and hydrogen-air coaxial mixing experimental data will be made. A brief study is also presented on the use of the Bradshaw method to calculate wake flow behind a thin flat plate.

# CHAPTER II

## DERIVATION OF THE COMPRESSIBLE TURBULENT
## KINETIC ENERGY EQUATION

### I.   TIME AVERAGE RULES

A derivation of the compressible turbulent kinetic energy equation will be made along with legitimate approximations to simplify the equation to useful form.  The equation can be developed entirely from the instantaneous form of the continuity and the momentum equations along with an averaging procedure.  The usual Eulerian time-averaged definition is used [27].  The time-averaged value of any dependent variable is defined by

$$\bar{A} = \lim_{t \to \infty} \frac{1}{2t} \int_{-t}^{t} A \, dt$$

Thus designation of the overscored quantity as a time-averaged quantity, the instantaneous quantity can be written as

$$A = \bar{A} + A'$$

where A' is the instantaneous fluctuation away from the mean.  The usual rules of time averaging are employed for the products of fluctuating quantities.  These are

$$\bar{A} = \overline{\bar{A} + A'} = \bar{\bar{A}} + \bar{A}' = \bar{A} + \bar{A}'$$

6

thus

$$\bar{A}' = 0$$

With

$$B = \bar{B} + B'$$

$$\overline{\bar{A}\,B'} = \bar{A}\,\overline{B'} = \bar{A}\,\overline{B'} = 0 \qquad \text{since} \quad \overline{B'} = 0$$

and

$$\overline{A\,B} = \overline{(\bar{A} + A')(\bar{B} + B')}$$

$$= \overline{\bar{A}\,\bar{B}} + \overline{\bar{A}\,B'} + \overline{\bar{B}\,A'} + \overline{A'B'}$$

$$= \bar{A}\,\bar{B} + \overline{A'B'}$$

At this point the compressible form of the instantaneous equations of motion will be stated followed by their conversion to their time-averaged form. By manipulation of the instantaneous and time-averaged equations, the compressible form of the turbulent kinetic energy equation will be derived. This treatment of the equation will be accomplished in Cartesian coordinates for simplicity. The generalized two-dimensional form of the final equations is used in succeeding chapters for both the plane two-dimensional wake and the axisymmetric two-stream jet mixing problems.

## II.  CONTINUITY

The instantaneous continuity equation is

$$\frac{\partial \rho}{\partial t} + \frac{\partial}{\partial x_i} (\rho U_i) = 0 \tag{1}$$

Using the time-averaged definition

$$\rho = \bar{\rho} + \rho'$$

$$U_i = \bar{U}_i + U_i'$$

where (') is used to designate the fluctuating quantity. Substituting into Equation 1 and time averaging gives

$$\frac{\partial}{\partial x_i} (\bar{\rho}\, \bar{U}_i + \overline{\rho' U_i'}) = 0 \tag{2}$$

which is the steady-state time-averaged form of the continuity equation.

### III. MOMENTUM

The instantaneous momentum equation is

$$\rho \frac{\partial U_i}{\partial t} + \rho U_j \frac{\partial U_i}{\partial x_j} = -\frac{\partial P}{\partial x_i} - \frac{\partial \sigma_{ij}}{\partial x_j} \tag{3}$$

where $\sigma_{ij}$ is the viscous stress tensor. Substituting in the instantaneous fluctuating properties we have

$$(\bar{\rho} + \rho') \frac{\partial (\bar{U}_i + U_i')}{\partial t} + (\bar{\rho} + \rho')(\bar{U}_j + U_j') \frac{\partial (\bar{U}_i + U_i')}{\partial x_j}$$

$$= -\frac{\partial \bar{P}}{\partial x_i} - \frac{\partial P'}{\partial x_i} - \frac{\partial \bar{\sigma}_{ij}}{\partial x_j} - \frac{\partial \sigma_{ij}'}{\partial x_j} \tag{4}$$

8

Taking the time average gives

$$(\bar{\rho}\ \bar{U}_j + \overline{\rho'U_j'})\frac{\partial \bar{U}_i}{\partial x_j} + \bar{\rho}\ \overline{U_j'\ \frac{\partial U_i'}{\partial x_j}} + \overline{\rho'(\bar{U}_j + U_j')\frac{\partial U_i'}{\partial x_j}}$$

$$= -\frac{\partial P}{\partial x_i} - \frac{\partial \bar{\sigma}_{ij}}{\partial x_j} \tag{5}$$

By multiplying the instantaneous continuity equation by the instantaneous velocity, $U_i$, time averaging and using Equation 2 gives

$$\overline{U_i'\ \frac{\partial}{\partial x_j}\ (\bar{\rho}\ U_j' + \rho'\bar{U}_j + \rho'U_j')} = 0 \tag{6}$$

By adding this term to Equation 5 and combining terms

$$(\bar{\rho}\ \bar{U}_j + \overline{\rho'U_j'})\ \frac{\partial \bar{U}_i}{\partial x_i} + \frac{\partial \bar{\rho}\ \overline{U_j'U_i'}}{\partial x_j} + \frac{\partial \overline{\rho'U_j'U_i'}}{\partial x_j} + \frac{\partial \overline{\rho'U_i'}\ \bar{U}_j}{\partial x_j}$$

$$= -\frac{\partial \bar{P}}{\partial x_i} - \frac{\partial \bar{\sigma}_{ij}}{\partial x_j} \tag{7}$$

which is the complete steady-state time-averaged form of the momentum equation.

## IV. TURBULENT KINETIC ENERGY

First the instantaneous momentum equation is multi-plied by $U_i$ and instantaneous continuity equation by $1/2\ U_i^2$.

Continuity

$$\frac{U_i^2}{2} \frac{\partial \rho}{\partial t} + \frac{U_i^2}{2} \frac{\partial}{\partial x_j} (\rho U_j) = 0$$

Momentum

$$\frac{\rho}{2} \frac{\partial U_i^2}{\partial t} + \frac{\rho U_j}{2} \frac{\partial U_i^2}{\partial x_j} = - U_i \frac{\partial P}{\partial x_i} - U_i \frac{\partial \sigma_{ij}}{\partial x_j}$$

Adding these two equations together gives

$$\frac{\partial}{\partial t} \left( \frac{\rho U_i^2}{2} \right) + \frac{1}{2} \frac{\partial \rho U_j U_i^2}{\partial x_j} = - U_i \frac{\partial P}{\partial x_i} - U_i \frac{\partial \sigma_{ij}}{\partial x_j}$$

Time averaging the steady-state form of this equation leaves

$$\frac{1}{2} \frac{\partial \overline{\rho U_j U_i^2}}{\partial x_j} = - \overline{U_i \frac{\partial P}{\partial x_i}} - \overline{U_i \frac{\partial \sigma_{ij}}{\partial x_j}} \tag{8}$$

Expanding the terms of this equation

$$\frac{1}{2} \frac{\partial}{\partial x_j} [ \overline{\rho} ( \overline{U}_i^2 \overline{U}_j + \overline{U}_j \overline{U_i'^2} + 2 \overline{U}_i \overline{U_i' U_j'} + \overline{U_i'^2 U_j'} )]$$

$$+ \frac{1}{2} \frac{\partial}{\partial x_j} [ 2 \overline{U}_i \overline{U}_j \overline{\rho' U_i'} + \overline{U}_j \overline{\rho' U_i'^2} + \overline{U}_i^2 \overline{\rho' U_j'}$$

$$+ 2 \overline{U}_i \overline{\rho' U_i' U_j'} + \overline{\rho' U_i'^2 U_j'} ]$$

$$= - \overline{U}_i \frac{\partial \overline{P}}{\partial x_i} - \overline{U_i' \frac{\partial P'}{\partial x_i}} - \overline{U}_i \frac{\partial \overline{\sigma}_{ij}}{\partial x_j} - \overline{U_i' \frac{\partial \sigma_{ij}'}{\partial x_j}} \tag{8a}$$

Multiply Equation 7 by $\overline{U}_i$ and subtract from Equation 8a

10

$$\frac{\overline{U}_i^2}{2} \frac{\partial \overline{\rho}\ \overline{U}_j}{\partial x_j} + \frac{\overline{U}_i^2}{2} \frac{\partial \overline{\rho' U_j'}}{\partial x_j} + \overline{\rho}\ \overline{U_i' U_j'}\ \frac{\partial \overline{U}_i}{\partial x_j}$$

$$+ \overline{\rho' U_i' U_j'}\ \frac{\partial \overline{U}_i}{\partial x_j} + \overline{\rho' U_i'}\ \overline{U}_j\ \frac{\partial \overline{U}_i}{\partial x_j} + \frac{1}{2} \frac{\partial \overline{\rho}\ \overline{U}_j \overline{U_i'^2}}{\partial x_j}$$

$$+ \frac{1}{2} \frac{\partial \overline{\rho}\ \overline{U_i'^2 U_j'}}{\partial x_j} + \frac{1}{2} \frac{\partial}{\partial x_j}\ \overline{\rho' U_i'^2}\overline{U}_j + \frac{1}{2} \frac{\partial}{\partial x_j}\ \overline{\rho' U_i'^2 U_j'}$$

$$= - \overline{U_i'\ \frac{\partial P'}{\partial x_j}} - \overline{U_i'\ \frac{\partial \sigma_{ij}'}{\partial x_j}} \tag{9}$$

The first two terms are identically zero as given by the time-averaged continuity equation. Changing the suffix on the pressure term from i to j, and after some rearranging, the compressible form of the turbulent kinetic energy equation is

$$U_j\ \frac{\partial}{\partial x_j}\ \underbrace{\left(\frac{1}{2}\rho\overline{U_i'^2} + \frac{1}{2}\overline{\rho' U_i'^2}\right)}_{\text{I}} + \underbrace{\overline{\rho' U_i'}\ U_j\ \frac{\partial U_i}{\partial x_j}}_{\text{II}}$$

$$+ \underbrace{\left(\frac{1}{2}\rho\overline{U_i'^2} + \frac{1}{2}\overline{\rho' U_i'^2}\right)\frac{\partial U_j}{\partial x_j}}_{\text{III}} - \underbrace{\overline{P'\ \frac{\partial U_j'}{\partial x_j}}}_{\text{IV}}$$

$$+ \underbrace{(\overline{\rho}\ \overline{U_i' U_j'} + \overline{\rho' U_i' U_j'})\ \frac{\partial U_i}{\partial x_j}}_{\text{V}}$$

$$+ \underbrace{\frac{\partial}{\partial x_j}\left(\overline{P' U_j'} + \frac{1}{2}\rho\overline{U_i'^2 U_j'} + \frac{1}{2}\overline{\rho' U_i'^2 U_j'}\right)}_{\text{VI}} + \underbrace{\overline{U_i'\ \frac{\partial \sigma_{ij}'}{\partial x_j}}}_{\text{VII}} = 0 \tag{10}$$

11

The bars over the mean flow quantities have been dropped for convenience. The seven labeled terms of the turbulent kinetic energy are:

I. Convection by mean flow

II. Turbulent mass flux times mean flow acceleration

III. Normal stress times mean dilatation

IV. Fluctuating pressure dilatation

V. Turbulence production

VI. Turbulent energy diffusion

VII. Viscous dissipation of turbulent energy

Equation 10 is an exact expression for the turbulent kinetic energy equation including compressibility. An order of magnitude analysis will be performed and simplifying approximations made to reduce this equation, and the continuity and momentum equations, to a more usable form. First, an approximation to the fluctuating density, $\rho'$, is developed. The instantaneous total enthalpy and equation of state for a thermally and calorically perfect gas are given by

$$H = h + \frac{U_i^2}{2} \tag{11}$$

$$P = \frac{\gamma - 1}{\gamma} \rho h \tag{12}$$

The instantaneous properties are defined

$$H = \bar{H} + H'$$

$$h = \bar{h} + h'$$

$$U = \overline{U} + U'$$

$$P = \overline{P} + P'$$

$$\rho = \overline{\rho} + \rho'$$

With these definitions, Equation 11 is written as

$$\overline{H} + H' = \overline{h} + h' + \frac{1}{2} (\overline{U}_i^2 + 2\overline{U}_i U_i' + U_i'^2)$$

Time averaging and taking the difference gives

$$H' = h' + \overline{U}_i U_i' + \frac{U_i'^2 - \overline{U}_i'^2}{2}$$

The last term is assumed to be an order of magnitude less than $\overline{U}_i U_i'$. Also $U'$, $V'$, and $W'$ are assumed to be of equal order and

$$\left|\frac{\overline{V}}{\overline{U}}\right|^2, \left|\frac{\overline{W}}{\overline{U}}\right|^2 \ll 1$$

Using Morkovin's [31] suggestion that $H' < h'$, these assumptions leave

$$h' + \overline{U} U' \simeq 0 \tag{13}$$

From the equation of state

$$\overline{P} + P' = \frac{\gamma - 1}{\gamma}[\overline{\rho}\ \overline{h} + \rho'\overline{h} + \overline{\rho}h' + \rho'h'] \tag{14}$$

The time average of Equation 14 is

$$\overline{P} = \frac{\gamma - 1}{\gamma} [\overline{\rho}\ \overline{h} + \overline{\rho'h'}] \tag{15}$$

Subtracting Equation 15 from Equation 14 leaves

$$P' = \frac{\gamma - 1}{\gamma}(\rho'\bar{h} + \bar{\rho}h' + \rho'h' - \overline{\rho'h'})$$

Bradshaw [25] suggests that the first and second terms on the right-hand side are the dominant terms when the Mach number fluctuation is much less than unity. This gives

$$\frac{\rho'}{\bar{\rho}} \simeq - \frac{h'}{\bar{h}} \tag{16}$$

Eliminating h' between Equations 13 and 16,

$$\frac{\rho'}{\bar{\rho}} \simeq \frac{\bar{U}\,U'}{\bar{h}}$$

or

$$\frac{\rho'}{\bar{\rho}} \simeq (\gamma - 1)\, M^2\, \frac{U'}{\bar{U}} \tag{17}$$

where M is the local time-averaged Mach number. This approximation will be used to simplify the continuity, momentum, and turbulent kinetic energy equations. It is also assumed that $(\gamma - 1)M^2$ is no greater than order unity. The reader is referred to Appendix A for the order of magnitude analysis of the continuity, momentum, and turbulent kinetic energy equations. The resulting equations are:

Continuity

$$\frac{\partial \rho U}{\partial x} + \frac{\partial}{\partial y}\,(\rho V + \overline{\rho'V'}) = 0 \tag{18}$$

14

Momentum

$$\rho U \frac{\partial U}{\partial x} + (\rho V + \overline{\rho'V'}) \frac{\partial U}{\partial y}$$

$$= - \frac{\partial P}{\partial x} - \frac{\partial}{\partial y} (\rho \overline{U'V'} + \overline{\rho'U'V'}) \tag{19}$$

Turbulent Kinetic Energy

$$\frac{\rho U}{2} \frac{\partial \overline{q}^2}{\partial x} + \frac{(\rho V + \overline{\rho'V'})}{2} \frac{\partial \overline{q}^2}{\partial y} + (\rho \overline{U'V'} + \overline{\rho'U'V'}) \frac{\partial U}{\partial y}$$

$$+ \frac{\partial}{\partial y} (\overline{P'V'} + \frac{1}{2} \rho \overline{q'^2V'} + \frac{1}{2} \overline{\rho'q'^2V'}) + \overline{U_i' \frac{\partial \sigma_{ij}'}{\partial x_j}}$$

$$+ \overline{\rho'U'} \cdot (U \frac{\partial U}{\partial x} + V \frac{\partial U}{\partial y}) - \frac{1}{2} \frac{\partial \overline{\rho'V'q'^2}}{\partial y} = 0 \tag{20}$$

In a manner similar to Bradshaw [24] the following definitions are made:

$$a_1 \equiv \frac{\tau}{\rho \overline{q}^2} \tag{21}$$

$$V_d \equiv \frac{(\overline{P'V'} + \frac{1}{2} \rho \overline{q'^2V'} + \frac{1}{2} \overline{\rho'q'^2V'})}{\rho \overline{q'^2}/2} \tag{22}$$

$$L \equiv \frac{\rho \left[\frac{\tau}{a_1 \rho}\right]^{3/2}}{\overline{U_i' \frac{\partial \sigma_{ij}'}{\partial x_j}}} \tag{23}$$

Using these definitions, neglecting the viscous stresses, letting the variable $V + \overline{\rho'V'}/\rho$ be defined as V, and defining the turbulent shear stress as

15

$$\tau \equiv - (\rho \overline{U'V'} + \overline{\rho'U'V'})$$

the continuity, momentum, and turbulent kinetic energy equations become

$$\frac{\partial \rho U}{\partial x} + \frac{\partial \rho V}{\partial y} = 0 \tag{24}$$

$$\rho U \frac{\partial U}{\partial x} + \rho V \frac{\partial U}{\partial y} = - \frac{\partial P}{\partial x} + \frac{\partial \tau}{\partial y} \tag{25}$$

$$\frac{\rho U}{2} \frac{\partial \left(\frac{\tau}{a_1 \rho}\right)}{\partial x} + \frac{\rho V}{2} \frac{\partial \left(\frac{\tau}{a_1 \rho}\right)}{\partial y} - \tau \frac{\partial U}{\partial y}$$

$$+ \frac{\partial}{\partial y} \left[\frac{V_d}{2} \frac{\tau}{a_1}\right] + \frac{\rho \left(\frac{\tau}{a_1 \rho}\right)^{3/2}}{L} + \rho D = 0 \tag{26}$$

The last term, $\rho D$, in Equation 26 is the same as the last two terms in Equation 20. Using the approximations given by Equation 17, the function D can be estimated as follows:

$$\overline{\rho'U'} = \rho \overline{U}'^2 \frac{U}{h}$$

$$\overline{\rho'V'} = \frac{\tau U}{h}$$

It has been noted by References 21 and 26 that $\overline{U}'^2 \approx \overline{q}^2/2$. Then

$$\overline{\rho'U'} \approx \frac{\tau}{2a_1} \frac{U}{h}$$

With these relations and by use of the momentum equation, $\rho D$

is approximated as

$$\rho D \simeq \frac{\tau}{2a_1\rho} \frac{U}{h}\left(- \frac{\partial P}{\partial x} + \frac{\partial \tau}{\partial y}\right) - \frac{\partial}{\partial y}\left(\frac{\tau U}{h}\right)\left(\frac{\tau}{2a_1\rho}\right) \tag{27}$$

This expression is rearranged to a more usable form:

$$\rho D \simeq - \frac{\tau}{2a_1\rho} \frac{U}{h} \frac{\partial P}{\partial x} - \tau\left[\frac{U}{h} \frac{\partial}{\partial y}\left(\frac{\tau}{2a_1\rho}\right) + \frac{\tau}{2a_1\rho} \frac{\partial}{\partial y}\left(\frac{U}{h}\right)\right] \tag{28}$$

This completes the development of the basic equations of motion in two-dimensional flow. The subsequent analysis in Chapter III uses the generalized two-dimensional equations (i.e., including axisymmetric flow).

# CHAPTER III

# CHARACTERISTIC AND COMPATIBILITY EQUATIONS

## I. BASIC ASSUMPTIONS AND DEVELOPMENT

If real·characteristics exist for Equations 24, 25, and 26, then this system ·of equations is hyperbolic [32]. However, prior to investigating the characteristics, additional assumptions· will be made to facilitate the development of the equations:

   a.  The flow is plane two-dimensional or axisymmetric.

   b.  The mixing process is a parallel two-stream turbulent mixing process.

   c.  The turbulent Prandtl and Schmidt numbers are unity, implying that the velocity, energy, and mass species profiles are similar.  Very near the initial plane of mixing where the mixing zone is undeveloped and dominated by the initial boundary layers, profile similarity does not exist. Thus, this assumption more properly applies to the fully developed mixing zone.

Equations 24, 25, and 26 are restated and used in generalized two-dimensional coordinates as follows:

Mass Continuity

$$\frac{\partial \rho U r^k}{\partial x} + \frac{\partial \rho V r^k}{\partial r} = 0 \tag{29}$$

18

Momentum

$$\rho U \frac{\partial U}{\partial x} + \rho V \frac{\partial U}{\partial r} = -\frac{dP}{dx} + \frac{1}{r^k}\frac{\partial r^k \tau}{\partial r} \tag{30}$$

Turbulent Kinetic Energy

$$\frac{\rho}{2}\left(U\frac{\partial}{\partial x} + V\frac{\partial}{\partial r}\right)\frac{\tau}{\rho a_1} + \frac{1}{r^k}\frac{\partial}{\partial r}\left[r^k\left(\frac{V_d}{2a_1}\right)\tau\right]$$

$$-\tau\frac{\partial U}{\partial r} + \frac{\rho}{L}\left(\frac{\tau}{\rho a_1}\right)^{3/2} + \rho D = 0 \tag{31}$$

where k is zero and one for plane two-dimensional flow and axisymmetric flow, respectively. The term D is still given by Equation 28.

If U, V, and $\tau$ are chosen as the dependent variables in Equations 29, 30, and 31, an expression for the density must be developed in terms of one or more of these three dependent variables. The density can be expressed in terms of U by use of the Crocco law since we have assumed the Prandtl and Schmidt numbers to be unity. From the equation of state

$$\rho = \frac{PM}{R_o T} \tag{32}$$

where M is the average molecular weight and $R_o$ is the universal gas constant. The local gas mixture is assumed to be calorically perfect, then

$$\rho = \frac{PC_p}{R_o h} \tag{33}$$

where $C_p$ is the average molar specific heat and h is the static enthalpy. Thus, in a two-stream compressible mixing process the density is a function of pressure, the molar specific heat, and enthalpy. The molar specific heat and enthalpy can be expressed in terms of velocity as will be seen. The axial pressure variation must be given. The log differential of Equation 33 is

$$\frac{1}{\rho}\frac{\partial \rho}{\partial x_i} = \frac{1}{C_p}\frac{\partial C_p}{\partial x_i} - \frac{1}{h}\frac{\partial h}{\partial x_i} + \frac{1}{P}\frac{\partial P}{\partial x_i} \tag{34}$$

where $x_1$ represents x and $x_2$ represents r. The average molar specific heat is

$$C_p = \Sigma\ Y_\alpha\ C_{p_\alpha} \tag{35}$$

where $Y_\alpha$ is the mole fraction of specie $\alpha$ given by

$$Y_\alpha = \frac{n_\alpha}{\Sigma n_\alpha} \tag{36}$$

and $n_\alpha$ is the moles of specie $\alpha$. For two-stream mixing where only two species need be considered

$$C_p = \frac{n_1}{n_1 + n_2}\ C_{p_1} + \frac{n_2}{n_1 + n_2}\ C_{p_2} \tag{37}$$

Lettinc $C_\alpha$ be the mass fraction

$$\frac{C_1}{C_2} = \frac{n_1 M_1}{n_2 M_2} \tag{38}$$

and substituting into Equation 37 gives

$$C_p = \frac{C_1 M_2 C_{p_1} + C_2 M_1 C_{p_2}}{C_2 M_1 + C_1 M_2} \tag{39}$$

Since $C_1 + C_2 = 1$

$$C_p = \frac{C_1 (M_2 C_{p_1} - M_1 C_{p_2}) + M_1 C_{p_2}}{C_1 (M_2 - M_1) + M_1} \tag{40}$$

Differentiating Equation 40

$$\frac{\partial C_p}{\partial x_i} = \left[ \frac{(M_2 C_{p_1} - M_1 C_{p_2}) - C_p (M_2 - M_1)}{C_1 (M_2 - M_1) + M_1} \right] \frac{\partial C_1}{\partial x_i}$$

and dividing by $C_p$

$$\frac{1}{C_p} \frac{\partial C_p}{\partial x_i} = \frac{M_1 M_2 (C_{p_1} - C_{p_2}) \frac{\partial C_1}{\partial x_i}}{\{C_1 (M_2 C_{p_1} - M_1 C_{p_2}) + M_1 C_{p_2}\}\{C_1 (M_2 - M_1) + M_1\}} \tag{41}$$

Note that mixing of perfect monatomic or diatomic gases gives

$$\frac{\partial C_p}{\partial x_i} = 0$$

since

$$C_{p_1} = C_{p_2}$$

21

By the assumption of unity turbulent Schmidt number the Crocco law gives

$$\frac{C_1 - C_{1o}}{C_{1j} - C_{1o}} = \frac{U - U_o}{U_j - U_o} \tag{42}$$

where the subscripts o and j refer to outer and inner (jet) boundary conditions, respectively. Differentiating Equation 42

$$\frac{\partial C_1}{\partial x_i} = \left(\frac{C_{1j} - C_{1o}}{U_j - U_o}\right)\frac{\partial U}{\partial x_i} \tag{43}$$

For convenience define

$$F_1 = \frac{M_1 M_2 (C_{p_1} - C_{p_2})\left(\frac{C_{1j} - C_{1o}}{U_j - U_o}\right)}{[C_1(M_2 C_{p_1} - M_2 C_{p_2}) + M_1 C_{p_2}][C_1(M_2 - M_1) + M_1]} \tag{44}$$

Then from Equations 41, 43, and 44

$$\frac{1}{C_p}\frac{\partial C_p}{\partial x_i} = F_1 \frac{\partial U}{\partial x_i} \tag{45}$$

From the assumption of unity turbulent Prandtl number, the Crocco law gives

$$\frac{H - H_o}{H_j - H_o} = \frac{U - U_o}{U_j - U_o} \tag{46}$$

where H is the total enthalpy defined by

$$H = h + \frac{U^2 + V^2}{2}$$

Assuming

$$\left(\frac{V}{U}\right)^2 << 1$$

$$H = h + U^2/2 \tag{47}$$

Differentiating Equations 46 and 47

$$\frac{\partial H}{\partial x_i} = \frac{H_j - H_o}{U_j - U_o} \frac{\partial U}{\partial x_i} \tag{48}$$

and

$$\frac{\partial H}{\partial x_i} = \frac{\partial h}{\partial x_i} + U \frac{\partial U}{\partial x_i} \tag{49}$$

By eliminating $\partial H/\partial x_i$ between Equations 48 and 49

$$\frac{\partial h}{\partial x_i} = \left(\frac{H_j - H_o}{U_j - U_o} - U\right) \frac{\partial U}{\partial x_i} \tag{50}$$

Again for convenience define

$$F_2 = \frac{1}{h}\left(\frac{H_j - H_o}{U_j - U_o} - U\right) \tag{51}$$

Then

$$\frac{1}{h} \frac{\partial h}{\partial x_i} = F_2 \frac{\partial U}{\partial x_i} \tag{52}$$

Combining Equations 34, 45, and 52 gives

23

$$\frac{1}{\rho} \frac{\partial \rho}{\partial x_i} = (F_1 - F_2) \frac{\partial U}{\partial x_i} + \frac{1}{P} \frac{\partial P}{\partial x_i} \tag{53}$$

This is the expression which will be used to express density gradients in terms of velocity gradients. Again, recall that $F_1$ equal to zero corresponds to mixing of thermally and calorically perfect monatomic or diatomic gases. Incompressible homogeneous mixing corresponds to $F_2$ equal to zero.

With Equation 53 and the equation of state the density gradient can be removed from explicity appearing in the continuity, momentum, and turbulent kinetic energy equations.

First the continuity equation is

$$[1 + U(F_1 - F_2)]\frac{\partial U}{\partial x} + V(F_1 - F_2)\frac{\partial U}{\partial r}$$

$$+ \frac{1}{r^k} \frac{\partial}{\partial r}(r^k V) + \frac{U}{P} \frac{dP}{dx} = 0 \tag{54}$$

The momentum equation is

$$U \frac{\partial U}{\partial x} + \left[V - \frac{\tau}{\rho}(F_1 - F_2)\right] \frac{\partial U}{\partial r}$$

$$= - \frac{(\gamma - 1)}{\gamma} \frac{h}{P} \frac{dP}{dx} + \frac{1}{r^k} \frac{\partial r^k (\tau/\rho)}{\partial r} \tag{55}$$

and the turbulent kinetic energy equation becomes

$$\frac{1}{2}\left[U \frac{\partial}{\partial x} + V \frac{\partial}{\partial r}\right]\left[\frac{\tau}{\rho a_1}\right] + \frac{1}{r^k} \frac{\partial}{\partial r}\left[r^k \left(\frac{V_d}{2a_1}\right)\frac{\tau}{\rho}\right]$$

$$+ \frac{V_d}{2a_1}\left(\frac{\tau}{\rho}\right)(F_1 - F_2)\frac{\partial U}{\partial r} - \frac{\tau}{\rho}\frac{\partial U}{\partial r}$$

$$+ \frac{1}{L}\left(\frac{\tau}{\rho a_1}\right)^{3/2} + D = 0 \qquad (56)$$

with

$$D = \frac{\tau}{2a_1\rho}\left(\frac{\gamma - 1}{\gamma}\right)\frac{U}{P}\frac{dP}{dx} - \frac{1}{2}\frac{\tau}{\rho}\frac{U}{h}\frac{\partial\left(\frac{\tau}{\rho a_1}\right)}{\partial r}$$

$$- \frac{1}{2}\frac{\tau}{\rho}\left(\frac{\tau}{a_1\rho}\right)\left(\frac{1 - F_2 U}{h}\right)\frac{\partial U}{\partial r} \qquad (57)$$

Note that the parameters $\tau$ and $\rho$ always appear together in Equations 54, 55, and 56 as $\tau/\rho$. For convenience $\tau/\rho$ will be written in the future as $\tau$.

At this point we assume the functions $a_1$, $V_d$, and L are functions only of the independent variables x and y. It should be remarked that $a_1$, $V_d$, and L also could be functions of U, V, and $\tau$ and that the resulting equations would be hyperbolic if the characteristics were real. However, they cannot in general be functions of the derivatives of the dependent variables, reference Courant and Friedrichs [32].

The method used for the development of the characteristic directions and compatibility equations is described in Appendix B. The method was shown to the author by Mr. Fran Loper of ARO, Inc. Other more involved methods exist and are described in References 32 and 33. The three

25

characteristic directions are

$$\frac{dr}{dx} = \infty \tag{58}$$

and

$$\left.\frac{dr}{dx}\right|_{L,R} = \frac{V + \frac{V_d}{2} - \frac{\tau}{2}(F_1 - F_2) - \frac{\tau U}{2h}}{U}$$

$$\pm \left\{ \left[\frac{V_d}{2} + \frac{\tau}{2}(F_1 - F_2) - \frac{\tau U}{2h}\right]^2 \right.$$

$$\left. + \tau \left[2a_1 - V_d(F_1 - F_2) + \frac{\tau}{h}(1 - F_2 U)\right] \right\}^{1/2} \div U \tag{59}$$

One characteristic direction is normal to the X-axis, the left characteristic direction is at an angle above the streamline, and the right characteristic direction is at an angle below the streamline. It is noted that the inclined characteristic directions are real provided

$$\left[\frac{V_d}{2} + \frac{\tau}{2}(F_1 - F_2) - \frac{\tau U}{2h}\right]^2$$

$$+ \tau \left[2a_1 - V_d(F_1 - F_2) + \frac{\tau}{h}(1 - F_2 U)\right] > 0 \tag{60}$$

For incompressible homogeneous mixing this expression reduces to

$$\frac{V_d^2}{4} + 2a_1\tau > 0$$

26

Both terms are always positive, thus the system of equations is hyperbolic.

The compatibility equation along the vertical characteristic is

$$[1 + U(F_1 - F_2)] \frac{1}{r^k} \frac{\partial (r^k \tau)}{\partial r}$$

$$- [V - \tau(F_1 - F_2) - U\tau(F_1 - F_2)^2]\frac{\partial U}{\partial r} + \frac{U}{r^k} \frac{\partial V r^k}{\partial r}$$

$$+ \left[U^2 - \frac{\gamma - 1}{\gamma} h[1 + U(F_1 - F_2)]\right]\frac{1}{P} \frac{dP}{dx} = 0 \qquad (61)$$

This equation can also be derived directly from the continuity and momentum equations simply by eliminating $\partial U/\partial x$ from the two equations. The compatibility equations along the inclined characteristics are

$$\tau\left[\frac{V_d}{2a_1}(F_1 - F_2) - 1\right]\left[\frac{\tau}{r}k - \frac{\gamma - 1}{\gamma} \frac{1}{P} \frac{dP}{dx} - U \frac{dU}{dx}\right]$$

$$- \left[G + \frac{U}{2a_1}\left(\frac{d\tau}{dx}\right)\right]\left[\frac{V_d}{2} + \frac{\tau}{2}(F_1 - F_2) - \frac{\tau U}{2h}\right]$$

$$\pm \left[\left[\frac{V_d}{2} + \frac{\tau}{2}(F_1 - F_2) - \frac{\tau U}{2h}\right]^2\right]$$

$$+ \tau\left[2a_1 - V_d(F_1 - F_2) + \frac{\tau}{h}(1 - F_2U)\right]\Big]^{1/2}\Big] = 0 \qquad (62)$$

where

$$G = \frac{\tau}{2a_1} \frac{1}{r^k} \frac{\partial}{\partial r}(V_d \ r^k) + \frac{1}{L}\left(\frac{\tau}{a_1}\right)^{3/2}$$

$$+ \frac{\tau}{2a_1}\left(\frac{\gamma - 1}{\gamma}\right)\frac{U}{P} \frac{dP}{dx} - \frac{U\tau}{2a_1^2} \frac{\partial a_1}{\partial x}$$

$$- \left(v + v_d - \frac{\tau U}{h}\right) \frac{\tau}{2a_1^2} \frac{\partial a_1}{\partial r} \tag{63}$$

This completes the development of the characteristics and their compatibility equations.

## II.  BOUNDARY CONDITIONS

### Symmetric Flow

For the symmetric two-dimensional flow, first- and second-regime mixing exist as illustrated in Figure 1. The first-regime boundary conditions are:

Outer Boundary

$$\tau = 0$$
$$U = U_o$$
$$V = V_o$$
$$V_d = V_{d_o} \tag{64}$$

Inner Boundary

$$\tau = 0$$
$$U = U_i$$

$U_o$ →

$U_j$ →

First Regime    Second Regime

₵
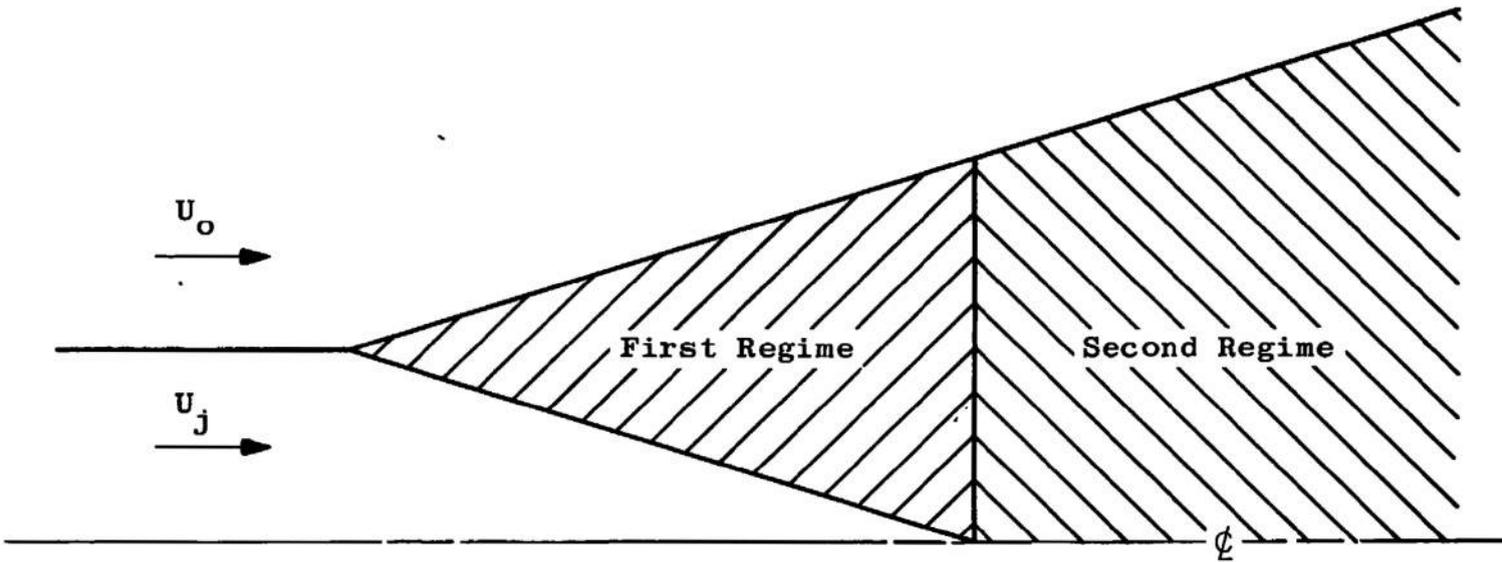
Figure 1.   Regimes of two-stream mixing.

$$V = 0$$

$$V_d = V_{d_i} \tag{65}$$

At both the inner and outer boundaries the slopes of the right and left characteristics reduce to

$$\left.\frac{dr}{dx}\right|_{L,R}^{b} = \frac{V + \frac{V_d}{2} \pm \left|\frac{V_d}{2}\right|}{U} \tag{66}$$

as can be seen from Equation 59. The superscript b is used to denote the boundary. More specifically, at the outer boundary with $V_d$ positive,

$$\left.\frac{dr}{dx}\right|_{L}^{bo} = \frac{V_o + V_{d_o}}{U_o} \tag{67}$$

and

$$\left.\frac{dr}{dx}\right|_{R}^{bo} = \frac{V_o}{U_o} \tag{68}$$

The left characteristic coincides with the outer boundary of the mixing layer. The right characteristic coincides with the streamline. At the inner boundary, with $V_d$ negative,

$$\left.\frac{dr}{dx}\right|_{L}^{bi} = \frac{V_i}{U_i} = 0 \tag{69}$$

and

$$\frac{dr}{dx}\bigg|_R^{bi} = \frac{V_{d_i}}{U_i} \tag{70}$$

The left characteristic coincides with the streamline at the inner boundary and the right characteristic coincides with the edge of the boundary. If the inner potential core flow is one dimensional, the left characteristic on the inner boundary has zero slope.

At both the inner and outer boundaries each term of the compatibility equations vanishes (Equation 62). Therefore, these equations provide no information at the mathematical boundaries. Normally, this would present some difficulty in solving the equations. This difficulty is avoided, however, because the outer boundary is arbitrarily defined to occur at the position where the U component of velocity is 1 per cent of the maximum velocity difference of the two streams. This criterion is for $U_j/U_o$ greater than unity. Likewise, the position of the inner boundary is defined to occur at 99 per cent of the velocity difference. At both of these defined boundaries a finite value of shear stress occurs. Consequently, the compatibility equations are not singular at these defined boundaries.

In the second regime the outer boundary conditions are the same as in the first regime, and the outer boundary is similarly defined. The inner boundary conditions, or line of symmetry boundary conditions, are

$$V = 0$$

$$\tau = 0$$

$$U = U_c$$

$$\frac{\partial U}{\partial r} = 0$$

$$V_d = 0 \tag{71}$$

The shear stress, vertical component of velocity, and diffusion velocity are zero by symmetry. These conditions give the slopes of both the right and left characteristics to be zero on the line of symmetry. The compatibility equations are singular and vanish on the line of symmetry.

The only unknown on the line of symmetry or centerline is $U_c$. Thus, one equation is needed to calculate $U_c$ and is obtained from either the continuity or momentum equation. Using the momentum equation (Equation 55) and taking the limit as r approaches zero gives

$$U_c \frac{\partial U_c}{\partial x} = - \frac{(\gamma - 1)}{\gamma} \frac{h}{P} \frac{dP}{dx} + (1 + k) \frac{\partial \tau}{\partial r} \tag{72}$$

By prescribing the pressure gradient and calculating the shear stress gradient from the value of $\tau$ and $r$ calculated from the first characteristic off the line of symmetry, $U_c$ can be calculated.

Unsymmetric Flow

If the flow is not symmetric, as is the case of mixing two semi-infinite streams, the vertical component of velocity at either of the two boundaries is not known a

priori. In this case, the vertical components of velocity at the two bouhdaries are related to one another. For incompressible flow, Mills [34] gives

$$\rho_i U_i V_i + \rho_o U_o V_o = 0 \tag{73}$$

The U component of velocity is either known or calculated from the potential flow.

CHAPTER IV

,

PARAMETER MODELING FOR FREE JET-MIXING

The purpose of this chapter is to establish physical-
ly perceptive models for the parameters $a_1$, $V_d$, and L for
axisymmetric-free jet mixing. Already these parameters have
been assumed to be at most functions of the independent
variables in the development of the characteristic and com-
patibility equations. Experimental data contained in the
literature will be used as a guide where possible. In
Chapter VI the models established here are used in the cal-
culation of several cases of axisymmetric jet mixing and the
calculations are compared with experimental data.

## I. TURBULENT KINETIC ENERGY-SHEAR
## STRESS PARAMETER

For the equilibrium boundary layer Bradshaw et al.
[24] observed that $a_1$ could be assumed a constant equal to
0.15. This value was used to obtain reasonable results in
the calculation of skin friction coefficient and velocity
and shear stress profiles for incompressible and compressible
adiabatic flows with and without pressure gradient. The
choice of $a_1$ equal to 0.15 was based on the turbulent
property measurements of Klebanoff [35]. For a two-
dimensional plane wake and an axisymmetric jet Lee and
Harsha [30] observed an average value of $a_1$ equal to 0.1

from several sources [36, 37, 38, and 39]. Recently they have revised their estimate to $a_1$ equal to 0.15 [40]. From the turbulent property data of Sami et al. [21] for a homogeneous axisymmetric jet exhausting into still air, Figure 2 was prepared to show the variation of $a_1$ with the non-dimensionalized independent variable $(r - r_i)/b$. It is shown that $|a_1|$ can be approximated reasonably well as a function of $(r - r_i)/b$ based on these data. The data shown are taken in both the first and second regimes ($3 < x/D < 10$). Wygnanski and Fiedler [41] have recently reported other turbulent intensity measurements in an incompressible and axisymmetric jet. Their measurements give $|a_1|_m$ approximately equal to 0.12 for $50 < x/D < 90$. Sami's data give $|a_1|_m$ approximately equal to 0.17 for $3 < x/D < 10$. On the centerline in the second regime $a_1$ equals zero since the shear stress is zero, but the turbulent kinetic energy is a finite value. The algebraic sign of $a_1$ is always the same sign as the shear stress since the turbulent kinetic energy is always positive. The experimental data used in this research for comparison with the theory are limited to $x/D < 18$; thus, a value of $a_1$ based on Sami's data is used in the calculations. An analytic function of the form

$$\frac{|a_1|}{|a_1|_m} = 4\frac{z}{z_o} - 3\left(\frac{z}{z_o}\right)^{4/3}, \quad z < z_o$$

$$\frac{|a_1|}{|a_1|_m} = 1, \quad z > z_o \tag{74}$$
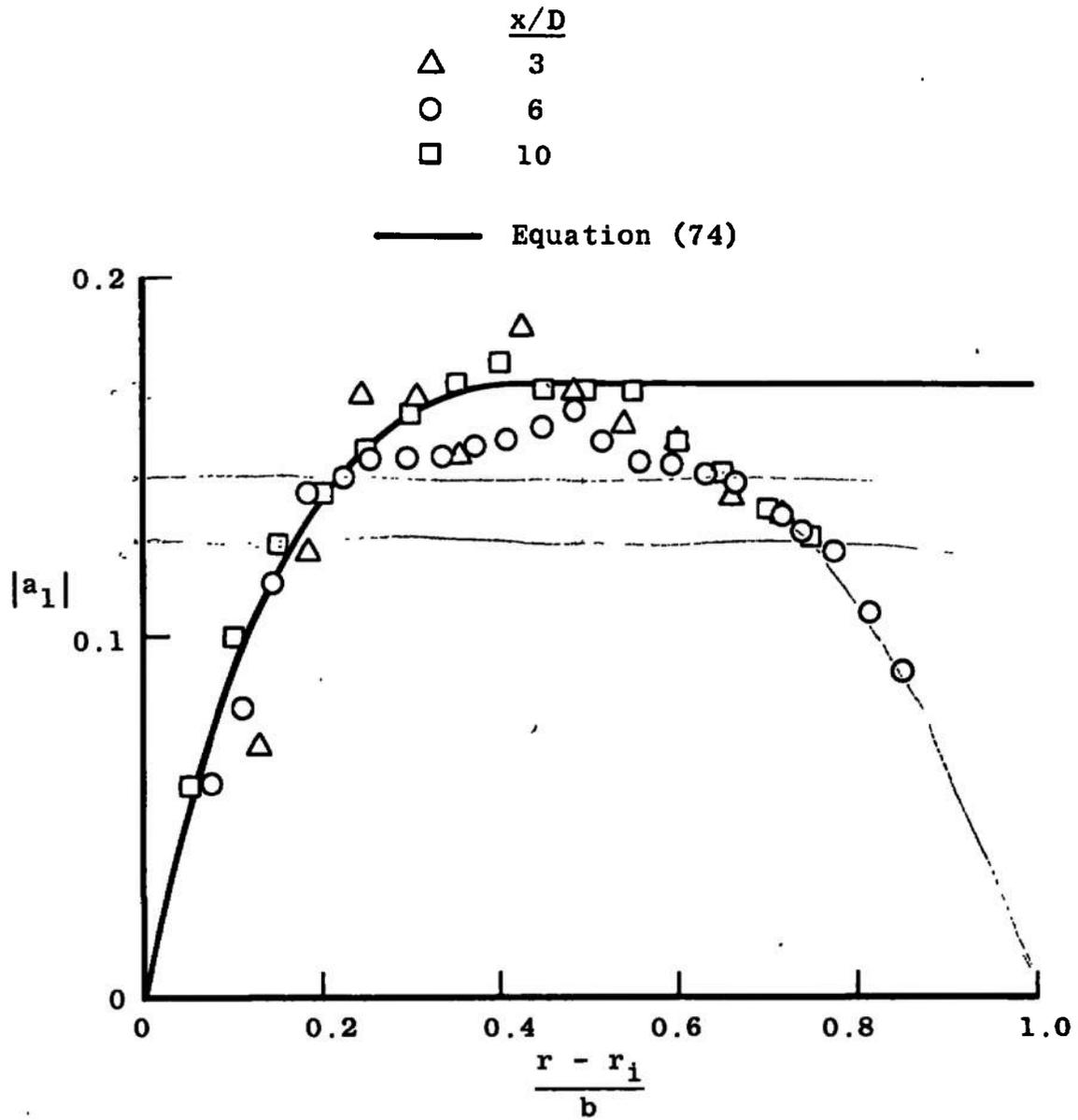
Figure 2. Variation of $a_1$ calculated from Sami's data.

where

$$Z = \frac{r - r_i}{b}$$

is used in the calculations. With $\left|a_1\right|_m$ equal to 0.17 and $Z_o$ equal to 0.4 this function is plotted in Figure 2 and is seen to fit Sami's data very well near the line of symmetry. In Chapter VI results of the calculations with other values of $\left|a_1\right|_m$ and $Z_o$ are discussed. For $Z > Z_o$, $a_1$ equal to a constant was found to be satisfactory in all calculations.

## II. DIFFUSION VELOCITY PARAMETER

The parameter $V_d$ is in effect the rate of diffusion of turbulent kinetic energy in the lateral direction. By assuming $V_d$ to be a function of the independent variables, x and r, the continuity, momentum, and turbulent kinetic energy equations were observed in Chapter III to form a hyperbolic set of equations for the three dependent variables U, V, and τ. The gradient diffusion models create a parabolic set of partial differential equations. The justification for the nongradient or diffusion velocity concept is based on the idea that the turbulent diffusion is primarily dominated by the effect of large eddies in free shear flow [28].

The functional form of the parameter $V_d$ was empirically derived by Bradshaw et al. [24] for the equilibrium boundary-layer case and adjustments were made by trial and

error until plausible solutions were obtained. In this study a similar approach is taken for the two-stream mixing problem. The value of $V_d$ can be empirically observed at the edge of the mixing layer by considering the entrainment of fluid into the mixing layer. Very near the edge of the turbulent mixing layer the production and dissipation of turbulent kinetic energy is small compared to convection and diffusion. Therefore, the turbulent kinetic energy equation reduces to

$$U \frac{\partial \overline{q}'^2}{\partial x} + V \frac{\partial \overline{q}'^2}{\partial r} + \frac{1}{r^k} \frac{\partial}{\partial r}(r^k V_d \overline{q}'^2) = 0 \qquad (75)$$

By assuming local similarity such that

$$\eta = \sigma \frac{r}{x}$$

where $\sigma$ is a constant, Equation 75 can be expressed as

$$\left[U \frac{\eta}{\sigma} - V\right] \frac{\partial}{\partial \eta} \overline{q}'^2 = \frac{1}{\eta^k} \frac{\partial}{\partial \eta}(\eta^k V_d \overline{q}'^2) \qquad (76)$$

Near the outer edge of the mixing zone the change of $(U\eta/\sigma - V)$, which is the entrainment, with respect to $\eta$ can be assumed to be small compared to the change of $\overline{q}'^2$ with respect to $\eta$ [24]. Thus, Equation 76 is rewritten as

$$\frac{\partial}{\partial \eta} \eta^k [(\frac{\eta}{\sigma} U - V)\overline{q}'^2] = \frac{\partial}{\partial \eta}(\eta^k V_d \overline{q}'^2) \qquad (76a)$$

Integrating this equation gives

$$V_d = \frac{\eta}{\sigma} U - V \tag{77}$$

The mass entrainment rate into one edge of the mixing layer is

$$\frac{dQ}{dx} = \frac{d}{dx} \int_0^b (2\pi r)^k \rho U dr \tag{78}$$

Also, the mass entrainment rate into the mixing layer is

$$\frac{dQ}{dx} = (2\pi b)^k \rho V_D \tag{79}$$

where $V_D$ is the lateral velocity of the mass being entrained into the mixing zone. Combining Equations 78 and 79 and with the aid of Leibnitz rule

$$V_D = U_b \frac{db}{dx} - \frac{1}{\rho_b b^k} \int_0^b \frac{\partial \rho U r^k}{\partial x} dr$$

and with the aid of the continuity equation this reduces to

$$V_D = U_b \frac{db}{dx} - V_b \tag{80}$$

where $U_b$ and $V_b$ are the boundary values of the velocity components. Since similarity has been assumed

$$\frac{db}{dx} = \frac{\eta}{\sigma}$$

Then Equations 77 and 80 give

39

$$V_d = V_D$$

Thus, the rate of turbulent diffusion at the boundary of the mixing zone is equal to the rate of mass entrainment. This observation permits use of mass entrainment measurements to establish the turbulent diffusion velocity at the boundary.

In the first regime of symmetric jet mixing, mass is entrained through the inner and outer boundaries. In the second regime of a symmetric jet mass is entrained only through the outer boundary and the net flux of turbulent kinetic energy being diffused across the line of symmetry is zero.

In the symmetric jet the turbulent diffusion velocity is finite on the inner boundary in the first regime, but as previously noted it is zero on the centerline in the second regime. Hence, the turbulent diffusion velocity at the end of the first regime experiences a finite discontinuity, or a transition zone exists over which the diffusion is altered. In either case it is obvious that the same function for the diffusion velocity could not apply to first-regime mixing as well as to second-regime mixing.

Following Bradshaw et al. [24] the turbulent diffusion velocity is normalized based on the local maximum absolute shear stress and a characteristic velocity, $U_{ch}$, such that

$$\frac{V_d}{U_{ch}} = \frac{|\tau|_{max}}{U_{ch}^2} \, f_{1,2}\left(\frac{r - r_i}{b}\right) \tag{81}$$

The subscripts, 1 and 2, denote the first and second regimes, respectively. For the equilibrium boundary-layer problem Bradshaw found the diffusion parameter, f, to be a universal function. Choice of the characteristic velocity is subject to some conjecture for the symmetric jet, but it is chosen as $(U_i - U_o)$, the <u>local</u> maximum velocity difference across the jet.

In establishing the function, $f((r - r_1)/b)$, the boundary values are established from empirical entrainment data. For the high velocity mixing boundary, data from the coaxial jet experiments by Chriss [18] and Paulk [19] are plotted in Figure 3 and compared with Bradshaw's [24] empirical result for the equilibrium boundary layer.

The agreement is reasonable and this suggests that a similar function exists for the high velocity mixing boundary, i.e.,

$$\left|\frac{V_d}{U_{ch}}\right|_{hV} = 10 \, \frac{|\tau|_{max}}{U_{ch}^2}$$

On the inner boundary in the first regime $f_1(0)$ is -10. The sign is negative since $V_d$ is negative on the inner boundary.

A similar correlation is also suggested in Figure 3 for the low velocity boundary, i.e.,

$$\left|\frac{V_d}{U_{ch}}\right|_{LV} = 2.5 \, \frac{|\tau|_{max}}{U_{ch}^2}$$

For $U_i > U_o$, $f_i(1)$ is 2.5. With the boundary conditions
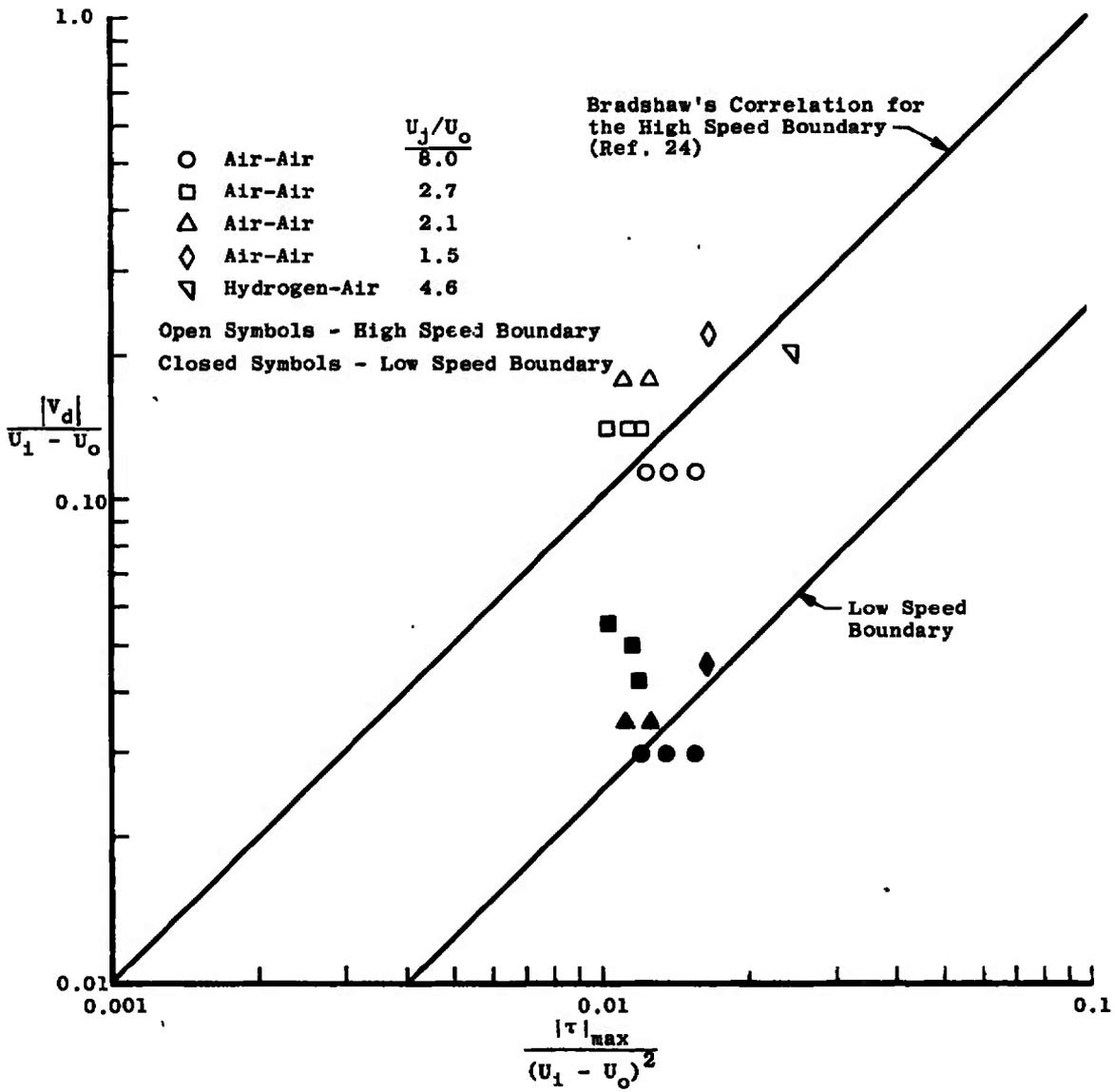
Figure 3.  Entrainment velocity correlation.

established for $f_1$, the complete function was established by trial and error by comparing calculated and experimental velocity and shear stress profiles. The resulting diffusion function is given in Figure 4. Ultimately, the diffusion function should be established experimentally. Negligible axial pressure gradients existed in the experiments and no pressure gradient was assumed in the trial and error calculations.

In the second regime $f_2(0)$ is zero by symmetry. At the outer boundary $f_2(1)$ was chosen as 2.5 to be continuous with its value in the first regime. Additional information can be derived from the turbulent kinetic energy equation for $f_2(0)$. Consider the turbulent kinetic energy equation written in the following form:

$$\frac{\partial u}{\partial r} = \frac{T}{\tau} \tag{82}$$

where

$$T \equiv \frac{U}{2} \frac{\partial \overline{q}'^2}{\partial x} + \frac{V}{2} \frac{\partial \overline{q}'^2}{\partial r} + \frac{1}{r^k} \frac{\partial}{\partial r}\left[ r^k \left( \frac{V_d}{2} \overline{q}'^2 \right) \right]$$

$$+ \left( \frac{V_d}{2} \overline{q}'^2 \right)(F_1 - F_2)\frac{\partial U}{\partial r} + \frac{1}{L}(\overline{q}'^2)^{3/2} + D \tag{83}$$

On the centerline $\partial U/\partial r$ and $\tau$ are zero. Therefore, T is not only zero on the centerline, but

$$\left. \frac{\partial T}{\partial r} \right|_{\mathcal{L}} = 0 \tag{84}$$
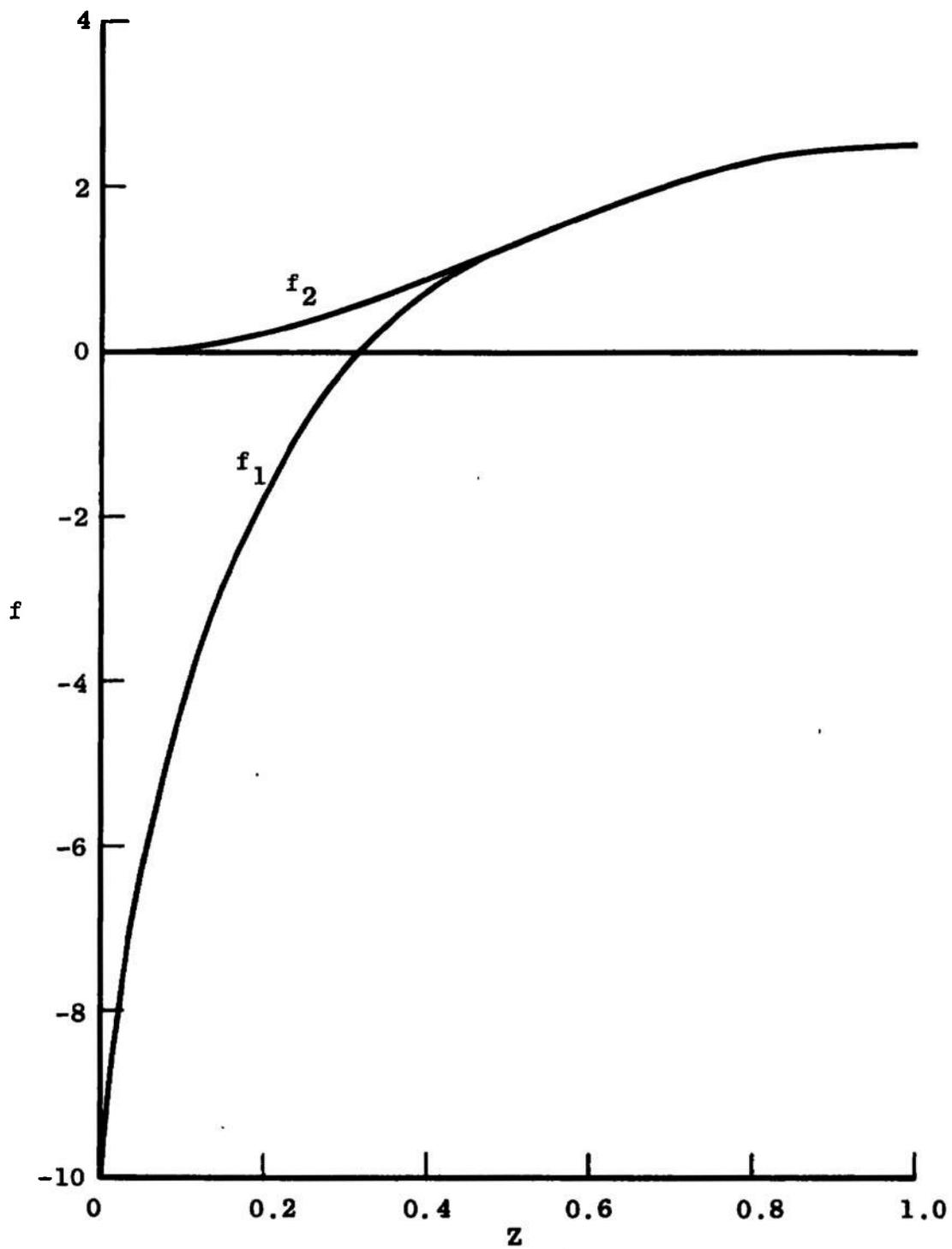
Figure 4.   Diffusion function for axisymmetric jet mixing.

which is obtained using L'Hospital's rule. Realizing that $\overline{q}'^2$ and U are symmetric functions, Equation 84 reduces further to

$$\frac{\partial^2 \ V_d \ \overline{q}'^2}{\partial r^2}\bigg|_{\underline{\mathcal{E}}} = \frac{\partial^2 \ V_d}{\partial r^2}\bigg|_{\underline{\mathcal{E}}} = 0$$

Using Equation 81 this gives

$$\frac{\partial^2 f}{\partial r^2}\bigg|_{\underline{\mathcal{E}}} = 0 \hspace{4cm} (85)$$

Using the boundary values established for $f_2$, the functional form was established by trial and error. The resulting function is given in Figure 4.

The negative values of the function for the first regime represent inward diffusion of turbulent kinetic energy, and the positive values represent outward diffusion of turbulent kinetic energy. In the first regime the diffusion function is zero at approximately the peak shear stress point.

## III.  DISSIPATION LENGTH PARAMETER

The dissipation length parameter, L, in the dissipation term of the turbulent kinetic energy equation is similar to the dissipation length used by Bradshaw et al. [24] and discussed by Townsend [26]. The parameter L is also analogous to the Prandtl mixing length as can be seen by neglecting the convection, diffusion, and compressibility

45

terms in the turbulent kinetic energy equation; hence, from Equation 31

$$\tau \frac{\partial U}{\partial y} = \frac{1}{L}\left(\frac{\tau}{a_1}\right)^{3/2}$$

which is rearranged to

$$|\tau| = L^2 |a_1|^3 \left(\frac{\partial U}{\partial y}\right)^2$$

This shows that the Prandtl mixing length theory actually equates the rate of local production and local dissipation of turbulent kinetic energy and consequently does not incorporate any history of the turbulent process. Including the convection and diffusion terms in the turbulent kinetic energy equation does add history to the turbulent structure behavior.

Following the approach of Lee and Harsha [30], L is taken to be proportional to the width, b, of the mixing layer such that

$$L = \frac{b}{K} \tag{86}$$

where K is a constant. From Sami's data [20 and 21] for an incompressible jet the value of K is plotted in Figure 5 versus the nondimensional jet width. Although there appears to be a slight variation in K with r, a constant and somewhat higher value equal to 0.85 was found to be more acceptable for the calculations presented in Chapter VI. In
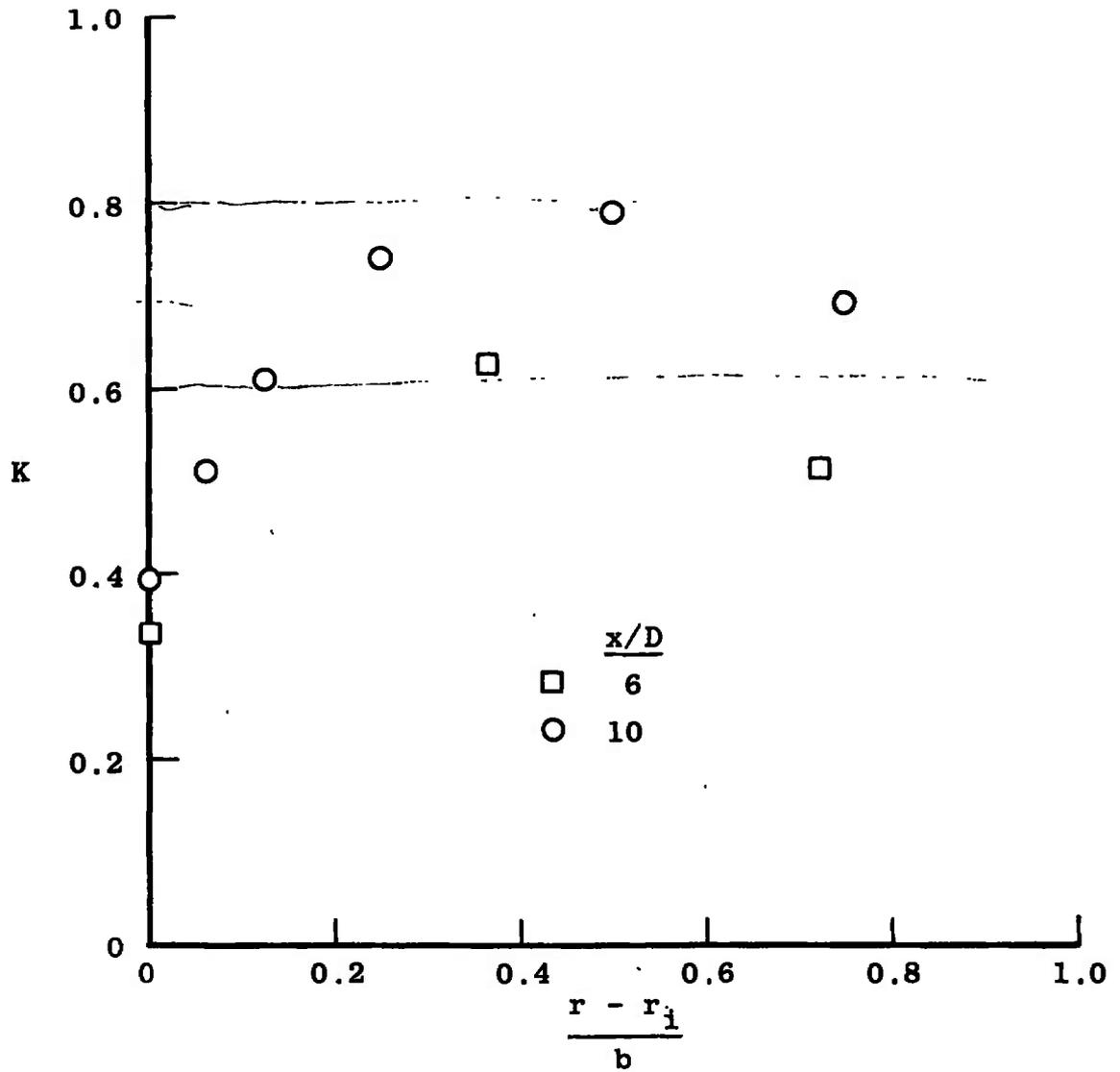
Figure 5.  Non-dimensional dissipation parameter calculated
from Sami's data.

Chapter VI it is shown that physically unrealistic velocity profiles are produced with K equal to 0.6 such that the peak velocity profile did not occur on the centerline. The sensitivity of the mixing calculation to K will be discussed in Chapter VI.

It is also of interest to note how L compares with the dissipation length reported by Bradshaw et al. [24] for the boundary layer. This is shown in Figure 6. Bradshaw's dissipation length parameter, denoted as L', is equivalent to $L |a_1|^{3/2}$. As Figure 6 shows, the two functions are remarkably similar except at the outer boundaries. Bradshaw included the effects of intermittency which is not included in the treatment of the mixing problem.
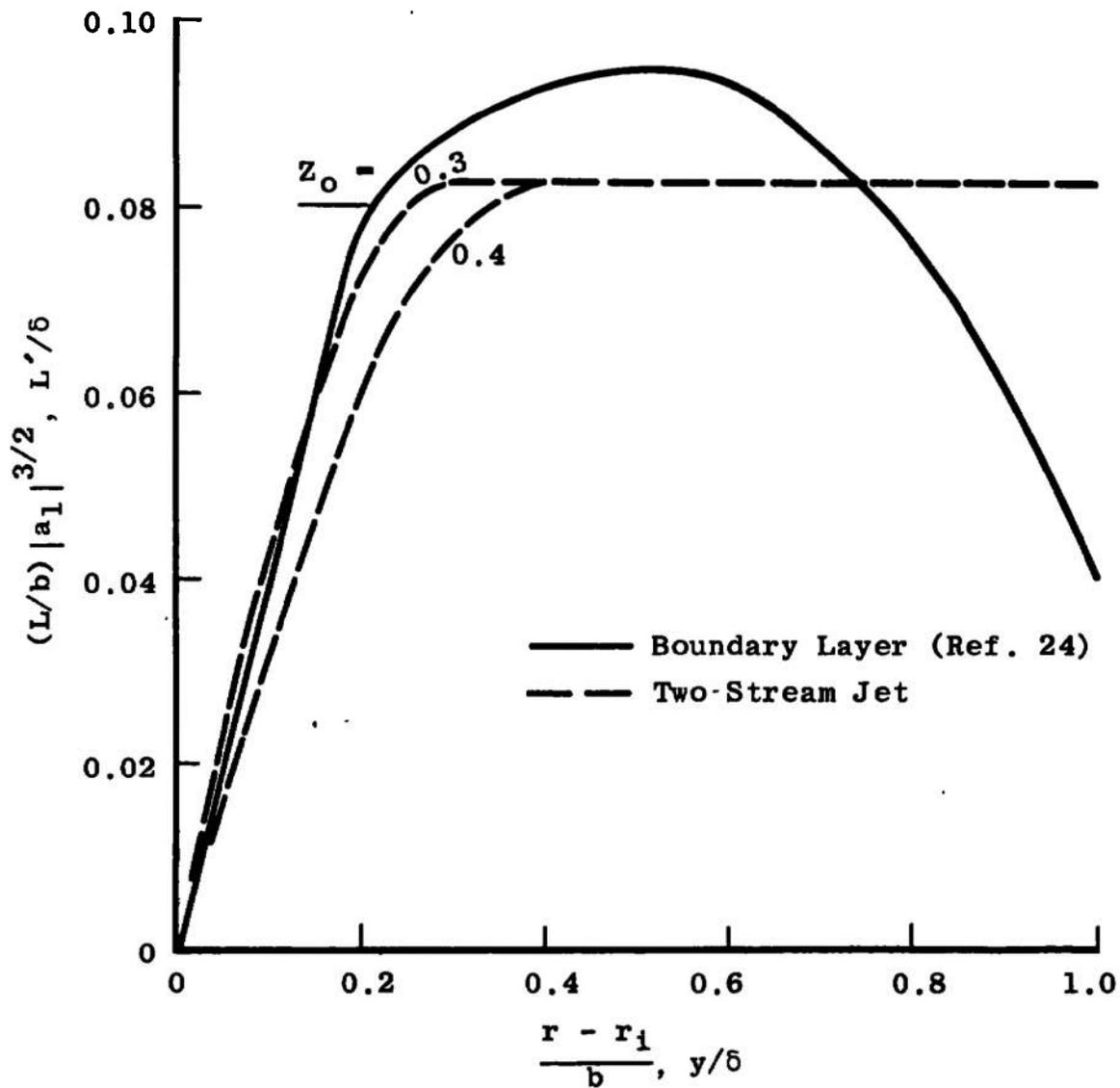
Figure 6. Dissipation length parameter in the boundary
layer and second-regime of the axisymmetric jet.

CHAPTER V

NUMERICAL PROCEDURES

I.  GENERAL APPROACH

The method of characteristics was used in solving the basic flow equations.  The characteristic slopes and corresponding compatibility equations were numerically solved in finite difference form on an IBM 360-50 computer.  The numerical equations were programmed in Fortran IV.  The numerical method used for the method of characteristics is basically Method II of Ralston and Wilf [39] with an implicit numerical integration scheme.  This method marches all the characteristics a constant $\Delta x$ before the next $\Delta x$ increment is taken.  This makes the method especially convenient for comparison of experimental data with the calculations since profiles of experimental data are generally taken and presented at a given x station.

II.  SUBROUTINES

Starting Line Subroutine

The vertical velocity component, V, does not appear in the differential equation along the inclined characteristics (Equation 66), but only in the differential equation along the vertical characteristic (Equation 65).  Therefore, V is calculated by direct integration along the vertical

characteristic with U and $\tau$ given on the initial profile.

## Field Point Subroutine

The field point subroutine is schematically illustrated in Figure 7. The objective is to calculate U, V, and $\tau$ on the new profile given their values on the old profile. In symmetric flow the most logical scheme is to proceed with the calculations from the inner boundary or line of symmetry to the outer boundary. In plane two-dimensional unsymmetric free shear flow the inner and outer boundary conditions are related to one another as given by Equation 73. In this case the calculations can be started from either boundary. The numerical procedure is to guess either $V_i$ or $V_o$ and iterate until Equation 73 is satisfied.

The numerical form of the characteristic and compatibility equations is expressed in Equations 87 through 91. The left characteristic equation is

$$
\begin{aligned}
r_3 - r_2 = \frac{\Delta x}{U_{23}} \Bigg[ V_{23} &+ \frac{V_{d_{23}}}{2} - \frac{\tau_{23}}{2}(F_1 - F_2)_{23} \\
&- \frac{\tau_{23}U_{23}}{2h_{23}} + \Bigg[ \left( \frac{V_{d_{23}}}{2} + \frac{\tau_{23}}{2}(F_1 - F_2)_{23} - \frac{U_{23}}{h_{23}} \right)^2 \\
&+ \tau_{23}[2(a_1)_{23} - V_{d_{23}}(F_1 - F_2)_{23} \\
&+ \frac{\tau_{23}}{h_{23}}(1 - F_2U)_{23}] \Bigg]^{1/2} \Bigg]
\end{aligned}
\tag{87}
$$

51

Old Profile     New Profile
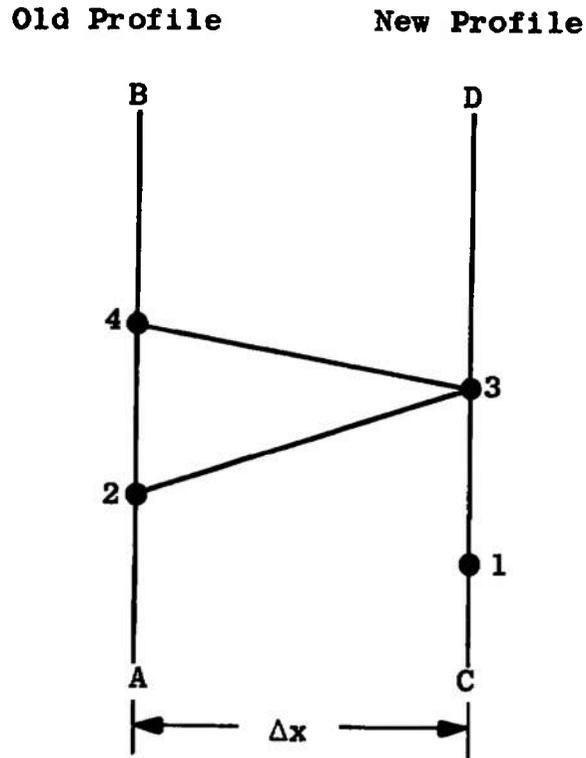
Figure 7. Schematic representation of the mesh point numerical method.

The right characteristic equation is

$$r_4 - r_3 = - \frac{\Delta x}{U_{43}} \left\{ V_{43} + \frac{V_{d_{43}}}{2} - \frac{\tau_{43}}{2}(F_1 - F_2)_{43} - \frac{\tau_{43}U_{43}}{2h_{43}} \right.$$

$$- \left[ \left( \frac{V_{d_{43}}}{2} + \frac{\tau_{43}}{2}(F_1 - F_2)_{43} - \frac{U_{43}}{h_{43}} \right)^2 \right.$$

$$+ \tau_{43} \left( 2(a_1)_{43} - V_{d_{43}}(F_1 - F_2)_{43} \right.$$

$$\left. \left. \left. + \frac{\tau_{43}}{h_{43}}(1 - F_2U)_{43} \right) \right]^{1/2} \right\} \qquad (88)$$

The compatibility equations along the characteristics in numerical form are as follows:

The left compatibility equation is

$$\tau_3 - \tau_2 + \frac{2(a_1)_{23}\tau_{23}}{\beta_{23}} \left[ \frac{V_{d_{23}}}{2(a_1)_{23}}(F_1 - F_2)_{23} - 1 \right] (U_3 - U_2)$$

$$= \frac{2(a_1)_{23}\Delta x}{U_{23}} \left\{ \frac{\tau_{23}}{\beta_{23}} \left[ \frac{V_{d_{23}}}{2(a_1)_{23}}(F_1 - F_2)_{23} - 1 \right] \right.$$

$$\left. \cdot \left[ \frac{\tau_{23}}{r_{23}}k - \left( \frac{\gamma - 1}{\gamma} \right)_{23} \frac{h_{23}}{P_{23}} \left( \frac{dP}{dx} \right)_{23} - G_{23} \right] \right\} \qquad (89)$$

where

$$\beta_{23} = \frac{V_{d_{23}}}{2} + \frac{\tau_{23}}{2}(F_1 - F_2)_{23} - \frac{\tau_{23}U_{23}}{2h_{23}}$$

$$+ \left\{ \left[ \frac{V_{d_{23}}}{2} + \frac{\tau_{23}}{2}(F_1 - F_2)_{23} - \frac{\tau_{23}U_{23}}{2h_{23}} \right]^2 \right.$$

$$\left. + \tau_{23} \left[ 2(a_1)_{23} - V_{d_{23}}(F_1 - F_2)_{23} + \frac{\tau_{23}}{h_{23}}(1 - F_2 U)_{23} \right] \right\}^{1/2}$$

and

$$G_{23} = \frac{\tau_{23}}{2(a_1)_{23}} \left[ \frac{V_{d_{23}}}{r_{23}} k + \left( \frac{dV_d}{dr} \right)_{23} \right] + \frac{1}{L_{23}} \left[ \frac{\tau_{23}}{(a_1)_{43}} \right]^{3/2}$$

$$+ \frac{\tau_{23}}{2(a_1)_{23}} \left[ \frac{\gamma - 1}{\gamma} \right]_{23} \frac{U_{23}}{P_{23}} \left( \frac{dP}{dx} \right)_{23} - \frac{\tau_{23}}{2(a_1)_{23}} U_{23} \left( \frac{\partial a_1}{\partial x} \right)_{23}$$

$$- \frac{\tau_{23}}{2(a_1)_{23}^2} \left[ V_{23} + \frac{V_{d_{23}}}{2} - \frac{\tau_{23}U_{23}}{h_{23}} \right] \left( \frac{\partial a_1}{\partial r} \right)_{23}$$

The right compatibility equation is

$$\tau_3 - \tau_4 + \frac{2(a_1)_{43}\tau_{43}}{\beta_{43}} \left[ \frac{V_{d_{43}}}{2(a_1)_{43}}(F_1 - F_2)_{43} - 1 \right] (U_3 - U_4)$$

$$= \frac{2(a_1)_{43}}{U_{43}} \Delta x \left[ \frac{\tau_{43}}{\beta_{43}} \left( \frac{V_{d_{43}}}{2(a_1)_{43}}(F_1 - F_2)_{43} - 1 \right) \right.$$

$$\left. \left( \frac{\tau_{43}}{r_{43}} k - \left[ \frac{\gamma - 1}{\gamma} \right]_{43} \frac{h_{43}}{P_{43}} \left( \frac{dP}{dx} \right)_{43} - G_{43} \right) \right] \qquad (90)$$

where

$$\beta_{43} = \frac{V_{d_{43}}}{2} + \frac{\tau_{43}}{2}(F_1 - F_2)_{43} - \frac{\tau_{43}U_{43}}{2h_{43}}$$

$$- \left\{ \left[ \frac{V_{d_{43}}}{2} + \frac{\tau_{43}}{2}\left( (F_1 - F_2)_{43} - \frac{U_{43}}{h_{43}} \right) \right]^2 \right.$$

$$+ \tau_{43}\left[ 2(a_1)_{43} - V_{d_{43}}(F_1 - F_2)_{43} \right.$$

$$\left. \left. + \frac{\tau_{43}}{h_{43}}(1 - F_2 U)_{43} \right] \right\}^{1/2}$$

and

$$G_{43} = \frac{\tau_{43}}{2(a_1)_{43}} \left[ \frac{V_{d_{43}}}{r_{43}} k + \left( \frac{dV_d}{dr} \right)_{43} \right] + \frac{1}{L_{43}} \left( \frac{\tau_{43}}{(a_1)_{43}} \right)^{3/2}$$

$$+ \frac{\tau_{43}}{2(a_1)_{43}} \left( \frac{\gamma - 1}{\gamma} \right)_{43} \frac{U_{43}}{P_{43}} \left( \frac{dP}{dx} \right)_{43} - \frac{\tau_{43}}{2(a_1)_{43}} U_{43} \left( \frac{\partial a_1}{\partial x} \right)_{43}$$

$$- \frac{\tau_{43}}{2(a_1)_{43}^2} \left[ V_{43} + \frac{V_{d_{43}}}{2} - \frac{\tau_{43}U_{43}}{h_{43}} \right] \left( \frac{\partial a_1}{\partial r} \right)_{43}$$

The vertical characteristic equation is

$$(V_3 - V_1)U_{31} = -\frac{V_{31}}{r_{31}} k (r_3 - r_1) - [1 + U_{31}(F_1 - F_2)_{31}]$$

$$\cdot \left[ (\tau_3 - \tau_1) + \frac{\tau_{31}}{r_{31}} k (r_3 - r_1) \right]$$

$$+ [V_{31} - \tau_{31}(F_1 - F_2)_{31} - U_{31}\tau_{31}(F_1 - F_2)^2_{31}](U_3 - U_1)$$

$$- \left[U^2_{31} - \left(\frac{\gamma - 1}{\gamma}\right)_{31} h_{31}[1 + U_{31}(F_1 - F_2)_{31}]\right]$$

$$\cdot \frac{1}{P_{31}}\left(\frac{dP}{dx}\right)_{31} (r_3 - r_1) \tag{91}$$

The double subscript notation indicates average values. For example, $U_{23}$ is $(U_2 + U_3)/2$. The single subscript notation is the value of the parameters at the designated mesh point. The calculation method proceeds as follows:

1. The position, $r_3$, is first approximated by projecting a left characteristic through point two to point three. The slope of this characteristic is calculated based on the average of values at point two and guessed values at point three. The first estimate of all the parameters at point three is taken as the average at the previously calculated point above point two and at point two.

2. A right characteristic is projected back through point three to make the first approximation of the position of point four. For the approximation of $r_4$ the same average values of the parameters are used as were used for the initial guess on the characteristic from point two to three.

.3. By linear interpolation, $U_4$, $V_4$, and $\tau_4$ are determined.

4. Using the right and left compatibility equations (Equations 89 and 90), the first calculated values of $U_3$ and $r_3$ are obtained.

5. Using the vertical compatibility equation (Equation 91), $V_3$ is calculated. Then the subroutine iterates through steps two to five until the calculations converge. The convergence criteria was arbitrarily set at $10^{-2}$ per cent on $U_3$, $V_3$, $\tau_3$, and $r_3$.

6. The process is repeated at other mesh points to obtain $U$, $V$, and $\tau$ over the whole range of $r$.

7. The new profile is then used as input for the next profile.

## Inner Boundary Subroutine

For the first-regime case the inner boundary mesh points are shown schematically in Figure 8a. The right characteristic on the boundary is line BD and is arbitrarily set at 99 per cent of the velocity difference between the inner and outer streams for $U_j > U_o$. The location of the boundary would be at 1 per cent of the velocity difference if $U_j < U_o$. With this criteron only $r_1$ and $\tau_1$ need to be calculated on the new profile since $U_1$ and $U_2$ are equal and $V_1$ is taken as zero in the symmetric flow problem. As was mentioned in Chapter III, $V_i$ is related to $V_o$ in plane two-dimensional unsymmetric flow and an iteration is required to satisfy this relation. The right characteristic equation, Equation 88, and its compatibility equation, Equation 90, are to be simultaneously solved for the two unknowns $r_1$ and $\tau_1$. At point three the flow properties are solved by the field point subroutine.

Old Profile　　　New Profile

A　　　　　　　　C

$\Delta x$

3

2 ●
B

1
D
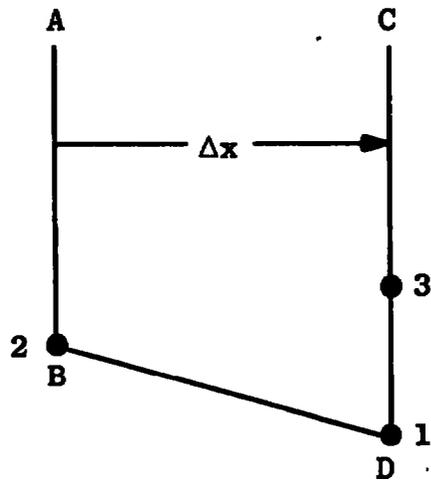
a.　First-Regime

Old Profile　　　New Profile

3

2 ●

C2　　　　　　　C1　　　— ¢ —
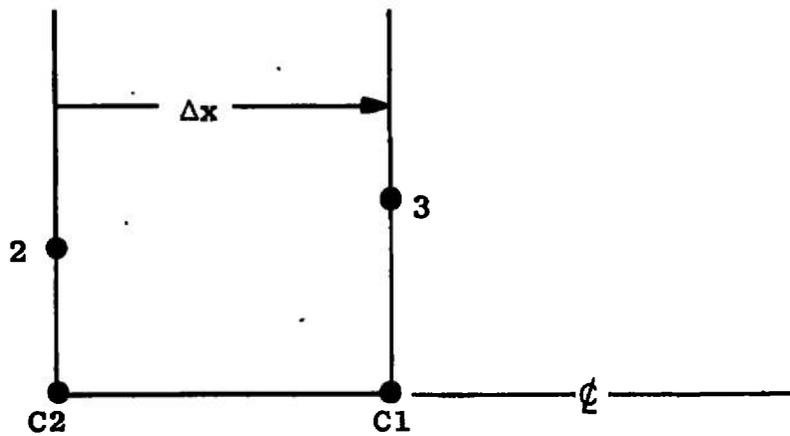
b.　Second-Regime

Figure 8.　Schematic of the inner boundary mesh points.

The second-regime inner boundary in symmetric flow requires an altogether different routine. The mesh points are schematically shown in Figure 8b. As was discussed in Chapter III, the problem is to calculate only the centerline velocity since the shear stress and vertical component of velocity are zero on the centerline. Equation 72 is used to calculate the centerline velocity, $U_{c_1}$, from conditions known on the old profile. This equation in finite difference form is

$$U_{c_{12}}(U_{c_1} - U_{c_2}) = -\left(\frac{\gamma - 1}{\gamma}\right)_{c_{12}} \frac{h_{c_{12}}}{P_{12}}\left(\frac{dP}{dx}\right)_{12}$$

$$+ (1 + k) \frac{\tau_{23}}{r_{23}} \Delta x \qquad (92)$$

Again at point three the flow properties are calculated by the field point routine. Calculation of the centerline velocity, $U_{c_1}$, is an implicit calculation to be consistent with the regular field point routine. This requires average values of $\tau$ and $r$ in Equation 92, i.e., $\tau_{23}$ and $r_{23}$, respectively. Therefore, the centerline velocity calculation was made in an iterative loop with the calculation of the properties at point three until it converged.

## Outer Boundary Subroutine

The outer boundary subroutine is the same in both the first and second regimes for symmetric flow and also can be

used for the plane two-dimensional unsymmetric flow case. The mesh points of the outer boundary are schematically shown in Figure 9. In this case the outer boundary is arbitrarily set at 1 per cent of the maximum velocity difference for $U_j > U_o$. The objective of this subroutine is to calculate $U$, $V$, $\tau$, and $r$ at point three. The left characteristic equation (Equation 87), its compatibility equation (Equation 89), the vertical compatibility equation (Equation 91) and the defined boundary condition for $U$ are used to solve for the four unknowns. Again an implicit calculation procedure is used. The first guessed values at point three are taken as those of point two.

The procedure for stopping the field point subroutine calculations and calling the outer boundary subroutine is as follows: If point one on the new profile is located by the field point subroutine such that the right characteristic passing through this point intersects the old profile at $r_4 > r_2$, point one is discarded and point one prime is used in the outer boundary calculations.

## III. LOGIC

The computer program logic is illustrated in Figure 10 for the symmetric two-dimensional jet mixing program.

## IV. STABILITY

The Courant-Friedrichs-Levy criterion
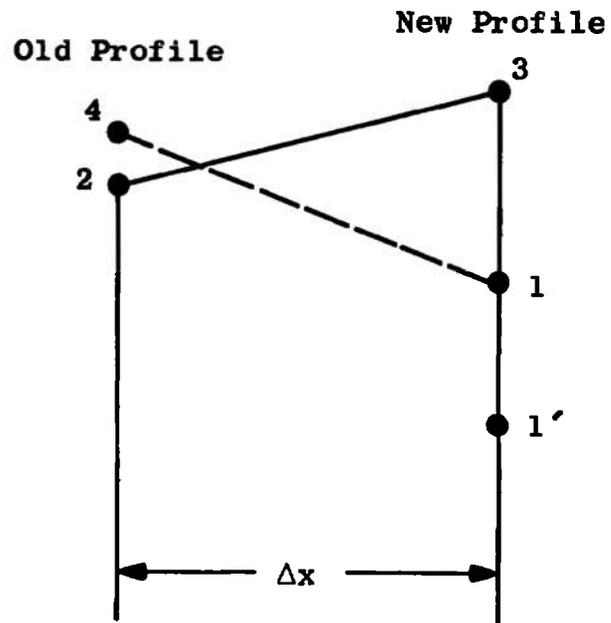
Figure 9. Schematic of the outer boundary mesh points.
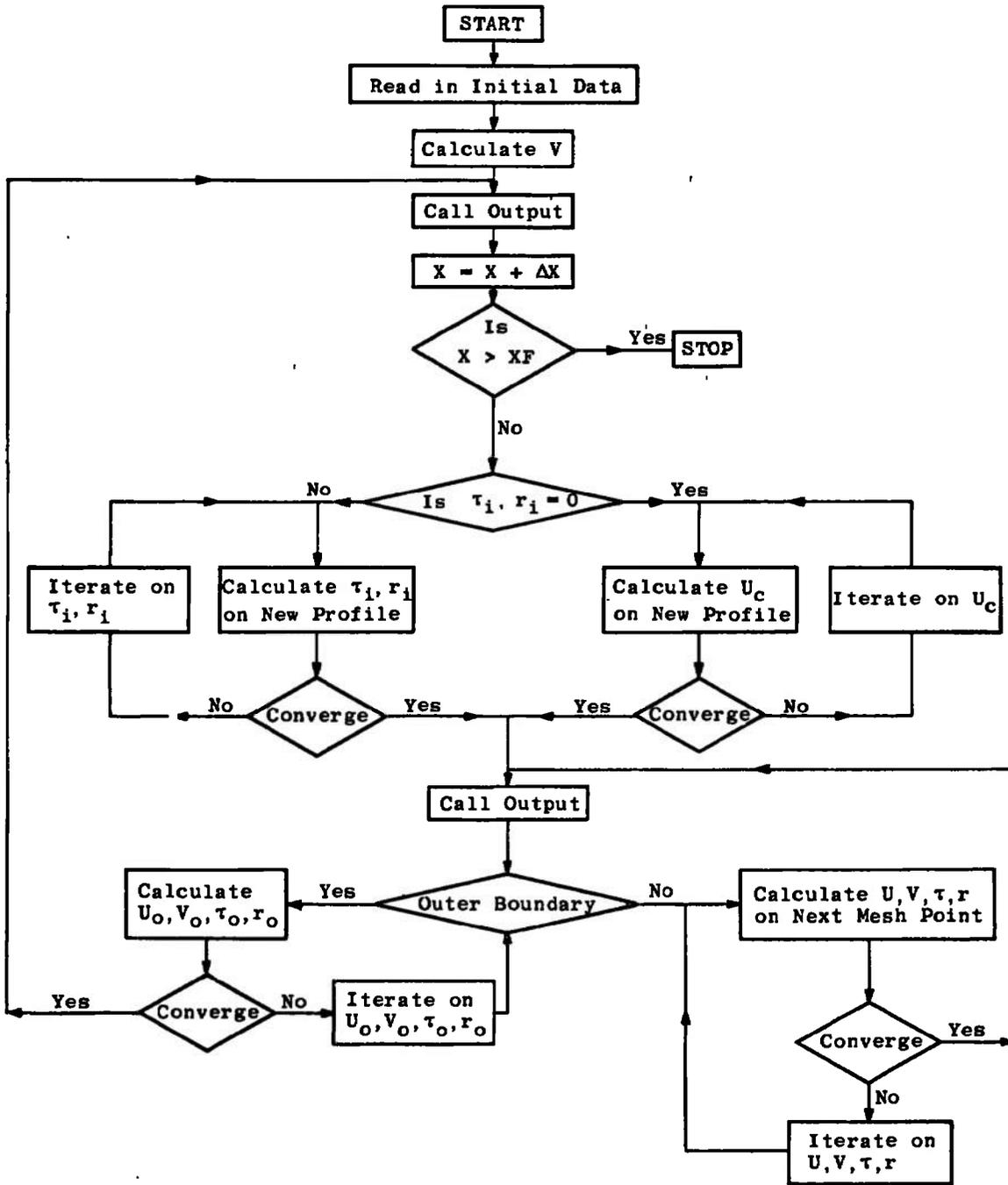
Figure 10. Flow diagram.

$$\Omega \equiv \frac{\Delta x}{\Delta r}\left(\frac{dr}{dx}\right)_{max} < 1 \qquad (93)$$

for a linear hyperbolic system of equations has so far proved sufficient for numerical stability. The term $\Delta r$ is the step size in the r-direction, $\Delta x$ is the step size in the x-direction and $(dr/dx)_{max}$ is the maximum slope of either the right or left characteristic. The step size in the computer program was chosen such that this criterion was satisfied. However, test calculations were made for $\Omega$ equal to 1.5 and no stability problems were encountered. Bradshaw, et al. [24] reports occasional instability near the wall for the boundary-layer problem unless $\Omega < 0.9$. This occurred when they used a least-squares linear extrapolation of the shear stress to the wall.

Early in the checkout phase of this computer program, a fourth-order Lagrangian curve fit was used for interpolation on the old profiles. This created an instability in the profiles near the centerline. The instability could be recognized by the growth of bumps in the profiles, particularly the velocity profile. The problem was eliminated by using a second-order Lagrangian (linear) curve fit.

## V. CONVERGENCE

A convergence criterion of 0.01 per cent was used on U, V, $\tau$, and r in the iteration which proved sufficient to the fourth significant figure. With this convergence criterion an average of four iterations for each mesh point on

the new profile was generally required.

## VI. COMPUTATIONAL TIME

The computational time depended on the number of mesh points chosen to start the calculation, the convergence criteria, and $\Delta x$. The number of mesh points chosen to start the calculations on the initial profile varied from 20 to 40. In first-regime calculations an additional point is picked up at each new profile along the inner boundary. In the second regime the number of mesh points remain constant. Generally, it was found better to use about twice as many mesh points in the inner half of the mixing zone as in the outer half to obtain an adequate plot of the shear stress profile. The program calculates along left characteristics which monotonically marches the mesh points away from the centerline. The program may require adding more mesh points near the centerline should the distance between the centerline and first mesh point become too great. The calculations reported in Chapter VI did not exceed 18 jet diameters from the initial plane of mixing, and did not require added mesh points.

The $\Delta x$ used in the mixing calculations was 0.12 jet diameters which satisfied the Courant-Friedrichs-Levy stability criterion in all cases calculated. This constant value of $\Delta x$ was chosen for the convenience of comparing the analytical calculation with the experimental data at particular x-stations. Should a variable $\Delta x$ be chosen by

letting $\Omega$ always equal unity the program would march faster.

As an example of the computing time, about 1.5 minutes are required for the program to march one jet diameter with 40 mesh points. No attempts were made to decrease the computing time since no more than 15 minutes were generally required to calculate the flow fields of interest.

## VII. ACCURACY

The numerical accuracy of the computer program was checked on each calculated profile by inserting the results into the integral form of the mass continuity and momentum equation. The details are given in Appendix C. Mass continuity was always satisfied within 2 per cent or better and momentum was always satisfied within 4 per cent or better.

CHAPTER VI

THEORETICAL CALCULATIONS FOR THE

AXISYMMETRIC JET

I.  SELECTION OF INITIAL PROFILE DATA

Analytical calculations are made and compared with
experimental data for hydrogen-air and air-air coaxial con-
stant pressure flow systems using the method of character-
istics discussed in Chapters III and V.  The hydrogen-air
experimental data is taken from Chriss' experiments [18]
and the air-air experimental data is taken from Paulk's
experiments [19].  Both sets of data were based on measure-
ments made in the same experimental apparatus.  Mixing cal-
culations are presented using initial velocity and turbulent
shear stress profiles in both the first and second regimes.
However, no calculations are made and presented for marching
the calculations from the first regime into the second
regime because the transition problem discussed in Chapter
IV remains to be solved.  The initial shear stress data
profiles were provided by Chriss and Paulk from their mean
flow measurements [18 and 19] using the momentum integral
method described by Peters et al. [42].

For first-regime calculations the initial starting
plane was chosen approximately 2.5 nozzle diameters from the
initial mixing plane, a location where reasonably accurate

velocity and turbulent shear stress profiles were obtained.

The analytical calculations to be presented for second-regime mixing generally used the second profile of experimental data in the second regime. The experimental turbulent shear stress profile was feared to be inaccurate on the first profile of experimental data. The turbulent shear stress data is based on evaluating X-derivatives of the momentum flux integral. In or near the transition regime these X-derivatives are probably not very accurate because of the rapid change in character of the flow from the first regime to the second regime.

The analytical calculations are presented first for hydrogen-air coaxial mixing and then for air-air coaxial mixing.

## II. HYDROGEN-AIR COAXIAL MIXING

Theoretical calculations are made and compared with experimental data for the case of a central jet of hydrogen coaxially exhausting with air into a plenum at constant pressure. The calculations are made for hydrogen-to-air velocity ratios ranging from 2.4 to 6.3. The maximum jet Mach number is about 0.6. Table I lists the bulk flow properties for the cases calculated and compared with experiment. Variations in the parameters $a_1$, K, and f are made to observe their sensitivity on the mixing calculations since basic measurements of these parameters are not available from the experiments. These calculations are made for a

TABLE I

HYDROGEN-AIR AXISYMMETRIC
MIXING FLOW CONDITIONS

| $U_j/U_o$ | $U_j$ ft/sec | $H_j/H_o$ | $H_j$ BTU/lb | $\rho_j/\rho_o$ |
|---|---|---|---|---|
| 2.4 | 1900 | 11.8 | $1.82 \times 10^3$ | 0.08 |
| 4.4 | 3200 | 11.6 | 1.78 | 0.09 |
| 6.3 ' | 3300 | 11.9 | 1.84 | 0.09 |
| 4.6 | 2880 | 7.7 | 1.98 | 0.14 |

second-regime case since their effect can be more readily observed over greater axial length. First, however, an example of a first-regime hydrogen-air mixing calculation is presented.

## First Regime

This example is presented for a central jet-to-outer stream velocity ratio of 4.6. The calculations start at an x/D of 2.7. Theoretical and experimental velocity and turbulent shear stress profiles are shown in Figures 11 and 12 at 3.57 and 4.53 nozzle diameters from the jet efflux.

The diffusion function, $f_1$, used in these calculations is that shown in Figure 4, page 44. The parameter K is chosen equal to 0.85. Two analytical functions for the parameter $a_1$ are used in these calculations for comparison. In one case it is assumed equal to -0.17 and in the other case it is a variable given by

$$\frac{|a_1|}{|a_1|_m} = 0.9\left[4\left(\frac{z}{z_o}\right) - 3\left(\frac{z}{z_o}\right)^{4/3}\right] + 0.1, \quad z < z_o$$

$$\frac{|a_1|}{|a_1|_m} = 1.0 \qquad\qquad z > z_o \qquad\qquad (94)$$

where $|a_1|_m$ and $z_o$ are equal to 0.17 and 0.4, respectively.

This function for $a_1$ is a modified form of Equation 74. Equation 74 could not be used for first-regime mixing since the inner boundary is defined where the shear stress is finite; consequently, the turbulent kinetic energy is
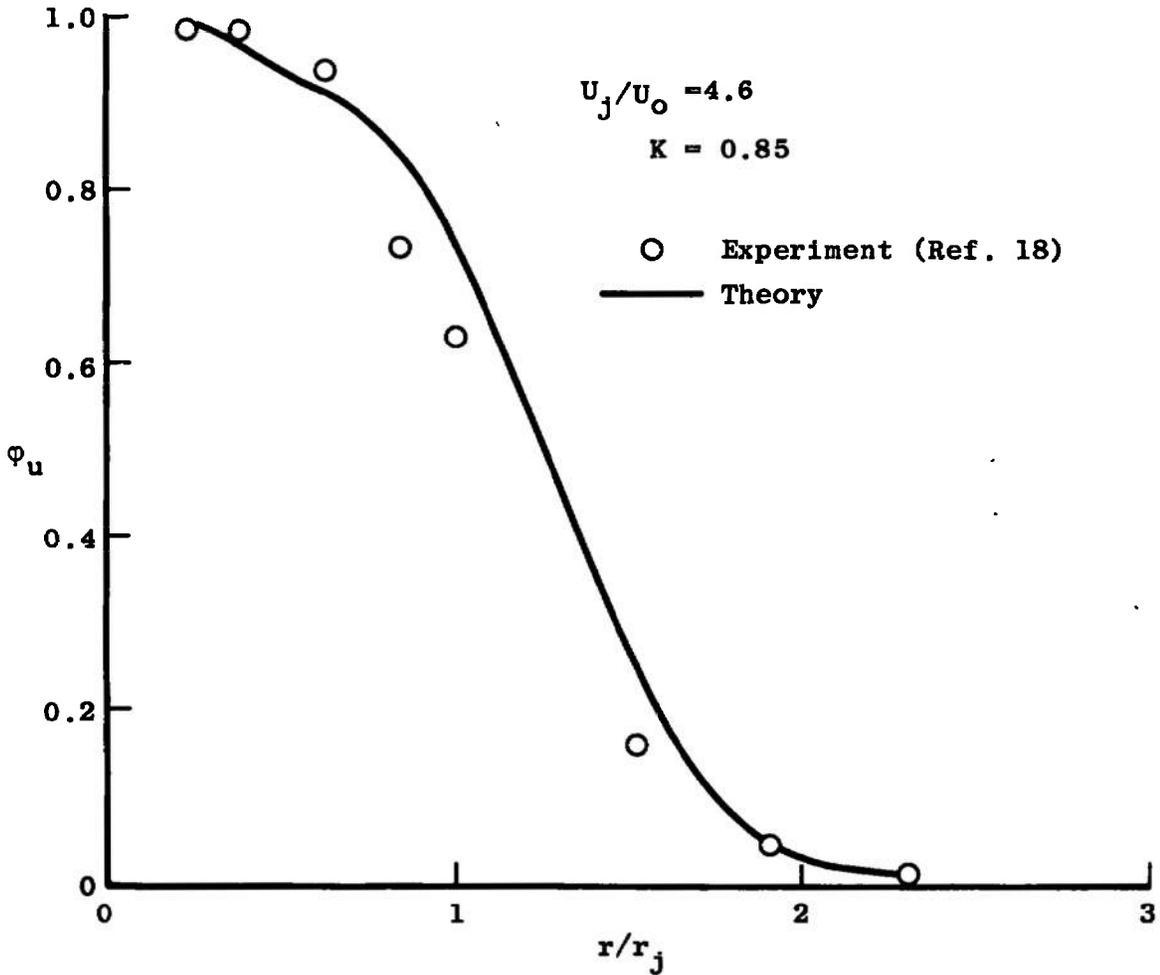
a. $x/D = 3.57$

Figure 11. First-regime velocity profiles for hydrogen-air mixing.

$U_j/U_o = 4.6$

$K \doteq 0.85$

O  Experiment (Ref. 18)

—— Theory
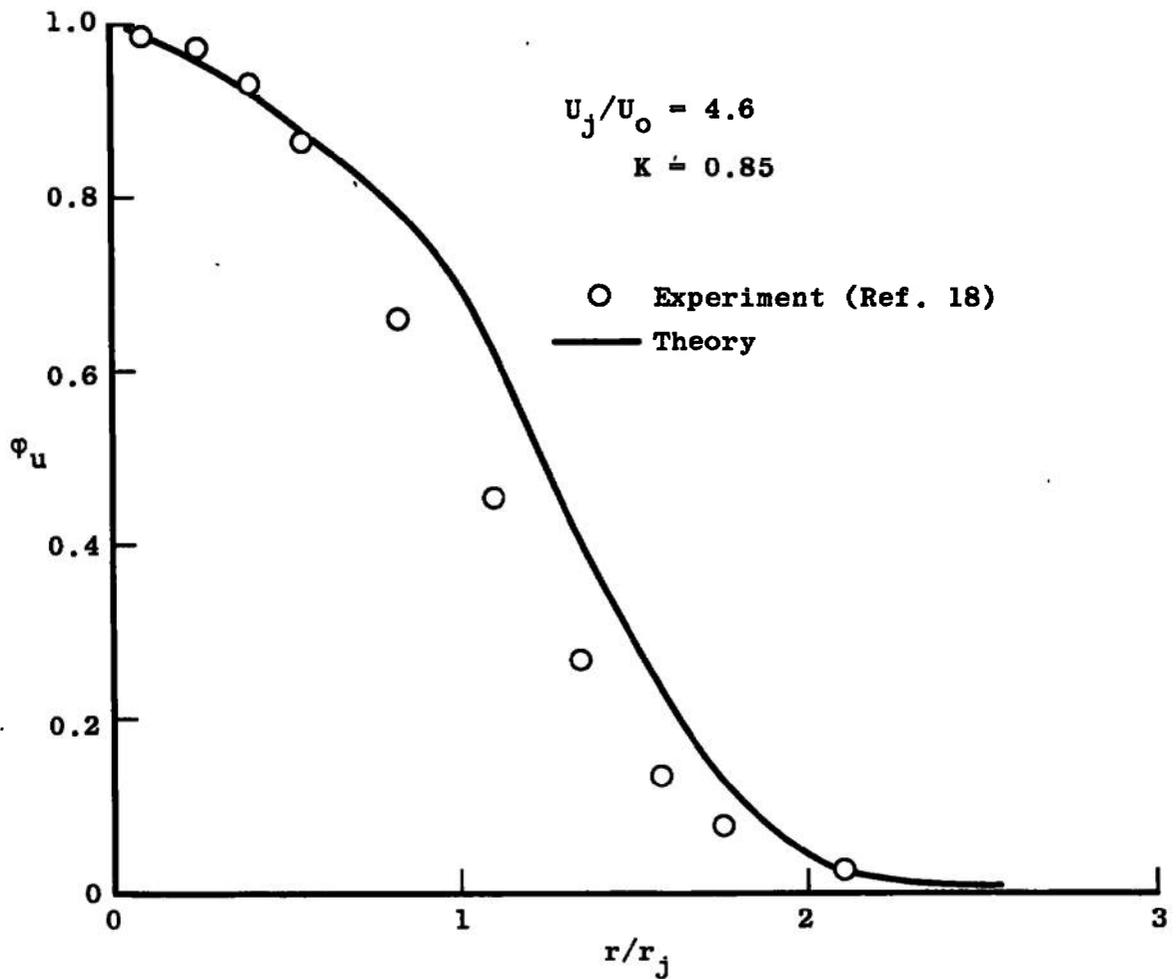
b.   x/D = 4.53

Figure 11.   (continued)
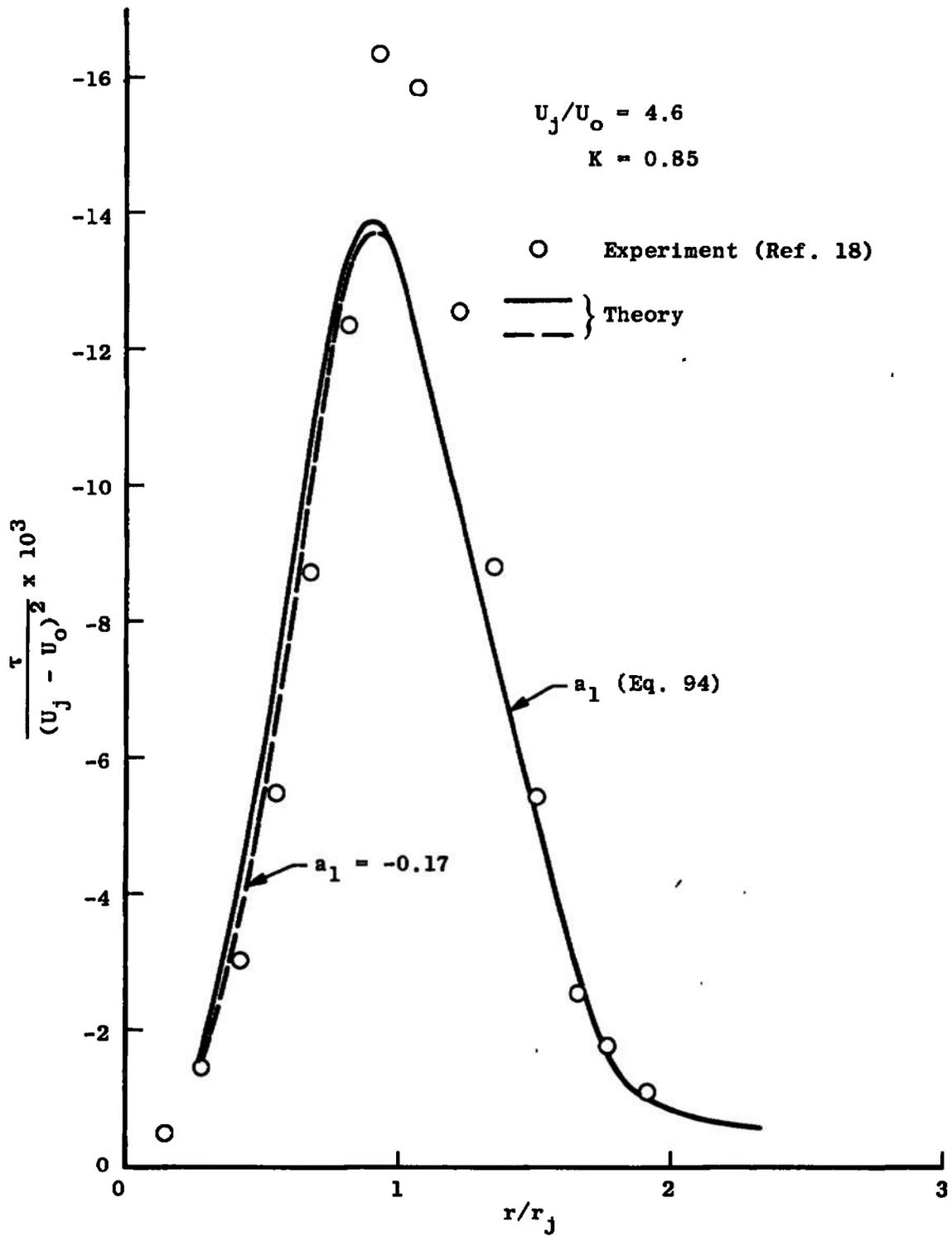
a. $x/D = 3.57$

Figure 12. First-regime turbulent shear stress profiles for hydrogen-air mixing.
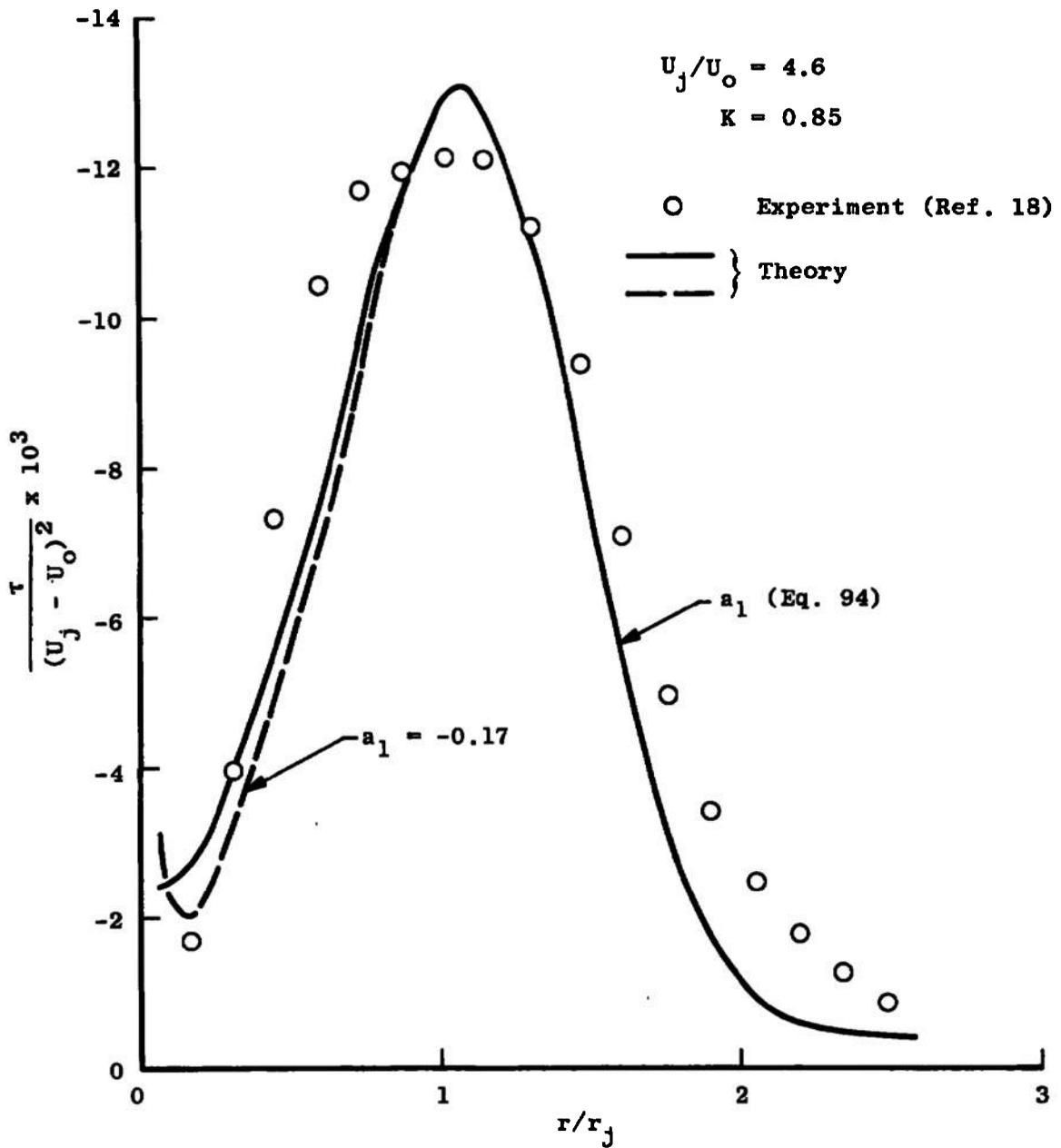
b.  x/D = 4.53

Figure 12.  (continued)

finite. Therefore, Equation 94 is used as an estimated approximation for the parameter $a_1$. The two functions used for $a_1$ do not produce enough difference in the velocity profiles to be seen on a plot of this scale. The shear stress profile near the inner boundary of the mixing zone is more sensitive to $a_1$, particularly near the end of the first regime. The proper shape of the shear stress profile is not produced by the analytical calculations near the inner boundary for either function of $a_1$ although the function given by Equation 94 seems to give the better result. The problem is not unexpected since the transition region is being approached. Also, a better function for $a_1$ is probably needed since Equation 94 is only an estimated approximation. Some improvement in the diffusion function may also be needed. Producing the proper shear profile at the end of the first regime is necessary before the marching integration can proceed from the first into the second regime. An improper shear stress profile at the end of the first regime will result in an improper decay of the centerline velocity in the second regime. With the exception of the problem just discussed, the velocity and shear stress profiles calculated agree reasonably well with the experimental data.

## Second Regime

Second-regime calculations are presented for the flow conditions given in Table I, page 68. First, the sensitivity of the calculations of velocity and shear stress profiles

and the centerline velocity and the peak shear stress decay to the parameters $a_1$, K, and $f_2$ is presented in Figures 13 through 29. The experimental data for the hydrogen-air velocity ratio of 4.4 is used for comparison and the initial profiles were selected at 6.5 jet diameters from the initial plane of mixing. For the best values of $a_1$, K, and $f_2$ found in these calculations, calculations for the other velocity ratio cases will be presented.

The empirical expression for $a_1$ used in the calculations is the analytical function given by Equation 74 in Chapter IV. The peak level of $a_1$ is established by $|a_1|_m$ and lateral position of this peak is established by $Z_o$. The sensitivity of $a_1$ on the calculations will be observed by choosing different constant values of $|a_1|_m$ and $Z_o$ while K and $f_2$ are held constant. In Figures 13 and 14 the center-line velocity and peak shear stress decay is observed to be relatively insensitive to $|a_1|_m$. The choice of $|a_1|_m$ equal to 0.17 based on Sami's data (discussed in Chapter IV) for an incompressible air jet is quite satisfactory in this case. This implies that the relation between the turbulent shear stress and turbulent kinetic energy is essentially independent of density effects, because there is an order-of-magnitude variation in density across the two coaxial flows. From this result perhaps one also could expect little or no compressibility effects on the function $a_1$. Bradshaw and Ferriss [25] found this to be the case for the adiabatic compressible boundary layer.
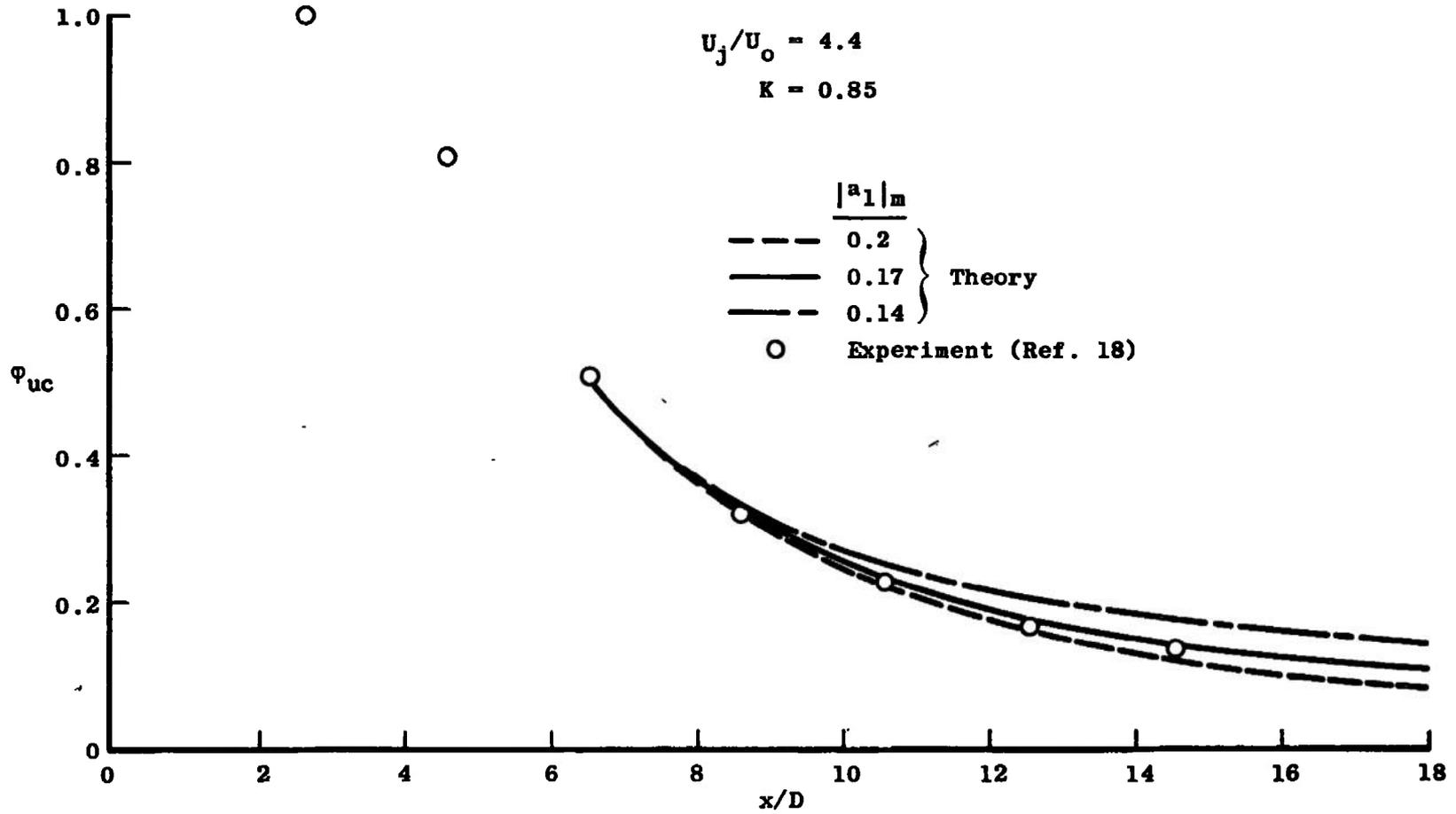
Figure 13. Effect of $|a_1|_m$ on the centerline velocity.
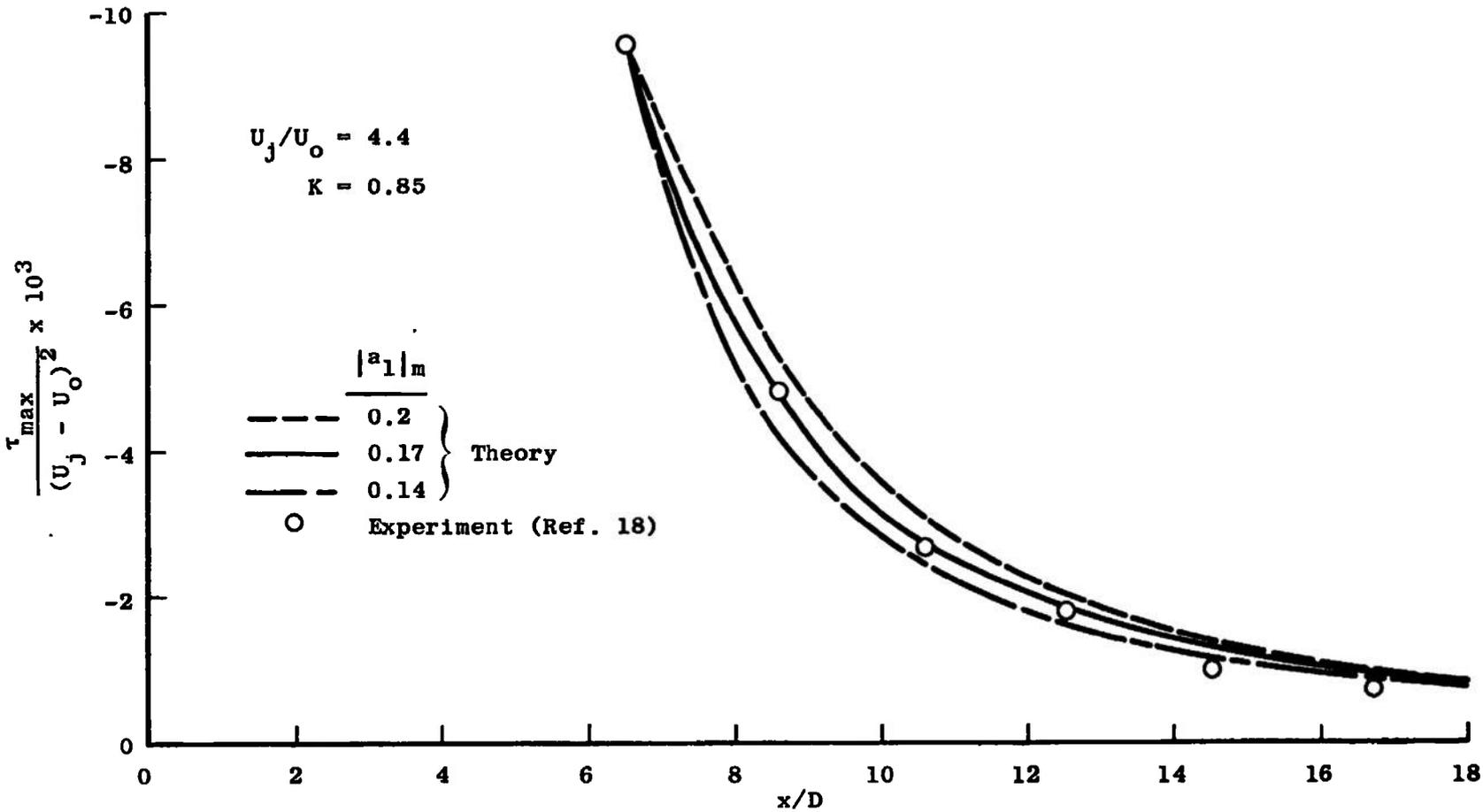
Figure 14.  Effect of $|a_1|_m$ on the peak shear stress.
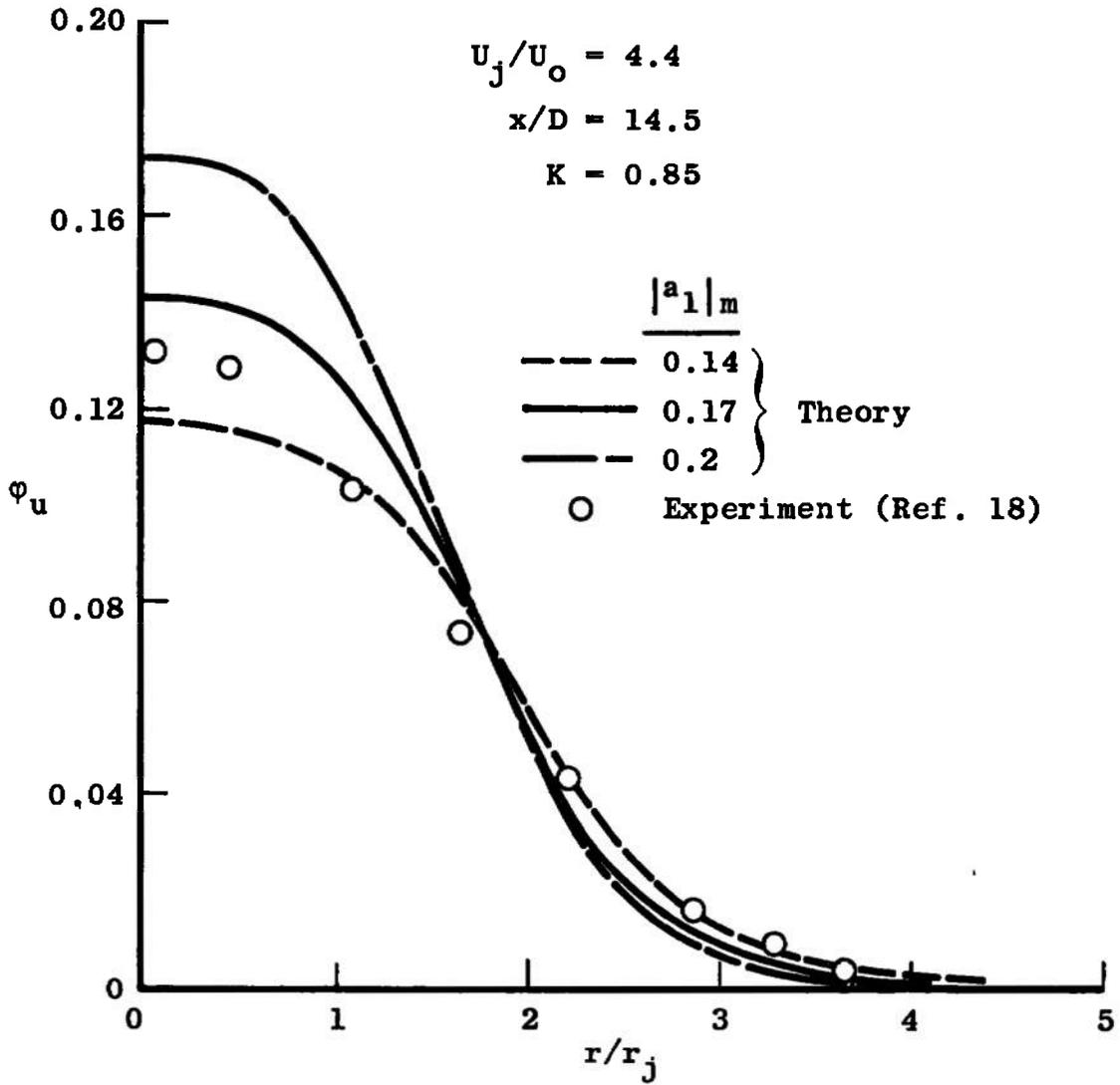
Figure 15.   Effect of $|a_1|_m$ on the velocity profile.
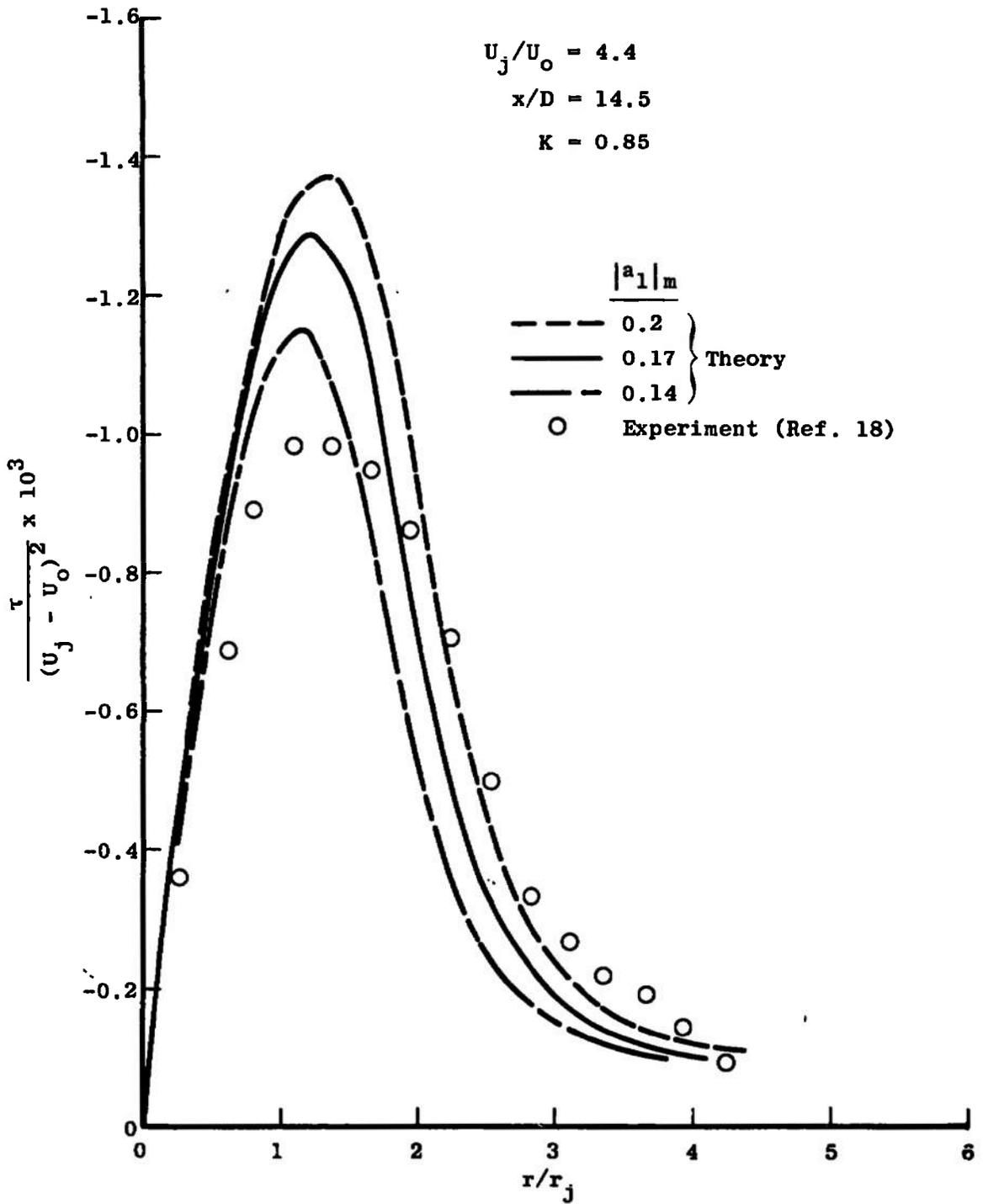
Figure 16.   Effect of $|a_1|_m$ on the shear stress profile.
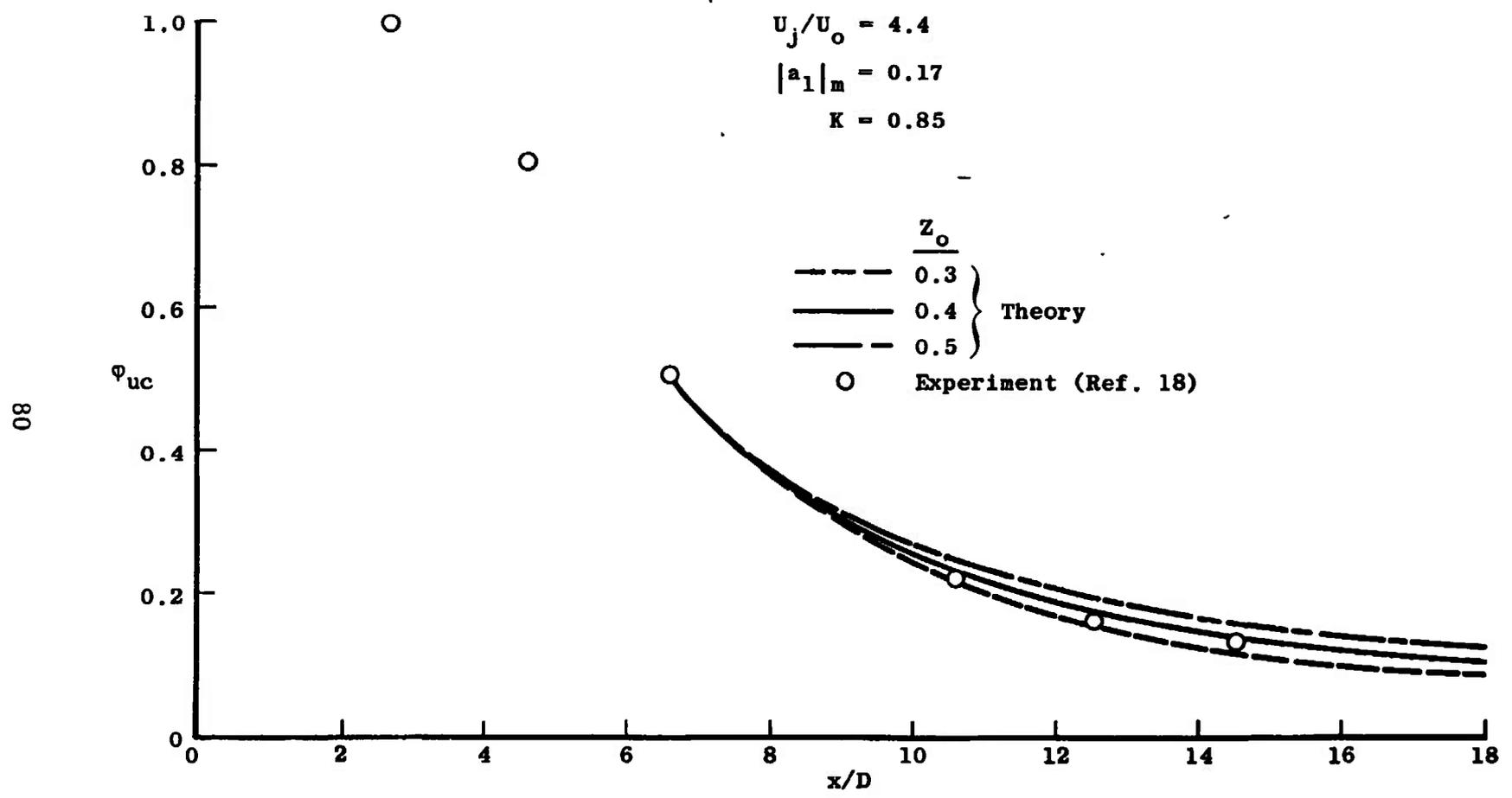
Figure 17.   Effect of $Z_o$ on the centerline velocity.
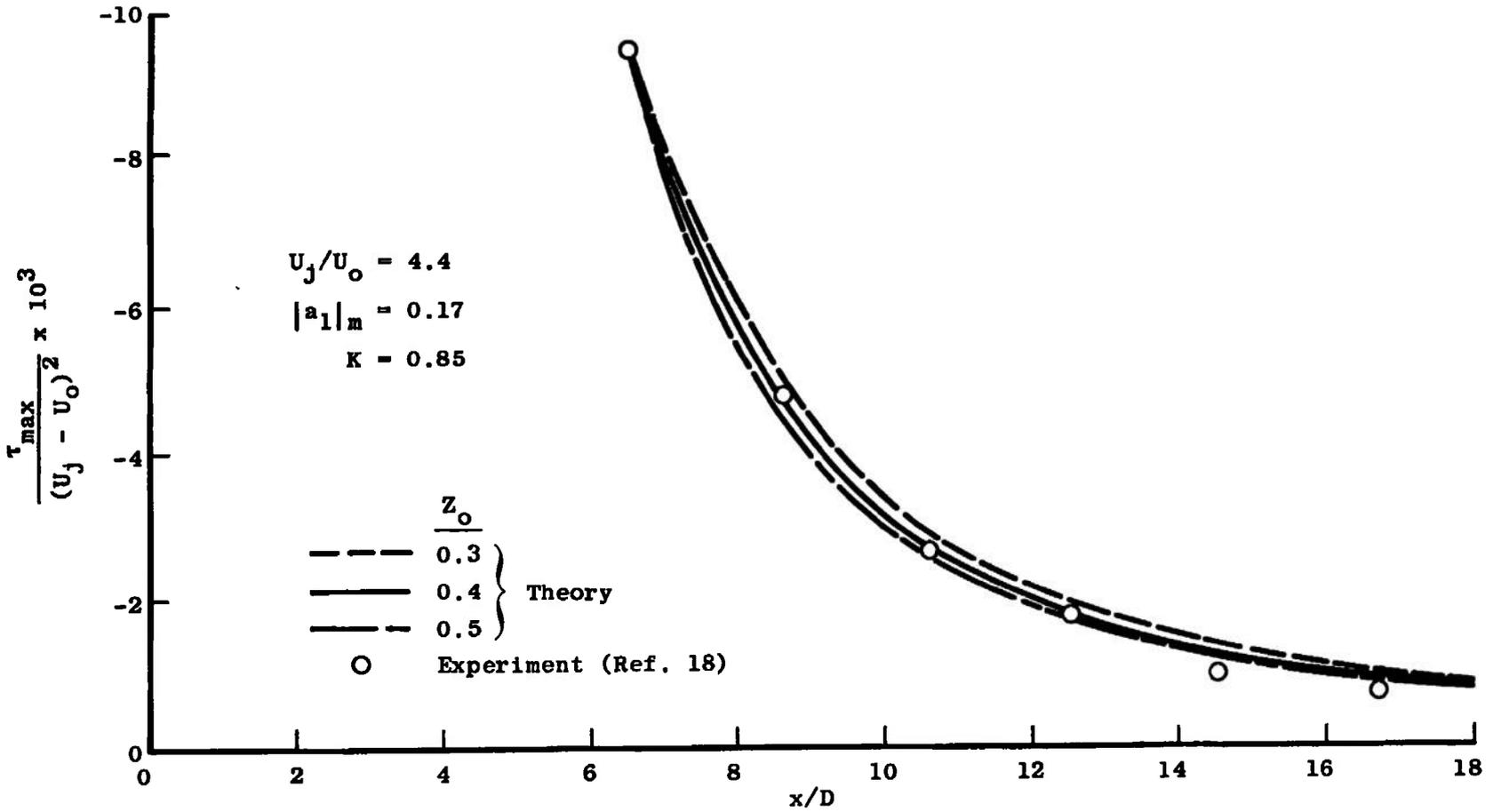
Figure 18. Effect of $Z_o$ on the peak shear stress.
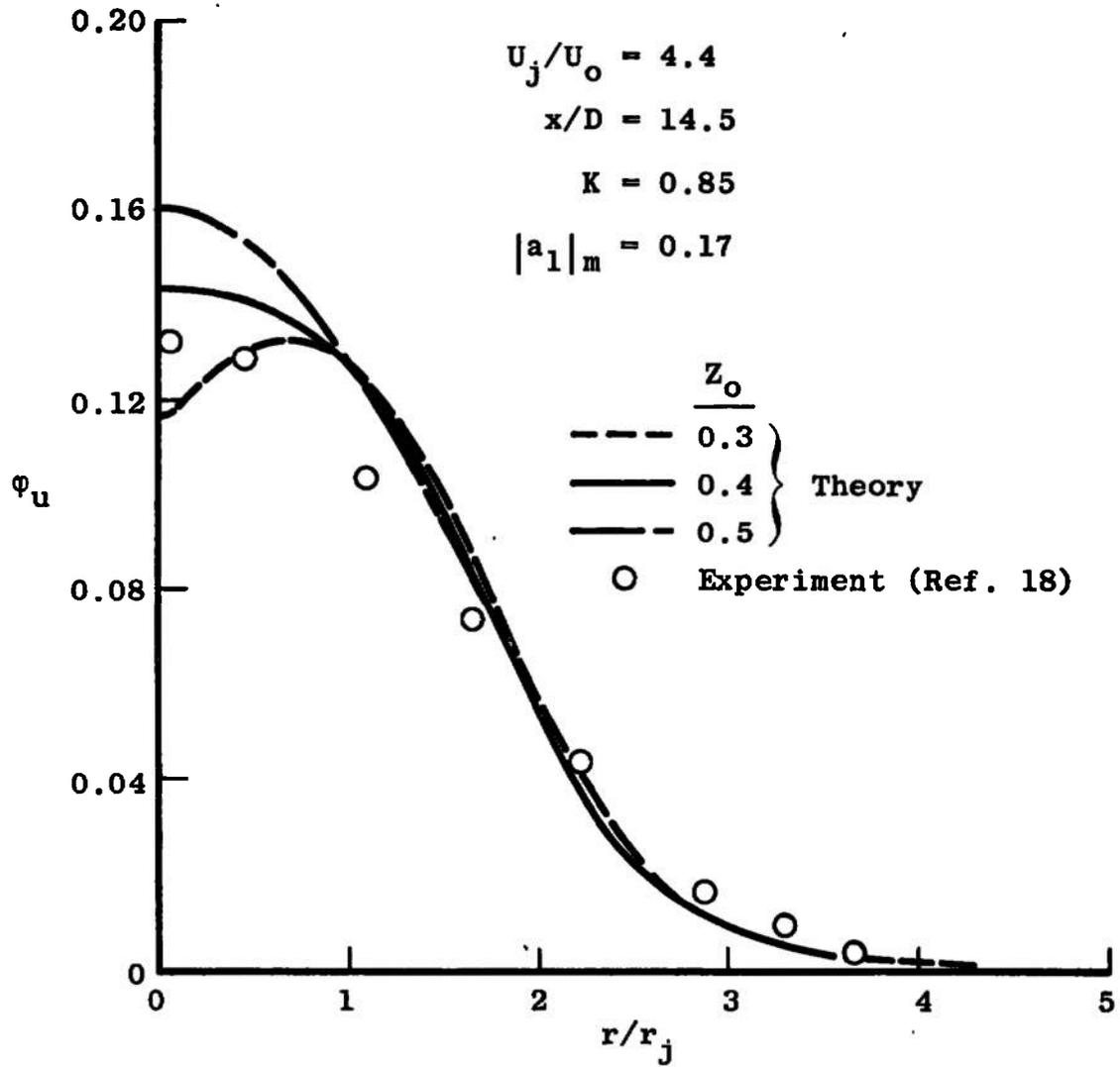
Figure 19.   Effect of $Z_o$ on the velocity profile.
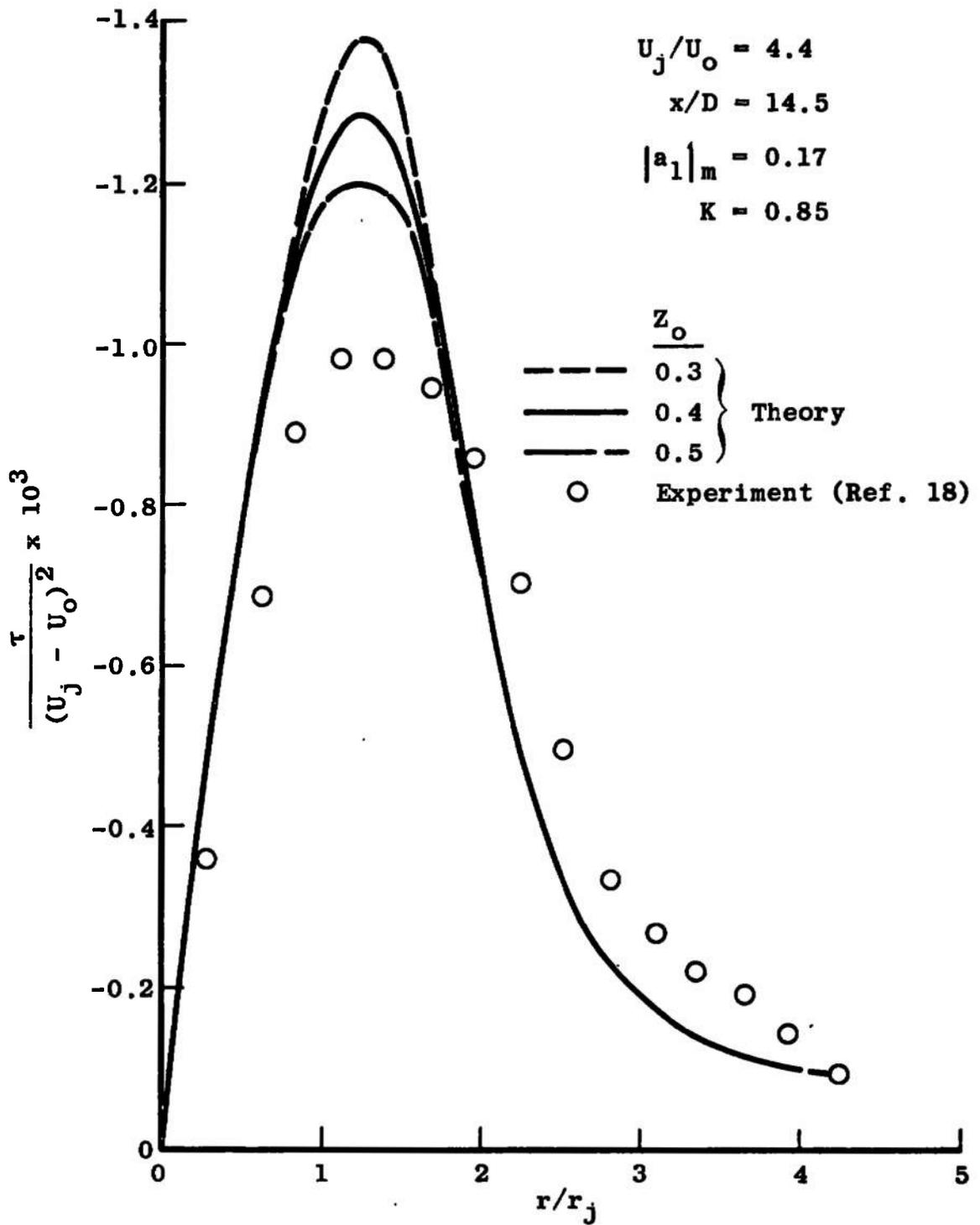
Figure 20. Effect of $Z_o$ on the shear stress profile.
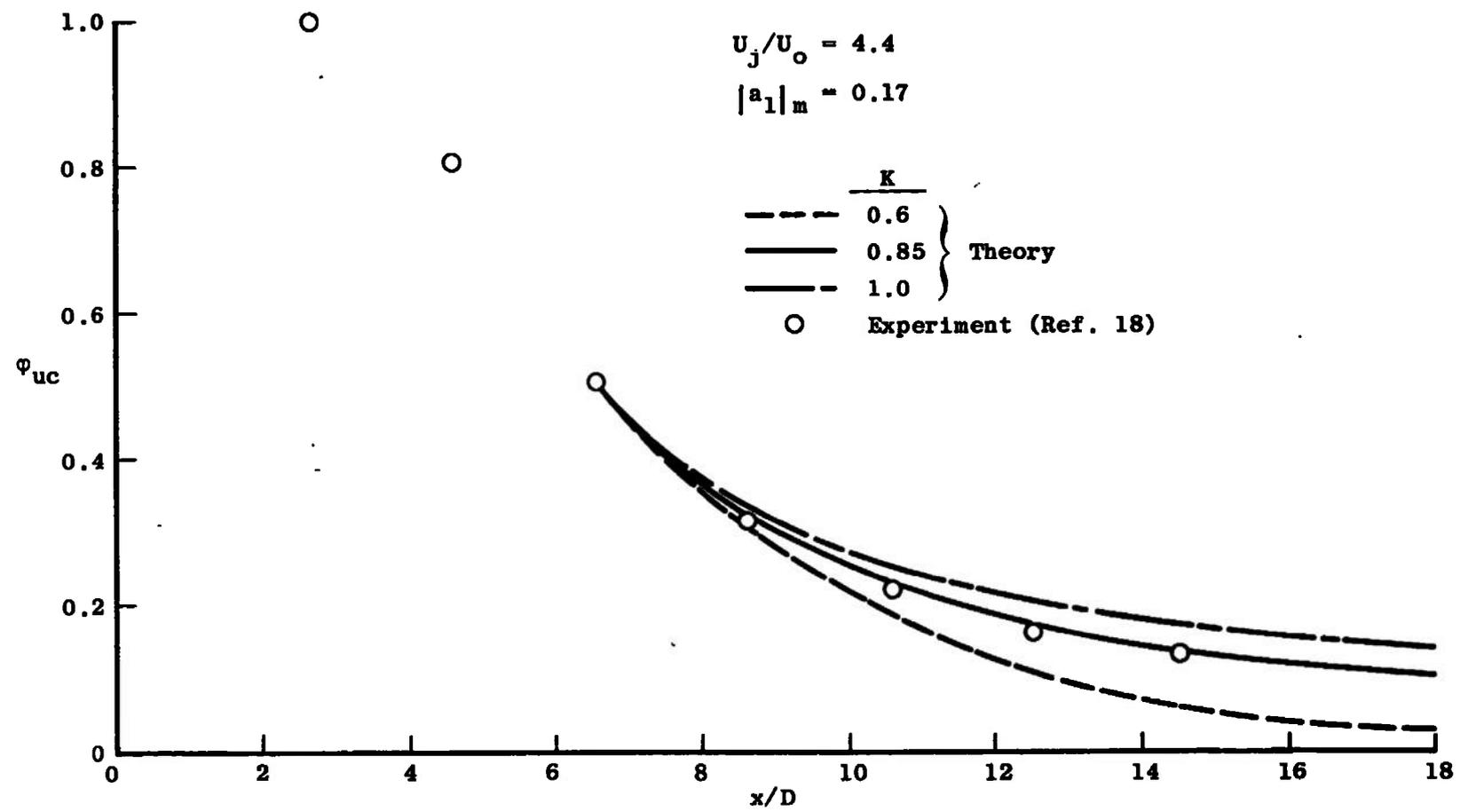
Figure 21.   Effect of K on the centerline velocity.
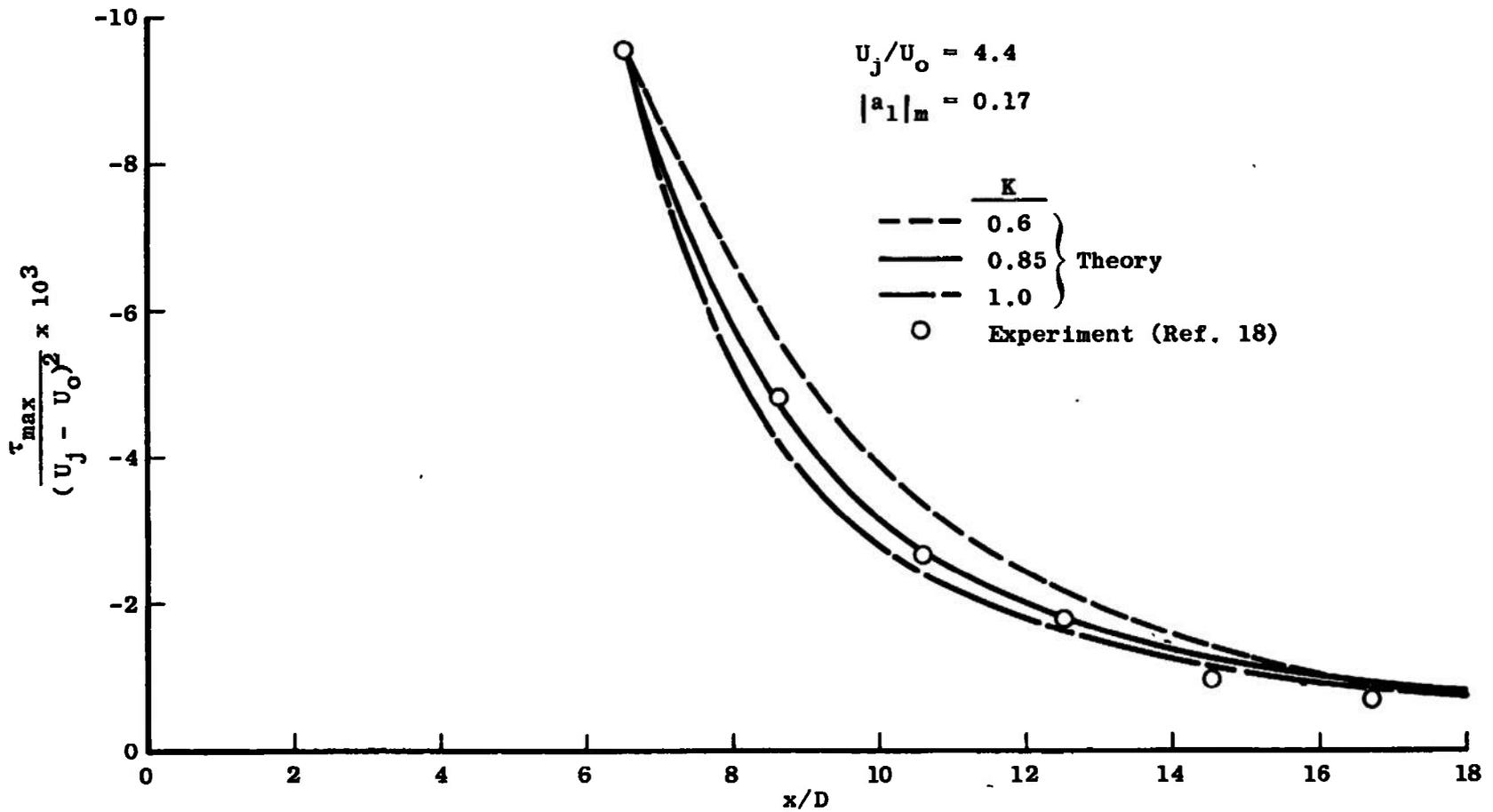
Figure 22. Effect of K on the peak shear stress.

$U_j/U_o = 4.4$

$x/D = 14.5$

$|a_1|_m = 0.17$

| | K | |
|---|---|---|
| - - - - | 0.6 | |
| ——— | 0.85 | Theory |
| — — | 1.0 | |
| ○ | | Experiment (Ref. 18) |

$\varphi_u$

$r/r_j$
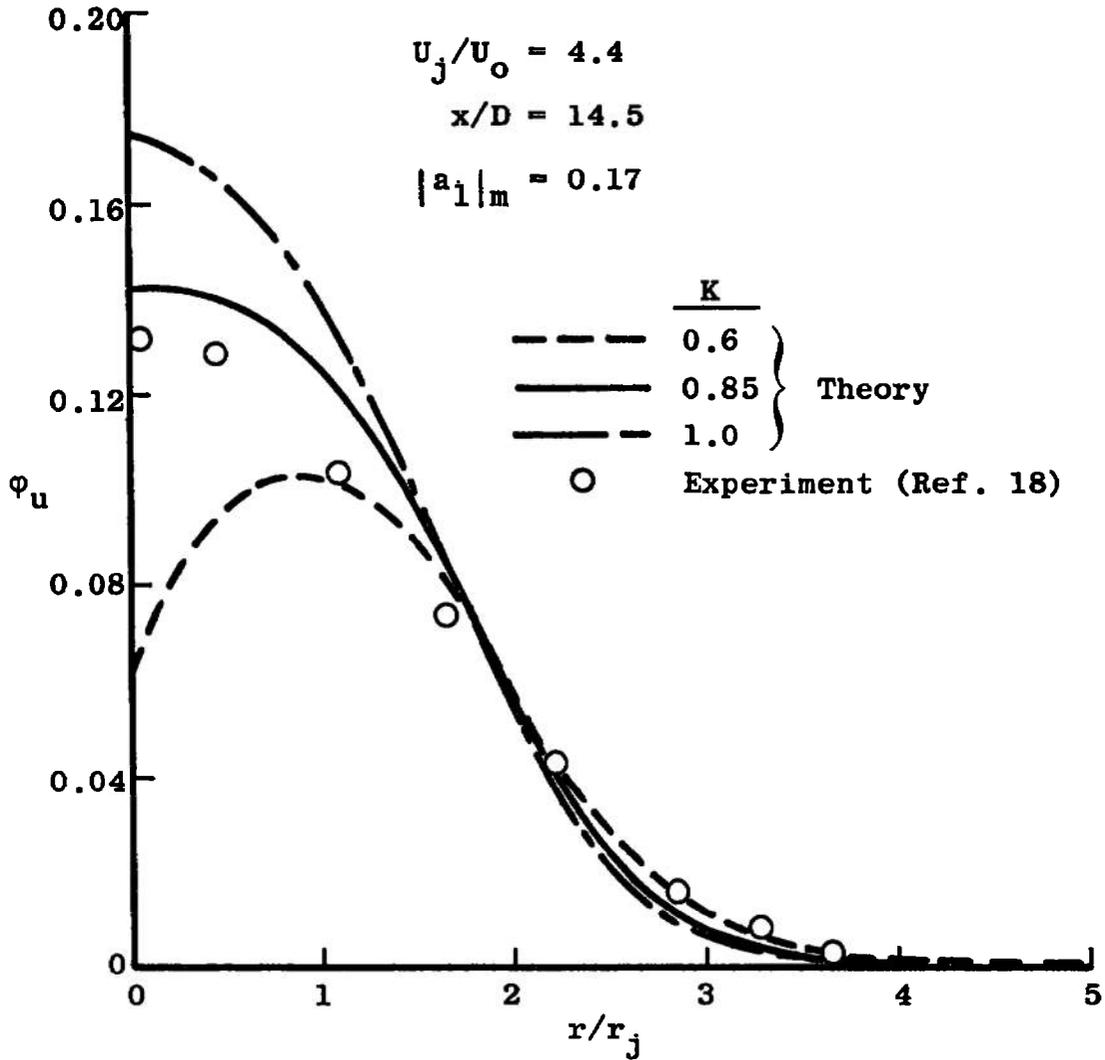
Figure 23. Effect of K on the velocity profile.
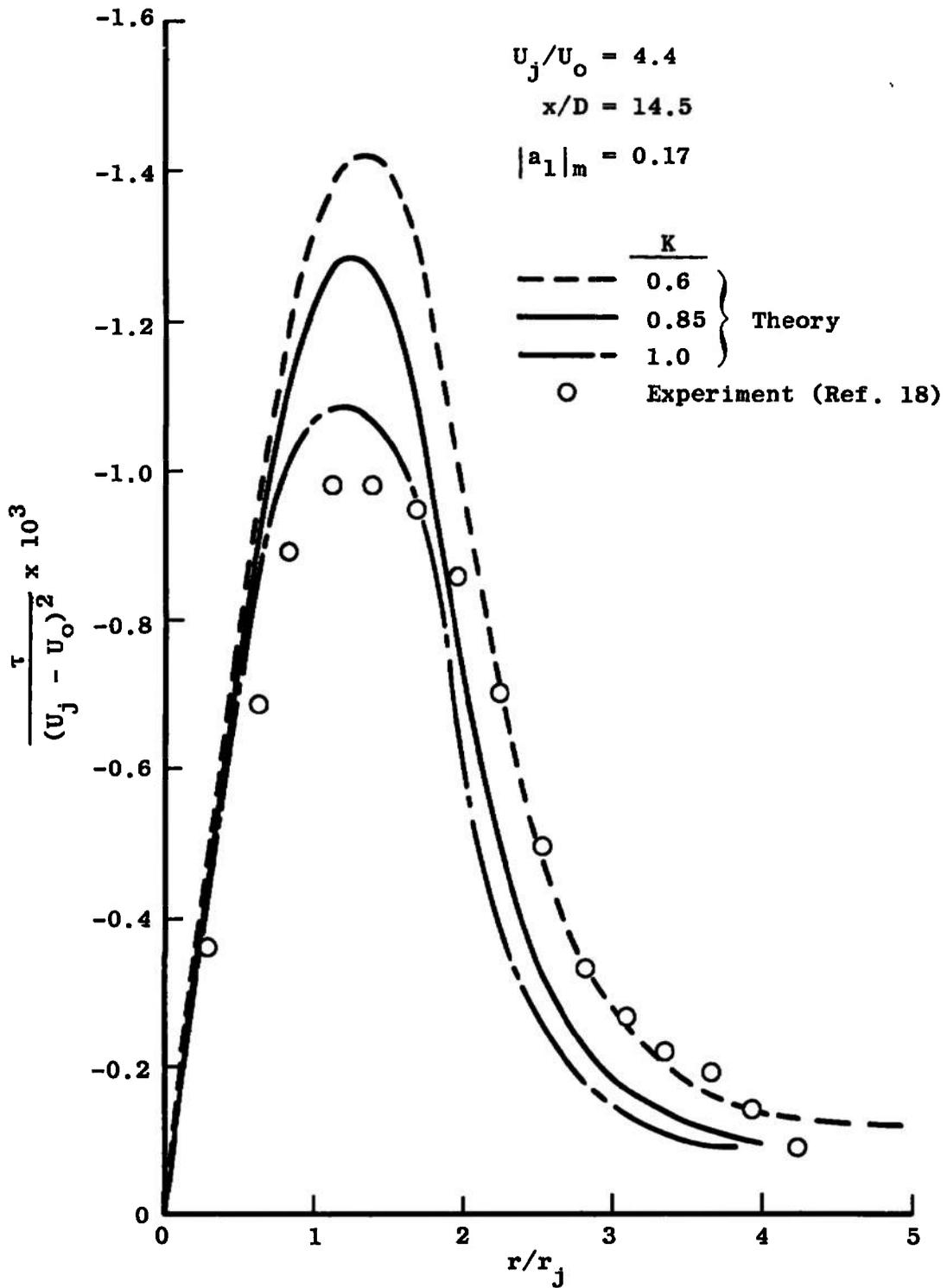
Figure 24.   Effect of K on the shear stress profile.
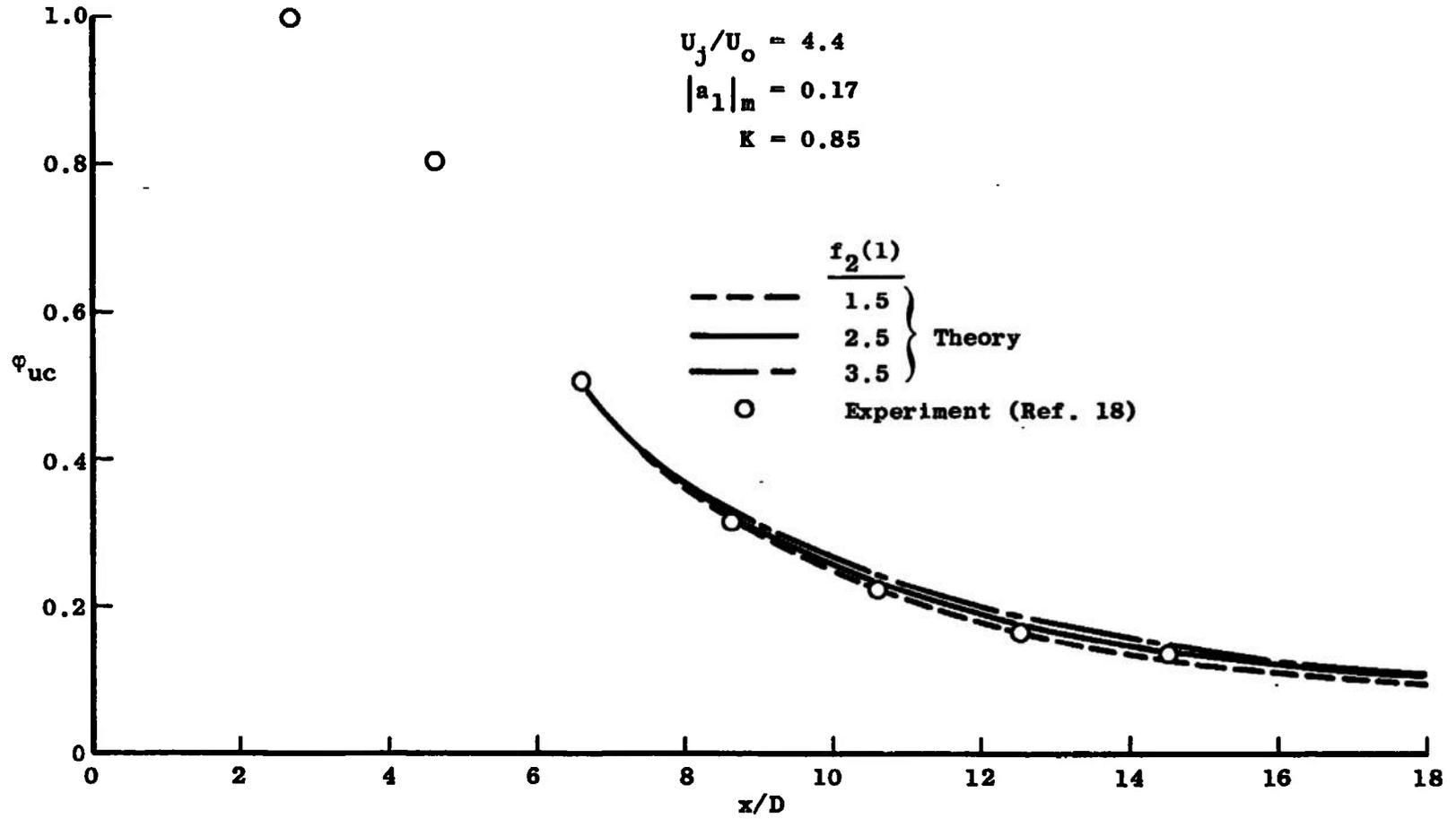
Figure 25. Effect of $f_2$ on the centerline velocity.
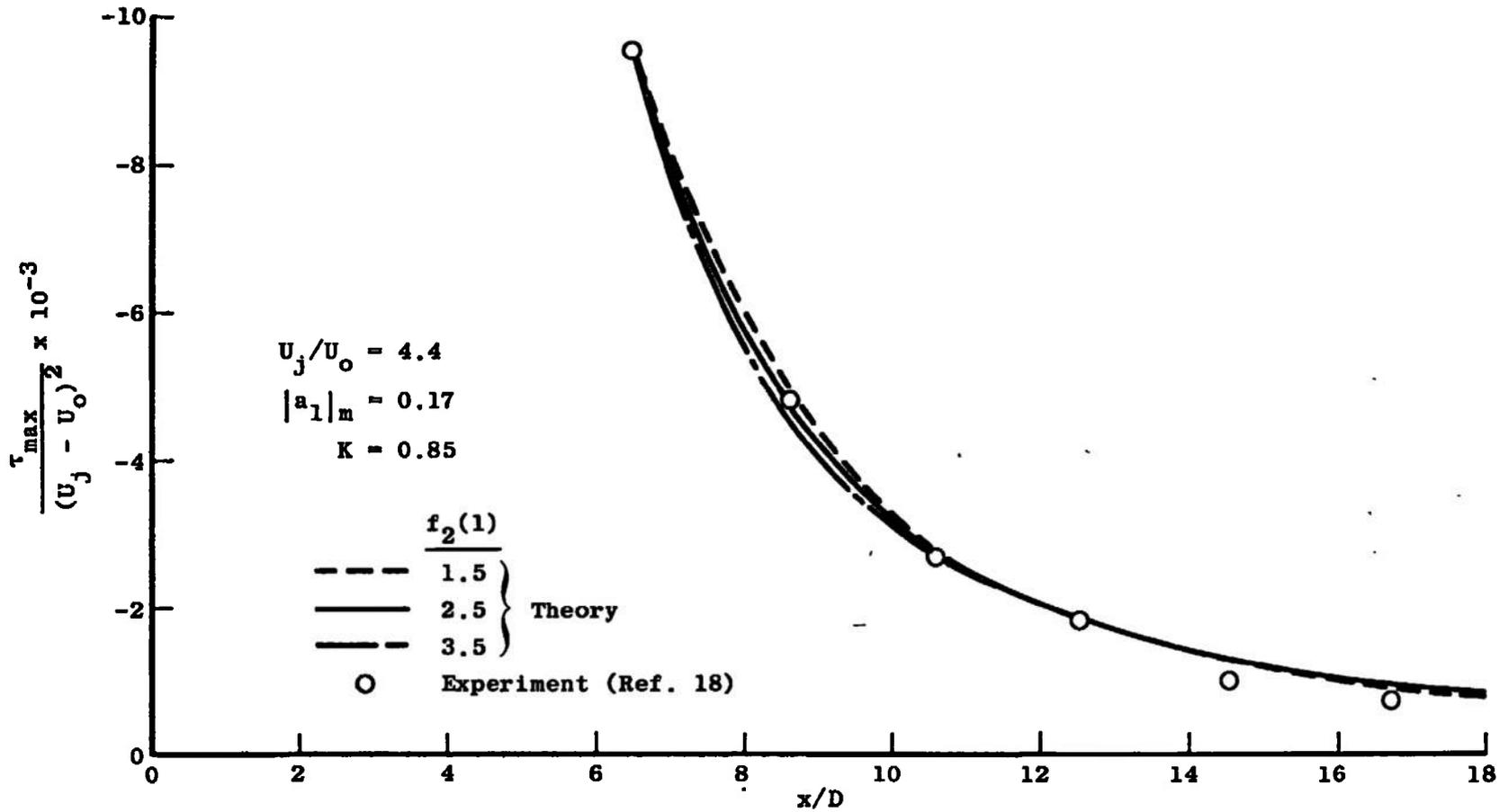
Figure 26.  Effect of $f_2$ on the peak shear stress.
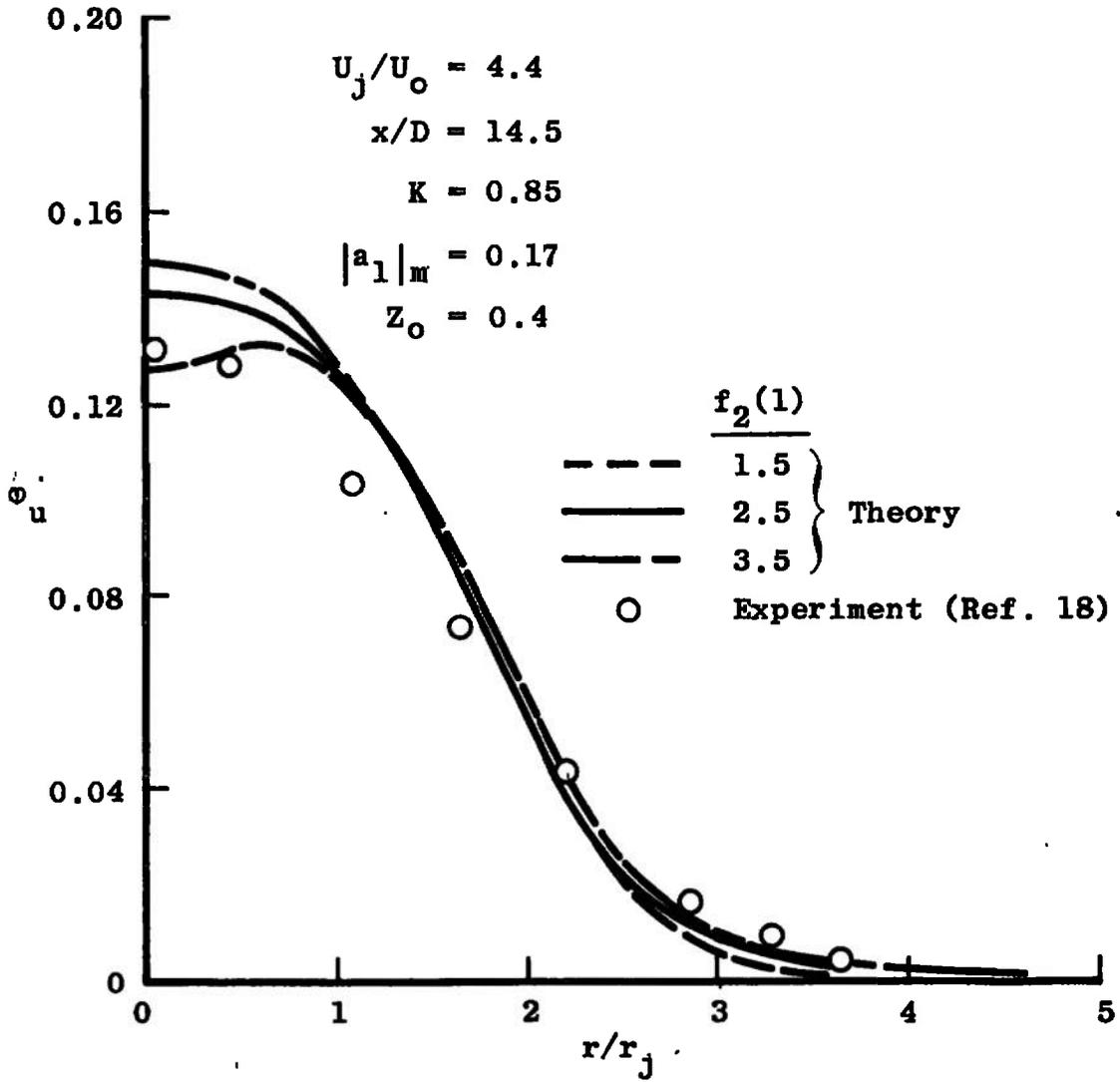
Figure 27. Effect of $f_2$ on the velocity profile.
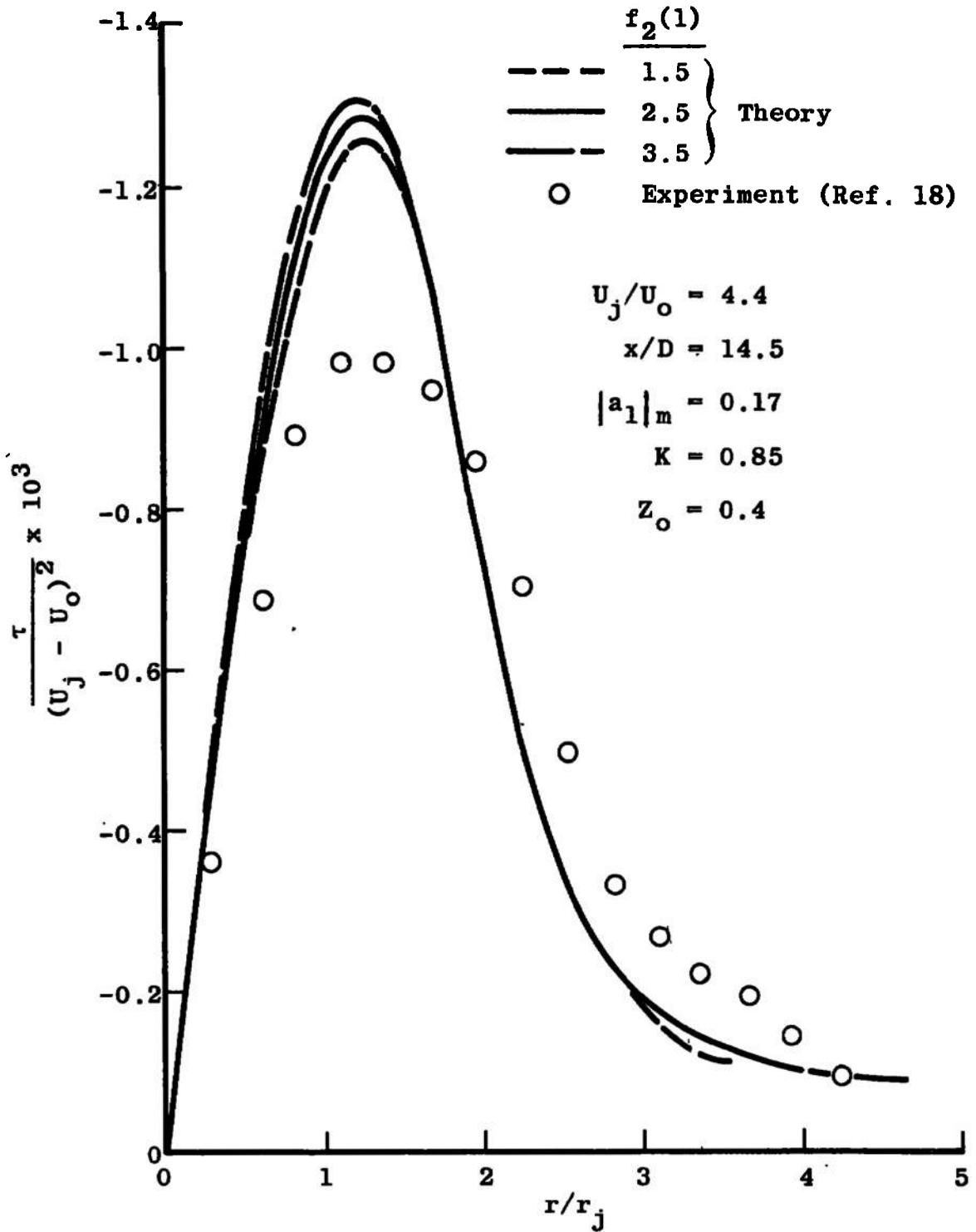
Figure 28. Effect of $f_2$ on the shear stress profile.
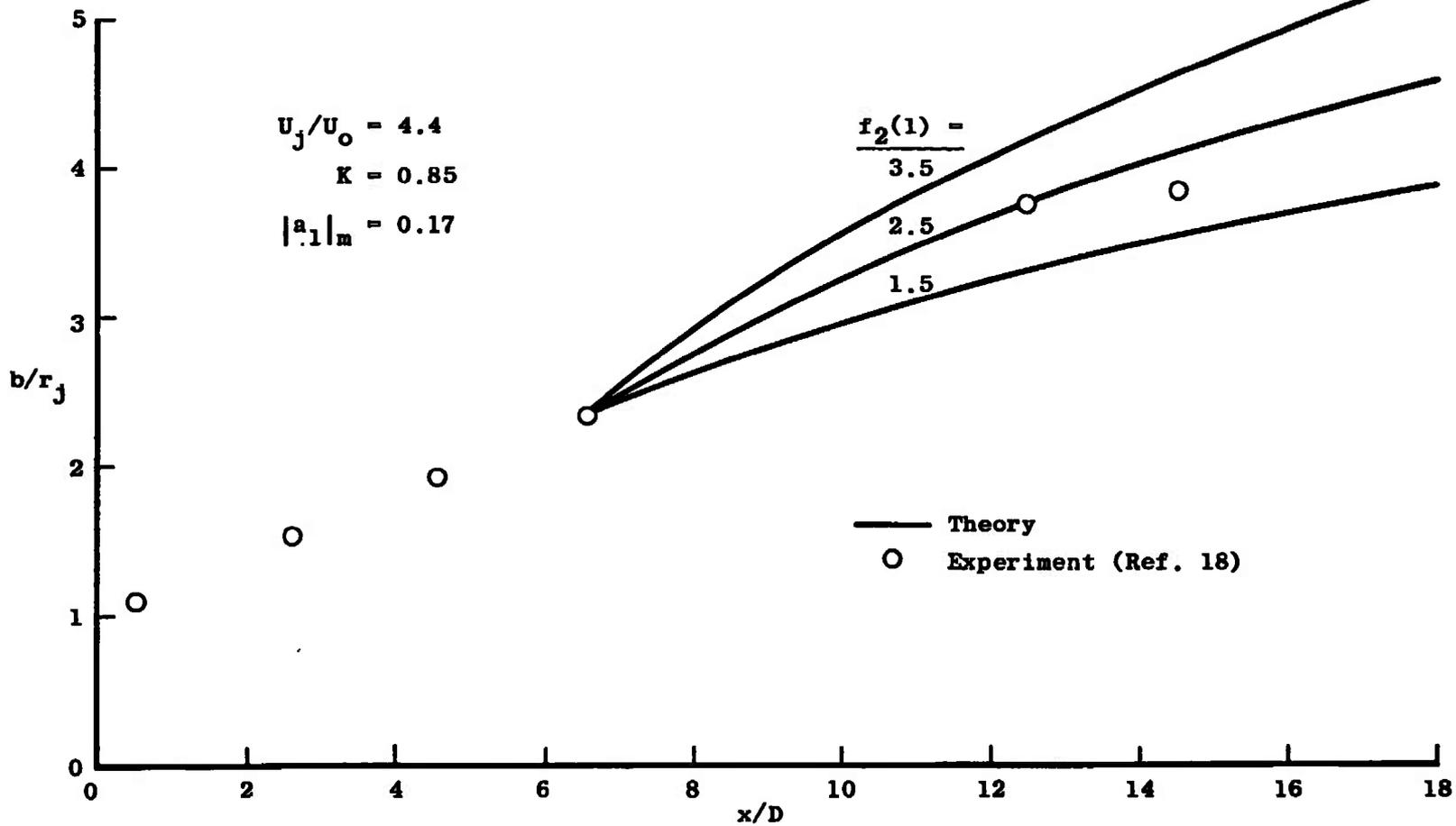
Figure 29.   Effect of $f_2$ on the mixing-boundary growth rate.

The effect of $|a_1|_m$ on the velocity and shear stress profiles at an x/D of 14.5 is shown in Figures 15 and 16, respectively. The velocity profile is more sensitive to $|a_1|_m$ near the centerline, whereas the shear stress is more sensitive away from the centerline. At this axial position the peak shear stress is overpredicted about 30 per cent. No conclusive reason can be given for this although there are several factors which could be the cause. For instance, the theory incorporates the assumption of unity Prandtl and Schmidt number which Chriss [18] has observed to be less than unity for hydrogen-air mixing.) A slight axial variation of $|a_1|_m$ , $Z_o$, and K may be closer to physical reality.

The sensitivity of the centerline velocity and peak shear stress calculations to $Z_o$ is shown in Figures 17 and 18. A relatively weak effect is observed here but as seen in Figure 19 the velocity profile shape is strongly affected near the centerline. In fact, a value of 0.3 for $Z_o$ is physically incorrect for this case since the peak velocity should occur on the centerline. Obviously, an improper balance and rate of change of convection, diffusion, pro- duction, and dissipation of turbulent kinetic energy near the centerline is created in the calculations. A reasonable velocity profile shape is produced with $Z_o$ equal to 0.4 or 0.5. The better choice is 0.4. This gives reasonable agreement with experimental data and also fits Sami's data very well in the use of Equation 74. This value of $Z_o$ is not always the best choice for other mixing flows as will be

shown later in this chapter. In Figure 19, page 82, variation in $Z_o$ is observed to produce a slight change in the peak shear stress.

Analytical calculations are made for K equal to 0.6, 0.85, and 1.0. The effect of this variation in K on the centerline velocity and peak shear stress decay is shown in Figures 21 and 22, pages 84 and 85. The effect on the lateral velocity and shear stress profiles is shown in Figures 23 and 24, pages 86 and 87. Too much velocity decay is produced near the centerline for K equal to 0.6 as observed in Figure 23. As with $a_1$, the velocity profile is most sensitive to K near the centerline. Of the three cases calculated K equal to 0.85 gives the best agreement with experimental data. This is a somewhat higher value of K than that calculated from Sami's experimental data and presented in Figure 5, page 47.

The diffusion velocity function, $f_2$, was formulated following the approach of Bradshaw et al. [24] as discussed in Chapter IV. The sensitivity of the velocity and turbulent shear stress calculations is obtained by scaling $f_2$ by three different constants such that $f_2(1)$ equals 1.5, 2.5, or 3.5. The effect on the centerline velocity and peak shear stress decay is shown in Figures 25 and 26, pages 88 and 89. The velocity profile is mainly affected near the centerline as observed in Figure 27, page 90. This centerline effect is caused by the influence that the diffusion velocity has on the mixing-layer thickness which in turn

affects $a_1$ and the energy dissipation term. Both of the latter parameters are functions of the mixing-layer thickness. In Figure 28, page 91, the shear stress profile is observed to be only slightly sensitive to a variation of $f_2$. A good measure of the proper choice of the diffusion function near the mixing boundary is its prediction of the mixing-layer growth rate. The results of these calculations are shown in Figure 29, page 92. Two conclusions are drawn. First, the form of the diffusion function chosen (Equation 81) predicts the mixing-layer growth rate very well. Secondly, the function, $f_2$, proposed in Figure 4, page 44, produces reasonable velocity and shear stress profiles. For $f_2(1)$ equal to 3.5 the mixing boundary spreads too fast and for $f_2(1)$ equal to 1.5 it spreads too slowly.

To summarize the sensitivity calculations analytical and experimental velocity profiles are presented in Figure 30 at 8.6, 12.5, and 14.5 jet diameters from the initial plane of mixing. The choices of $|a_1|_m$, $Z_o$, $K$, and $f_2(1)$ are 0.17, 0.4, 0.85, and 2.5, respectively. Although the calculated velocity profiles agree well with the experimental data with this combination of values of the parameters, other better combinations of these parameters may exist. A detailed experimental study of the turbulent structure is needed to better assess these parameters.

Calculations on the remaining velocity ratio cases listed in Table I, page 68, are presented in Figures 31 through 33. The "best" values of $|a_1|_m$, $K$, and $f_2$ found
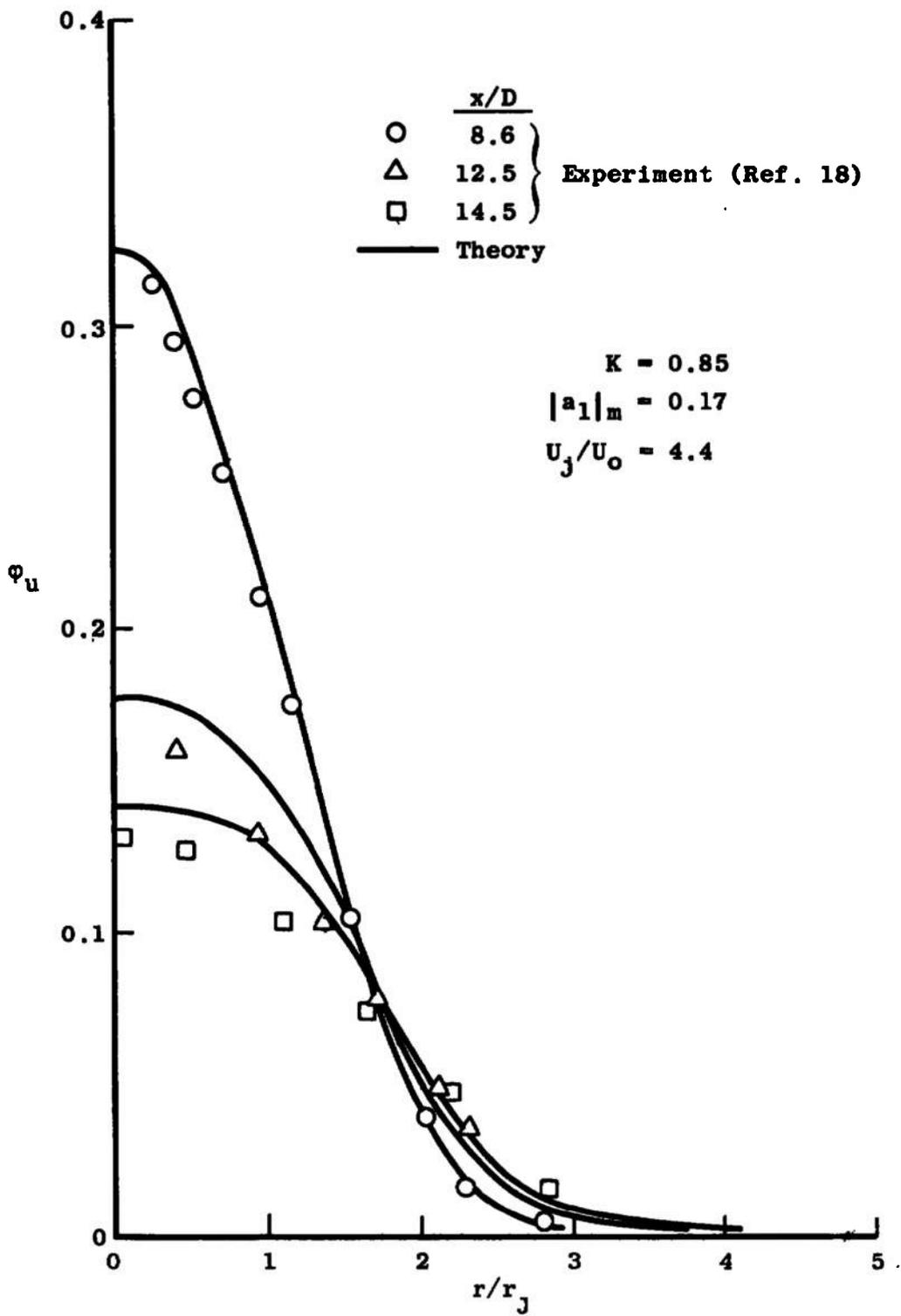
Figure 30. Lateral velocity profiles.
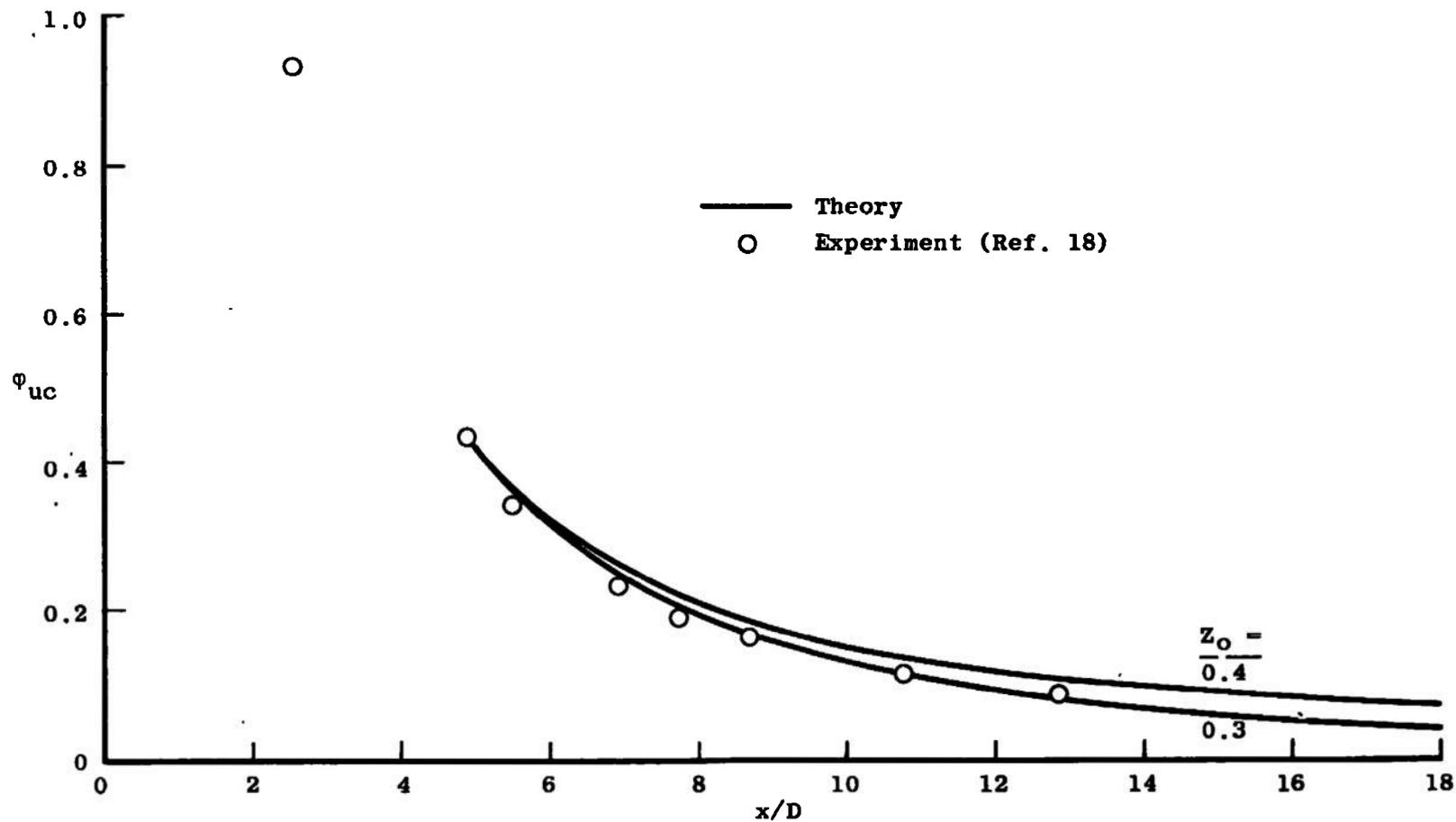
a. Centerline Velocity Decay

Figure 31. Velocity and turbulent shear stress calculations for $U_j/U_o$ = 2.4.
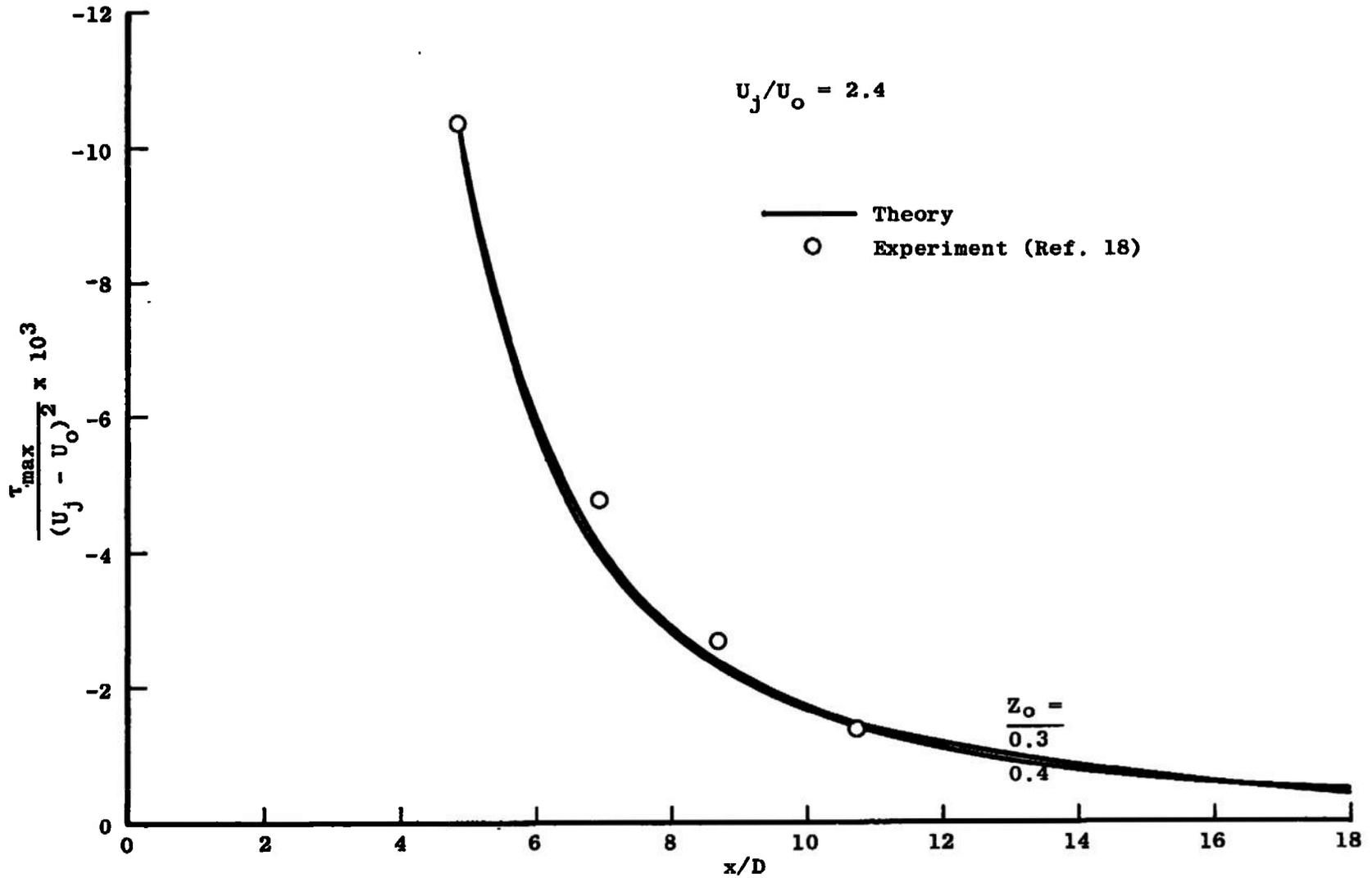
b.  Peak Turbulent Shear Stress Decay
Figure 31.  (continued)
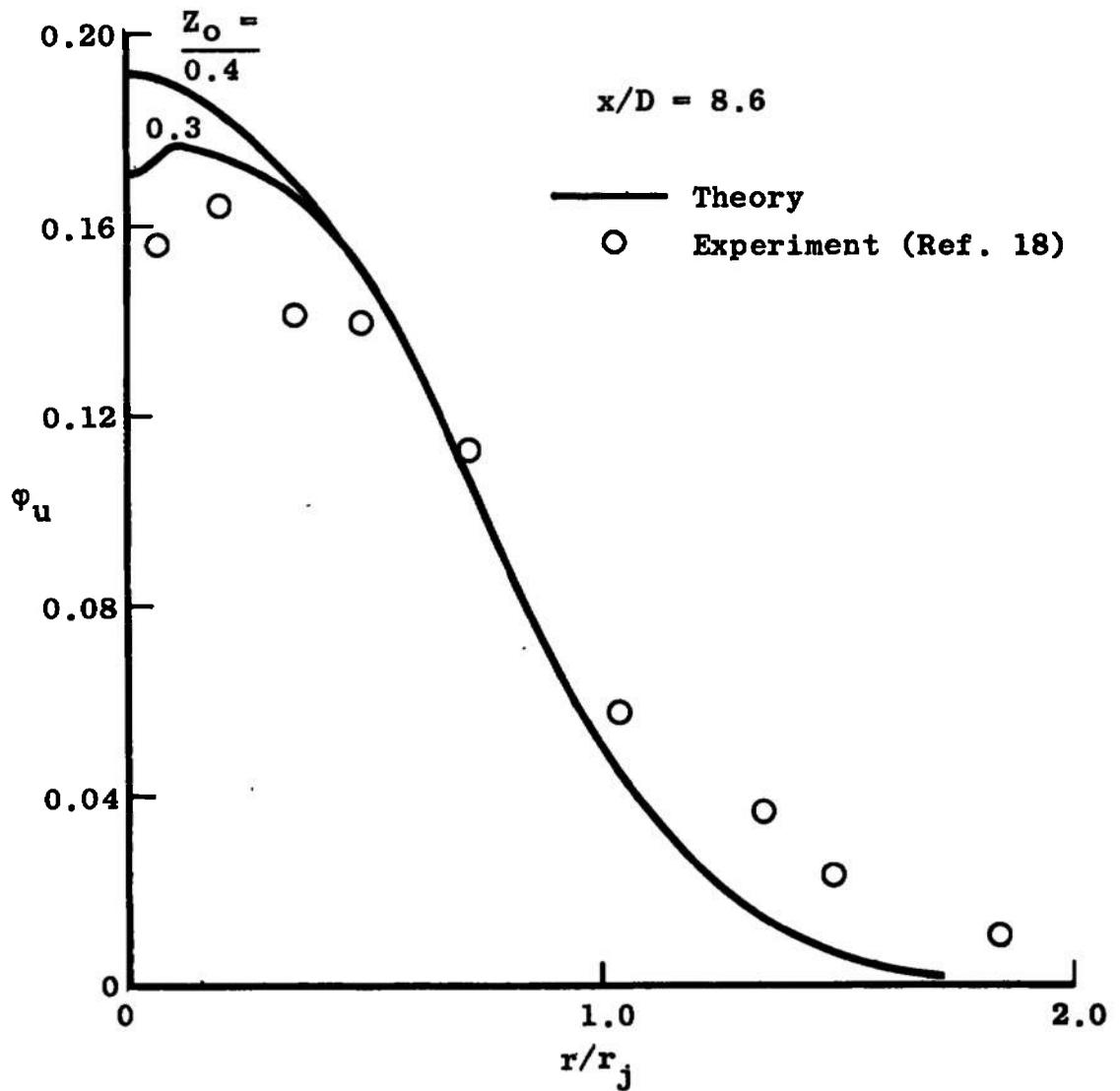
c.   Velocity Profile

Figure 31.   (continued)
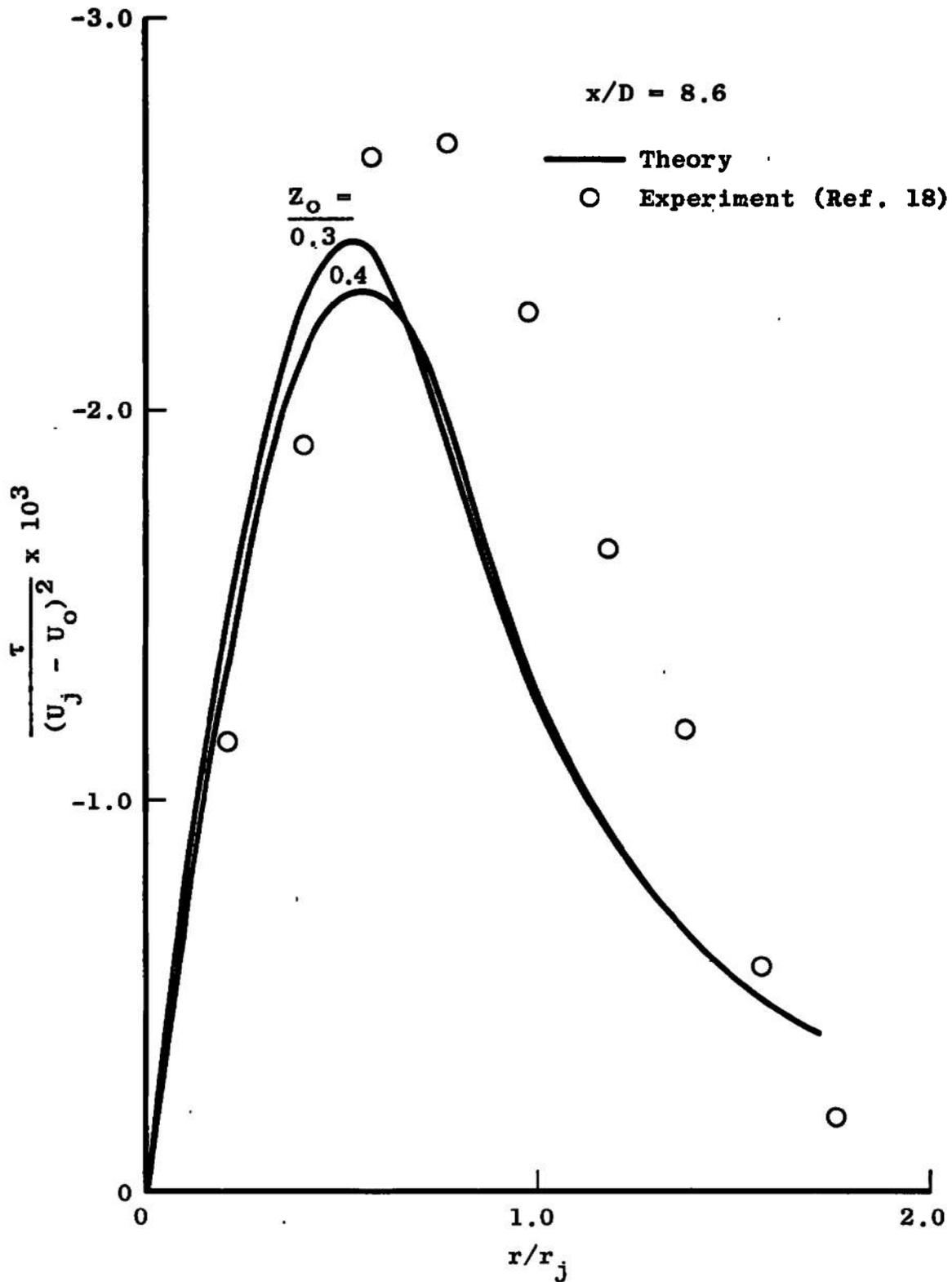
d.  Turbulent Shear Stress Profile
Figure 31.   (continued)
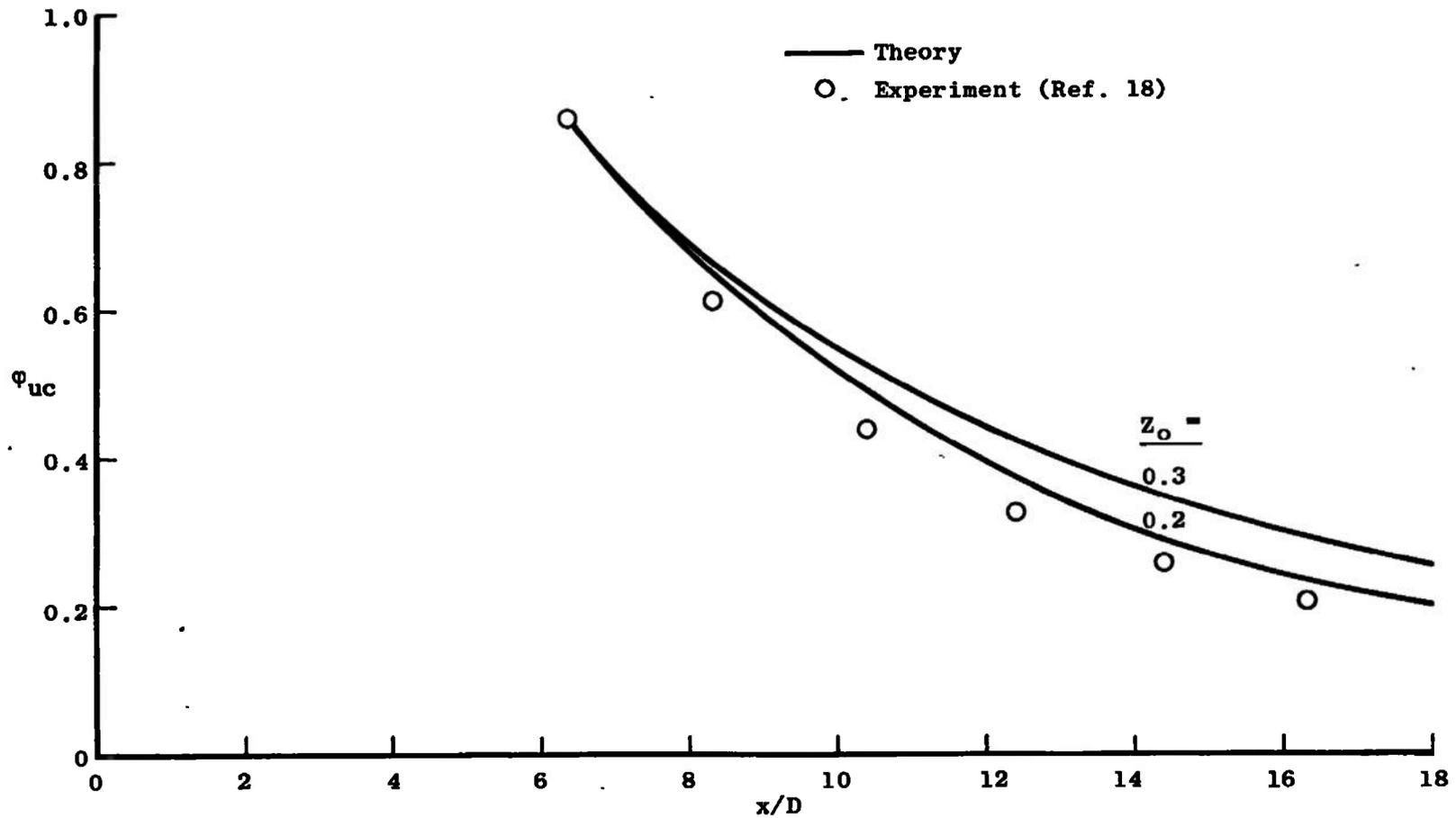
a. Centerline Velocity Decay

Figure 32. Velocity and turbulent shear stress calculations for $U_j/U_o = 4.6$.
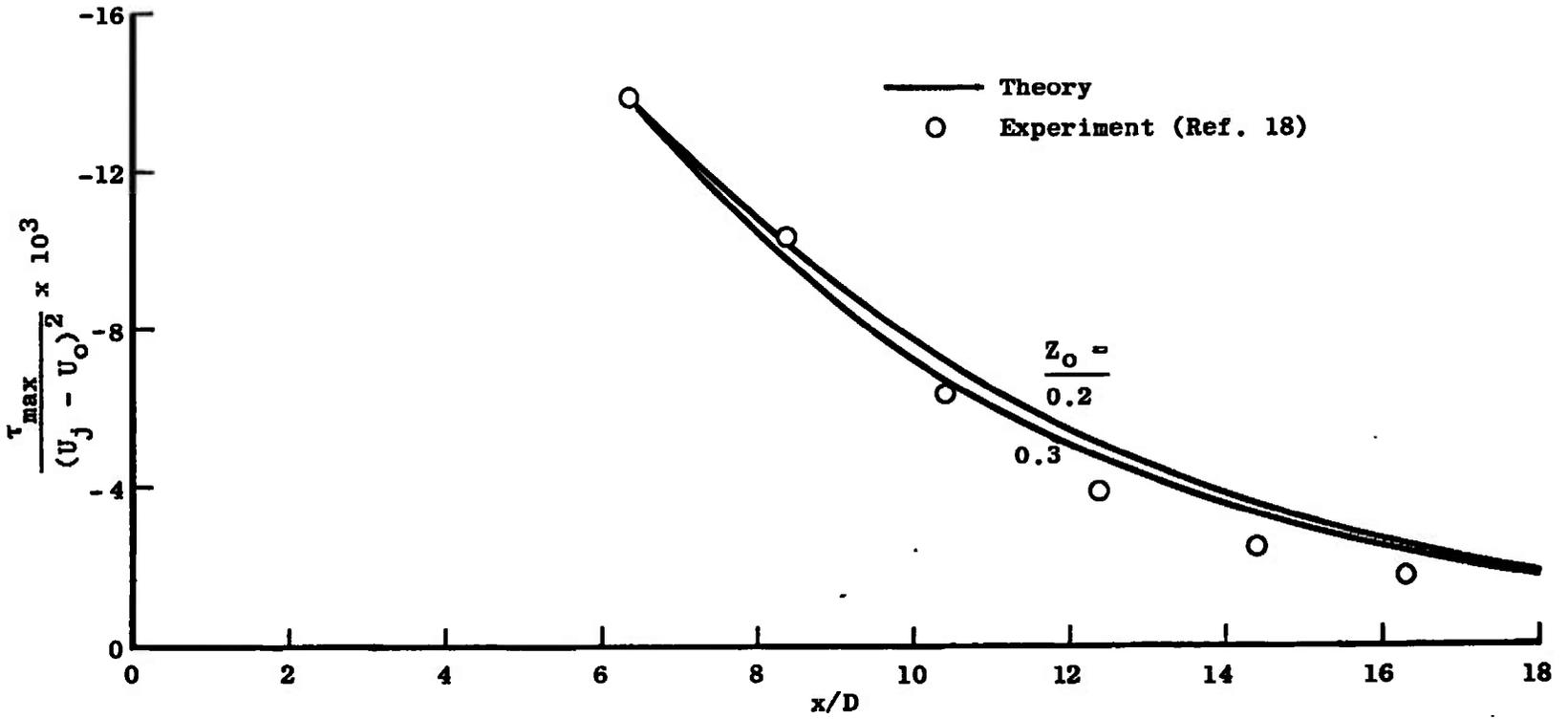
b.  Peak Turbulent Shear Stress Decay

Figure 32.  (continued)
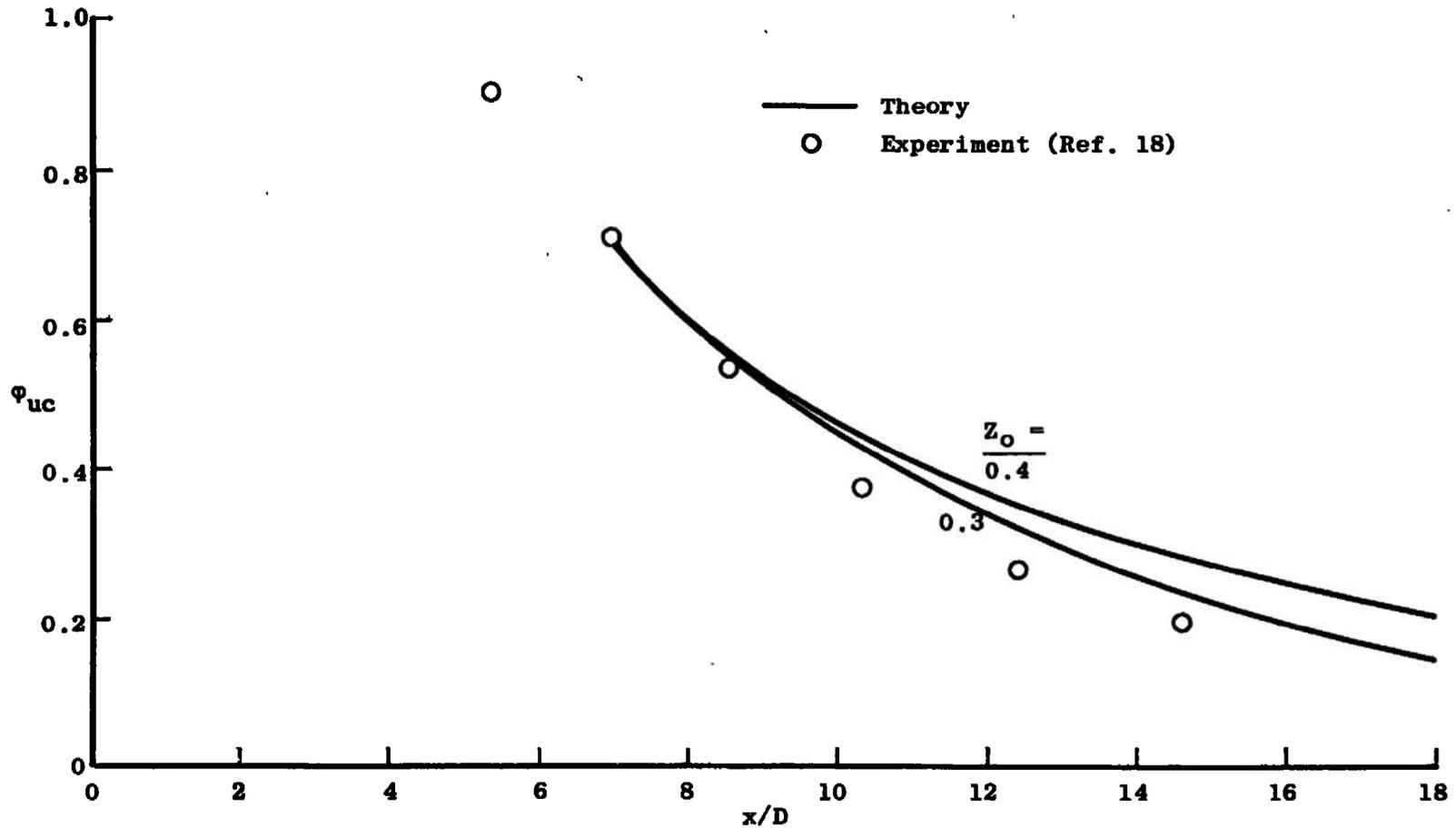
a.   Centerline Velocity Decay

Figure 33.   Velocity and turbulent shear stress calculations for
$U_j/U_o = 6.3$.
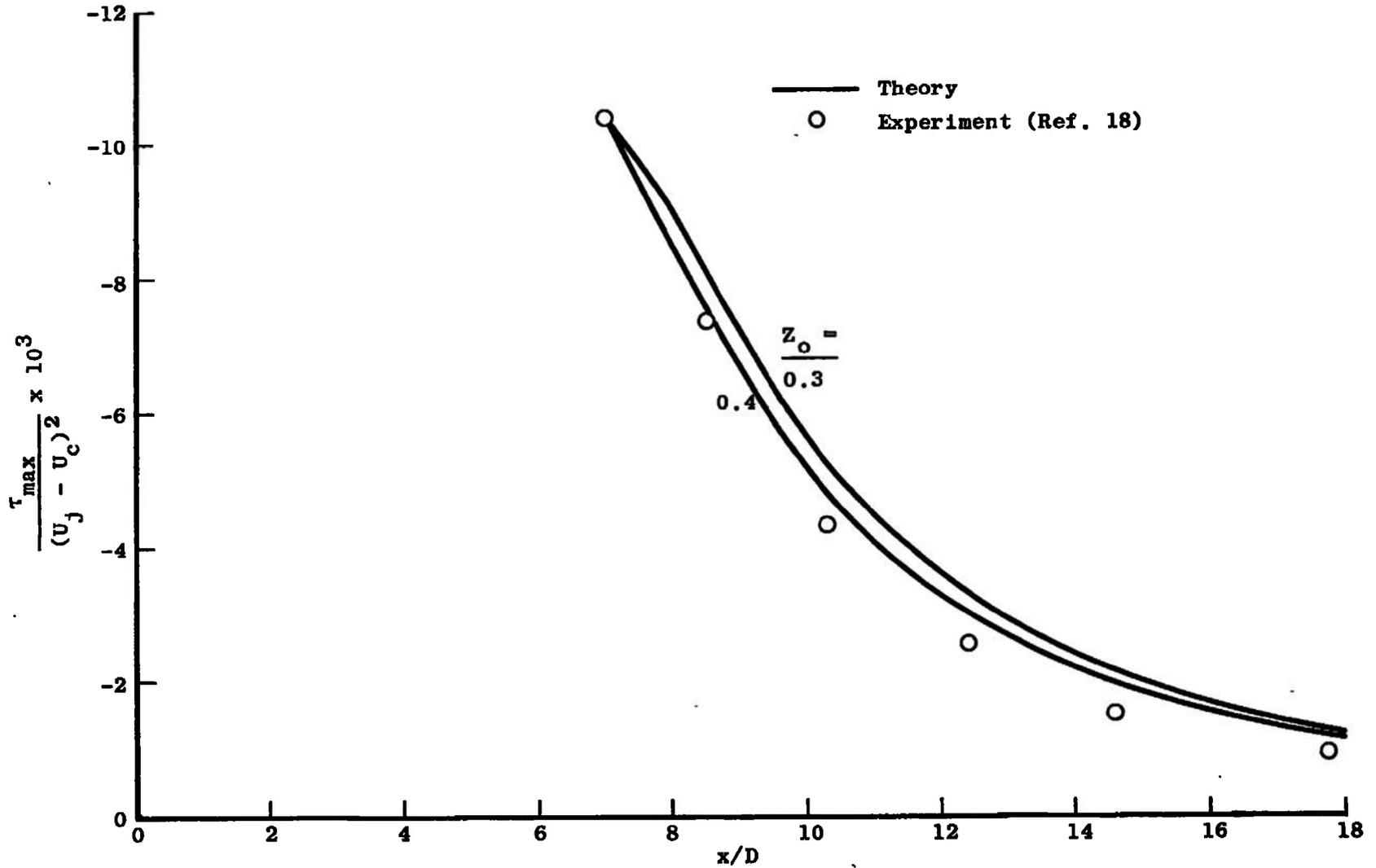
b. Peak Turbulent Shear Stress Decay

Figure 33. (continued)

in the sensitivity calculations are used and are found to work very well. However, the best value for $Z_0$ is observed to vary from one case to the other. This suggests that $a_1$ is not a universal function of $Z$. An estimate for $Z_0$ equal to $Z$ at $\tau_{max}$ was found to work occasionally but not always. Still, a better analytical function for $a_1$ is desired near the line of symmetry. A choice of $a_1$ equal to -0.17 over the outer mixing zone works well.

## III.  AIR-AIR COAXIAL MIXING

The air-air mixing calculations are made for a central jet-to-outer stream velocity ratio of 8.0. The nominal inviscid jet and outer stream velocities are 400 and 50 ft/sec, respectively. The maximum Mach number in the mixing flow field is approximately 0.35, low enough to be considered incompressible flow. Both first-regime and second-regime calculations are presented and compared with experimental data. The functions for the parameters $\left|a_1\right|_m$, $K$, $f_1$, and $f_2$ used for the hydrogen-air mixing calculations are used here.

First Regime

The initial profiles of experimental data were taken at 2.6 jet nozzle diameters from the nozzle exit. Velocity and shear stress profiles are calculated and compared with experimental data at 4.4 jet nozzle diameters from the initial plane of mixing, a position less than one-half nozzle diameter from the end of the first regime. These

results are shown in Figures 34 and 35. As with the hydrogen-air first-regime calculations the same two functions for $a_1$ are used in these analytical calculations. Similar to the hydrogen-air results no detectable differences are observed in the velocity profiles for the two functions of $a_1$ used. The shear stress profile also exhibits an improper shape near the inner boundary. Otherwise, the theoretical profile calculations agree well with the experimental velocity and shear stress profiles. These observations generally agree with the results of the hydrogen-air mixing calculations.

## Second Regime

One second-regime theoretical calculation is made for coaxial air streams. The experimental data for a jet-to-outer stream velocity ratio of 8.0 is taken from Reference 19. Plots of the centerline velocity and peak shear stress decay are shown in Figures 36 and 37. The theoretical calculations were made for $|a_1|_m$ and K equal to 0.17 and 0.85, respectively, the same numerical values as were used for the hydrogen-air calculations. The diffusion function, $f_2$, is also the same as that used for the hydrogen-air calculations. The centerline velocity agrees well with the experimental data. The peak shear stress experimental data are scattered; consequently, good agreement of the theory with experimental data is not expected. The results do indicate that the peak shear stress decay is properly predicted.
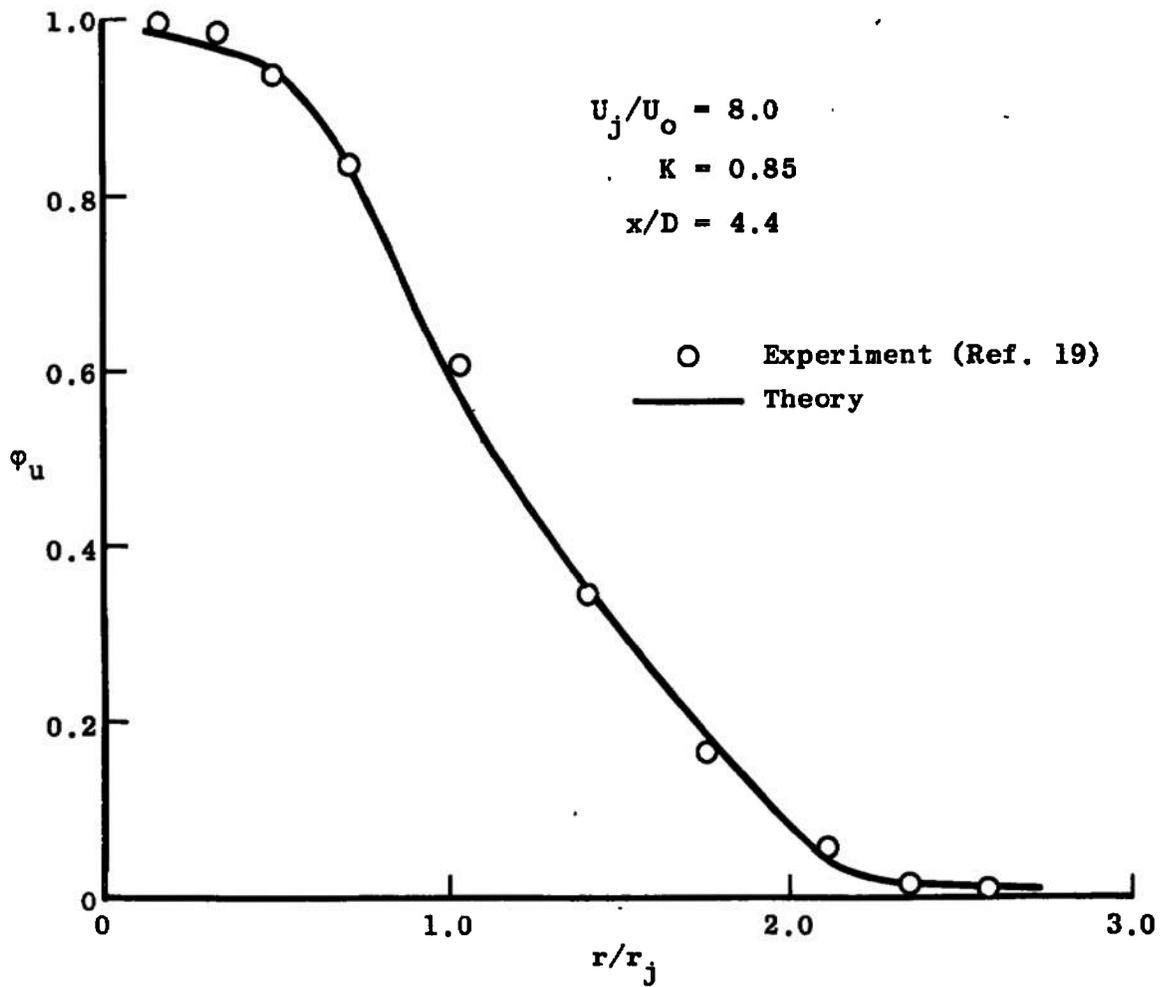
Figure 34. First-regime velocity profile for air-air mixing.
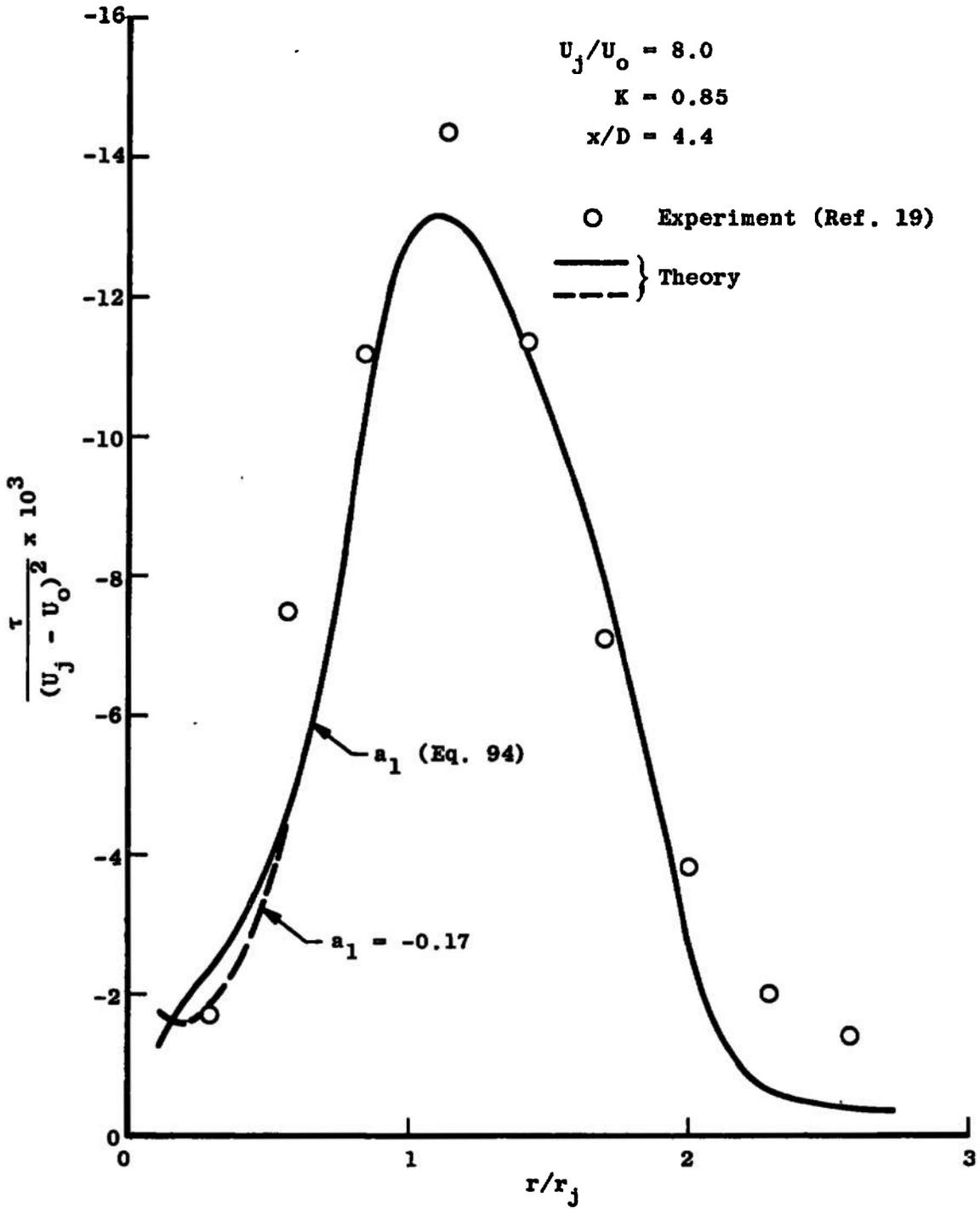
Figure 35. First-regime turbulent shear stress profile for air-air mixing.
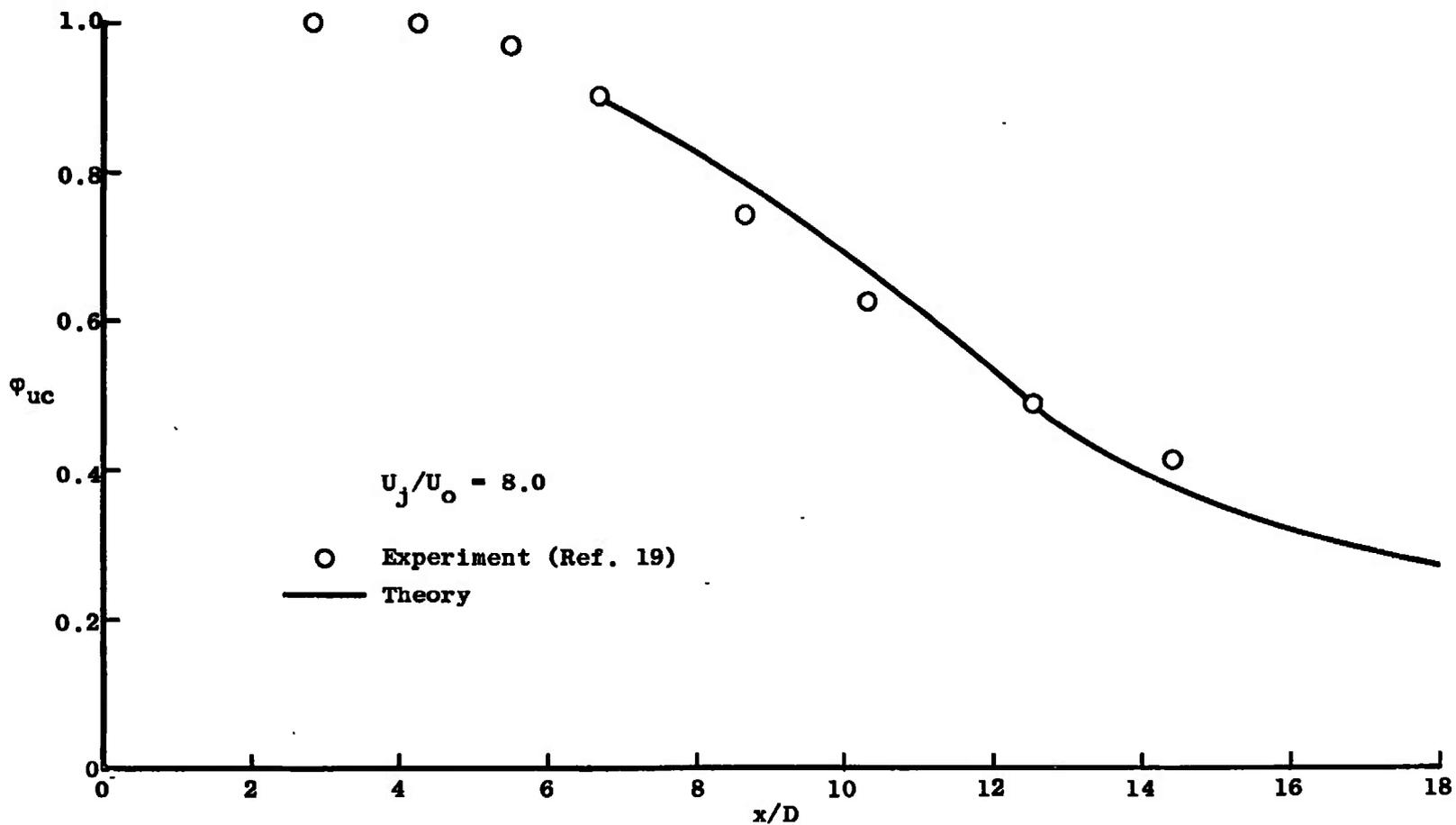
Figure 36.  Centerline velocity decay for air-air mixing.
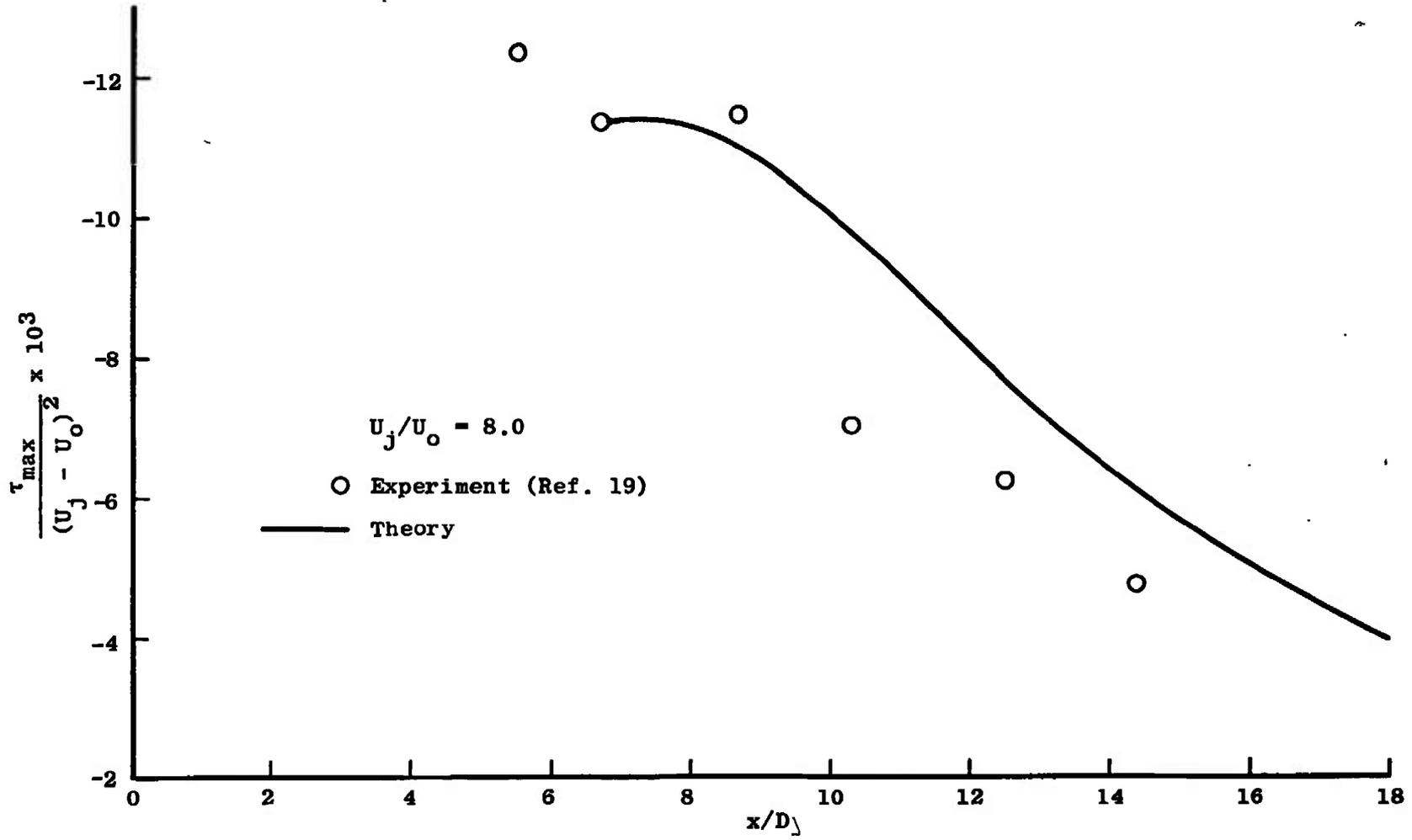
Figure 37.  Peak shear stress decay for air-air mixing.

## IV.  OTHER THEORETICAL CALCULATIONS

### Compressibility

In the development of the turbulent kinetic energy
equation term D (Equation 28) appears as the result of
including density fluctuation terms.  If this term and the
other density fluctuation terms are neglected the form of
the turbulent kinetic energy equation left is the incom-
pressible form.  Calculations were made for hydrogen-air and
air-air mixing to determine the effect of D on the results.
The effect is very small.  Differences only in the fourth
significant figure in the calculations of U, V, and τ were
observed.  Therefore, the term can be neglected at least for
subsonic incompressible hydrogen-air and air-air mixing.
For supersonic mixing it may be necessary to include D in
the calculations.

### Vertical Component of Velocity

A typical result of the calculated vertical component
of velocity is shown in Figure 38 for hydrogen-air and air-
air coaxial mixing.  In the air-air mixing case the stream-
lines have positive slope near the centerline and negative
slope in the outer mixing zone.  Therefore, the mass flux is
decreasing near the line of symmetry although the net mass
flux is increasing in the mixing zone.  In the hydrogen-air
mixing case a very different behavior is observed.  The
streamlines have negative slope over most of the mixing
zone.  The mass flux near the centerline is increasing even
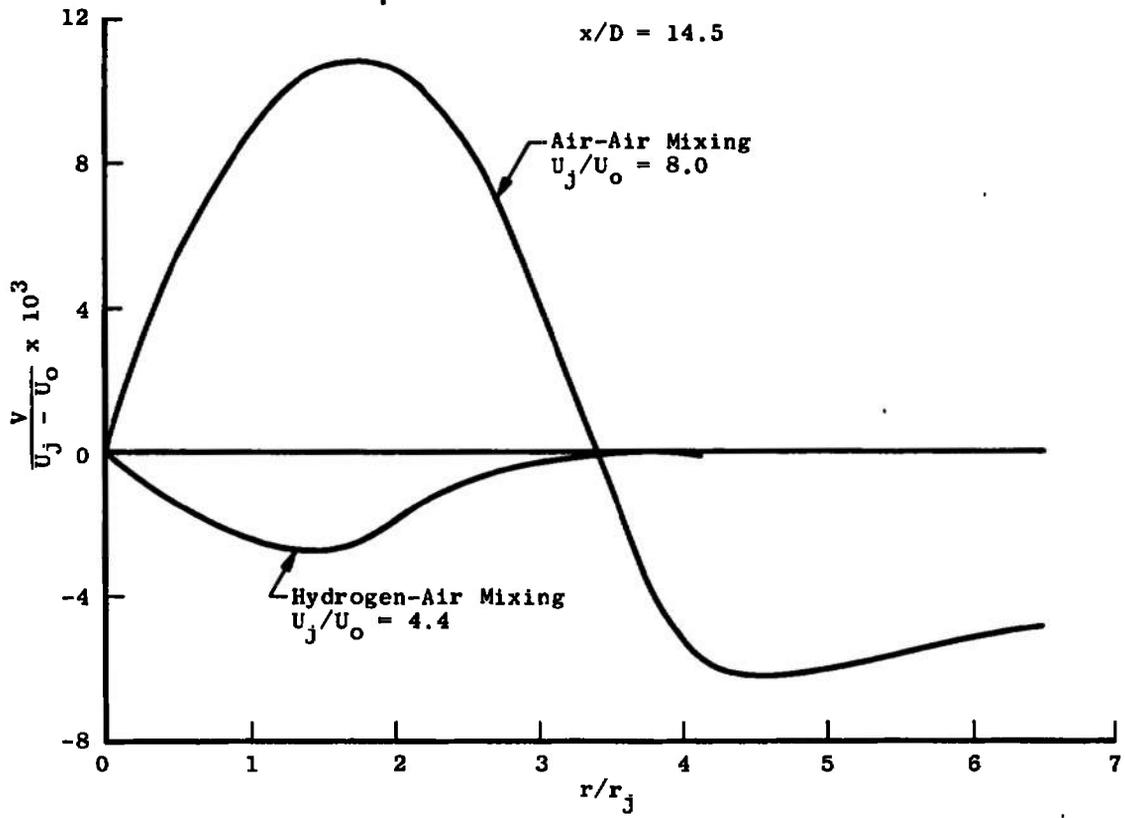
Figure 38. Calculated vertical component of velocity.

though the velocity decays.  This is primarily caused by the displacement of the light hydrogen with the heavier air through the action of turbulent mixing.

# CHAPTER VII

## THEORETICAL CALCULATIONS FOR THE

## TWO-DIMENSIONAL SYMMETRIC WAKE

The results of a brief study on extending the theo-
retical method, presented in Chapters II and III, to a two-
dimensional symmetric wake is presented in this chapter.
Theoretical calculations are made and compared with the
experimental data of Reference 44 for an incompressible
turbulent wake behind a thin flat plate.  Before presenting
the results, a brief discussion is given on the choice of
functions for the turbulent kinetic energy-shear stress
parameter, the diffusion velocity, and the energy dissipa-
tion.

## I.  PARAMETER MODELING

Basically, the same functional forms as were developed
for the coaxial jet mixing problem are used for the wake
problem.

### Turbulent Kinetic Energy-Shear Stress Parameter

The turbulent kinetic energy-shear stress parameter,
$a_1$, is in part arbitrarily chosen to be given by Equation 74
with $|a_1|_m$ and $Z_o$ equal to 0.15 and 0.25, respectively.  The
value of $Z_o$ selected is strictly arbitrary.  The value of
$|a_1|_m$ selected is based on that recommended by Reference 40
for plane two-dimensional wakes.

Diffusion Velocity Parameter

The diffusion velocity parameter used is given by Equation 81 where the characteristic velocity, $U_{ch}$, is chosen as $U_o - U_c$. The diffusion function, f, used in the calculations is arbitrarily selected to be the same as given in Figure 4, page 44, for $f_2$ but scaled up by a factor of four to provide the proper high-velocity mixing boundary condition, i.e., to give $f_2(1)$ a value of 10.0.

Dissipation Length Parameter

The dissipation length parameter, L, is again given by Equation 86. From trial-and-error calculations a constant value of 0.53 for K was found to be satisfactory for the wake.

II.   RESULTS AND DISCUSSION

The initial starting profile for the wake calculations is taken at the end of the flat plate. The general numerical procedures are the same as are described in Chapter V for second-regime mixing calculations with one exception. Once the position, y, of the left characteristic nearest the line of symmetry exceeds its initial value by a factor of two, a new mesh point was added by linear interpolation halfway between the line of symmetry and the first mesh point. The results of these calculations are presented in Figures 39 through 42. The centerline velocity is plotted versus the distance from the end of the flat plate. This distance is nondimensionalized by the turbulent boundary
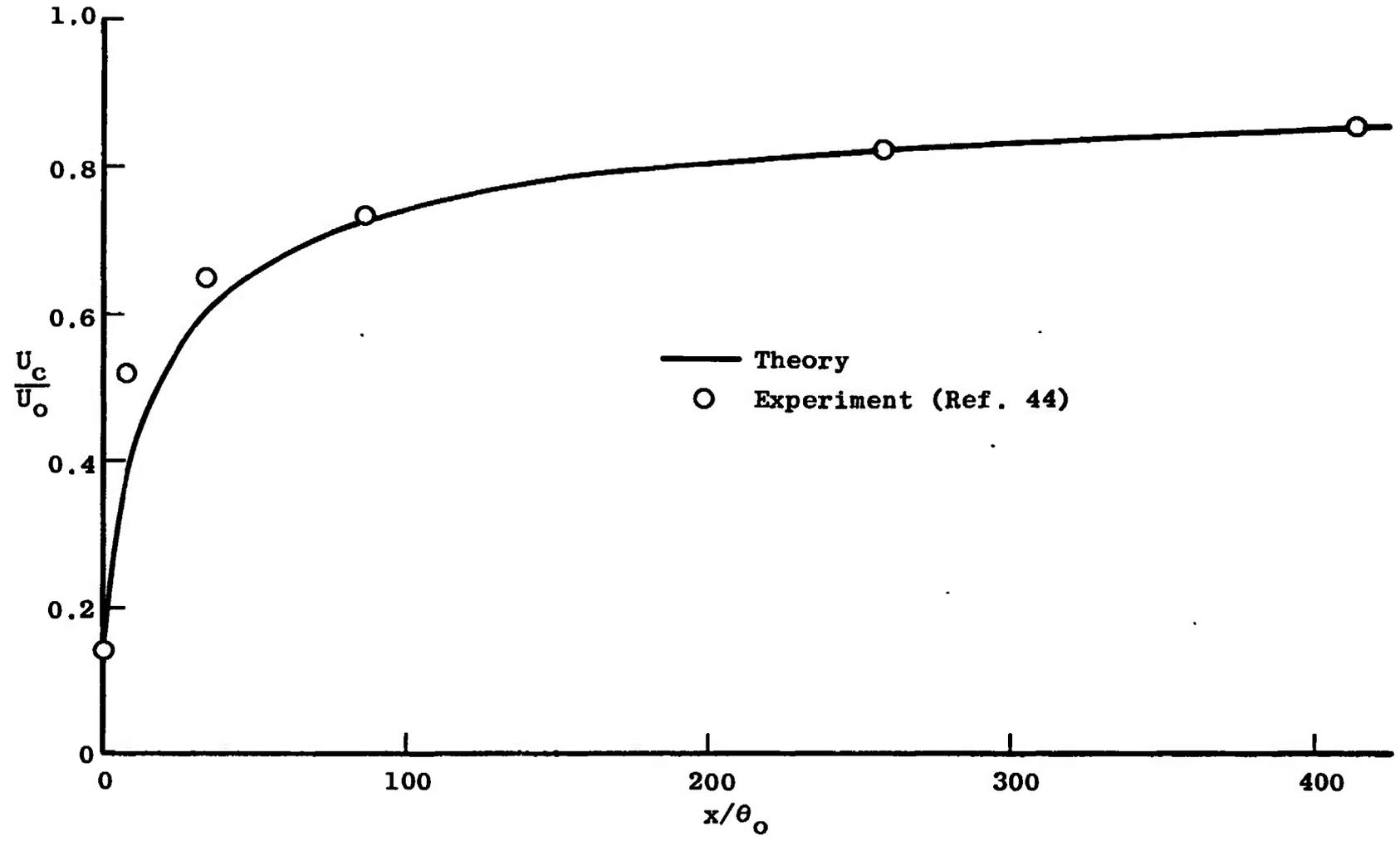
Figure 39.   Centerline velocity in the wake of a thin flat plate.
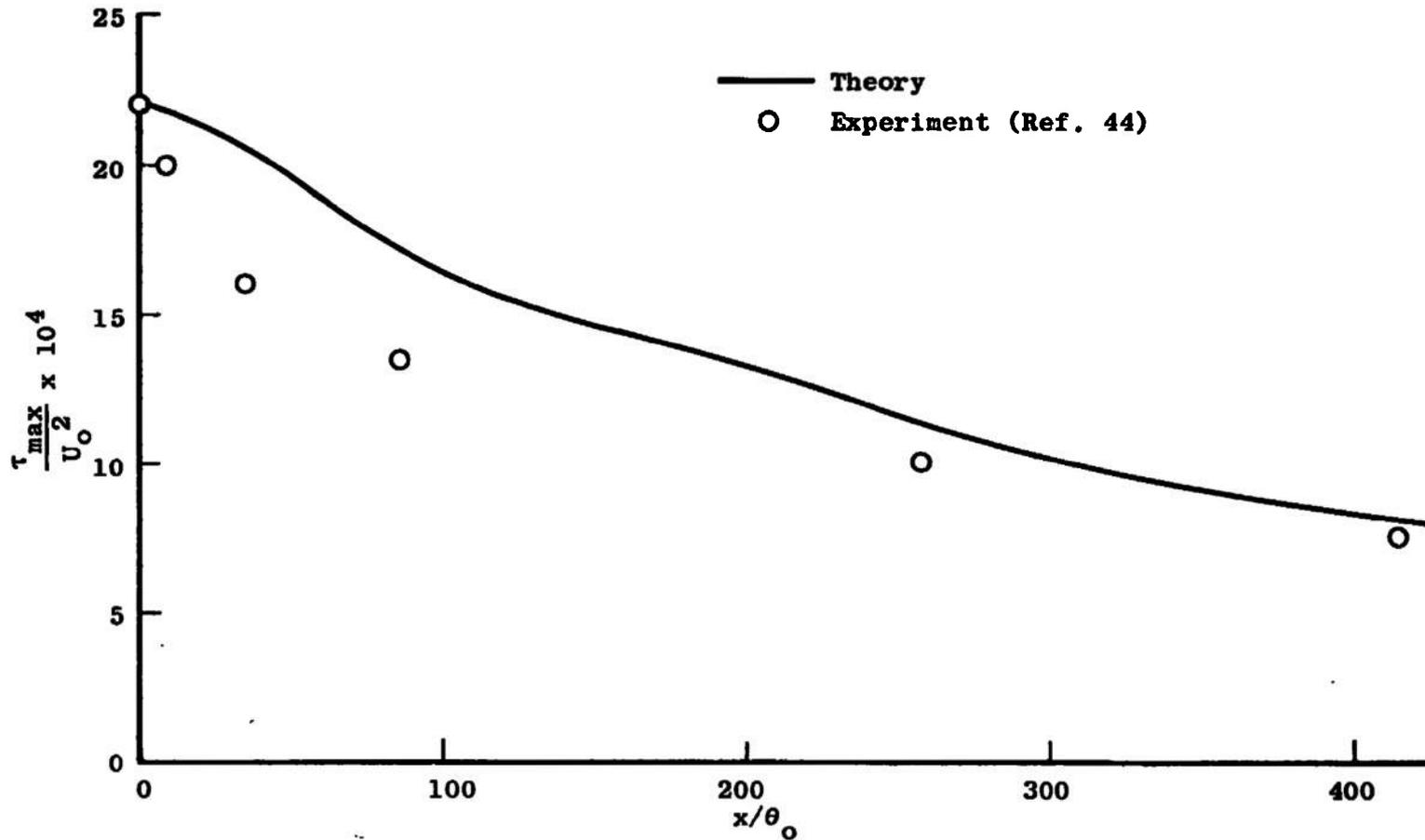
Figure 40. Maximum turbulent shear stress in the wake of a thin flat plate.
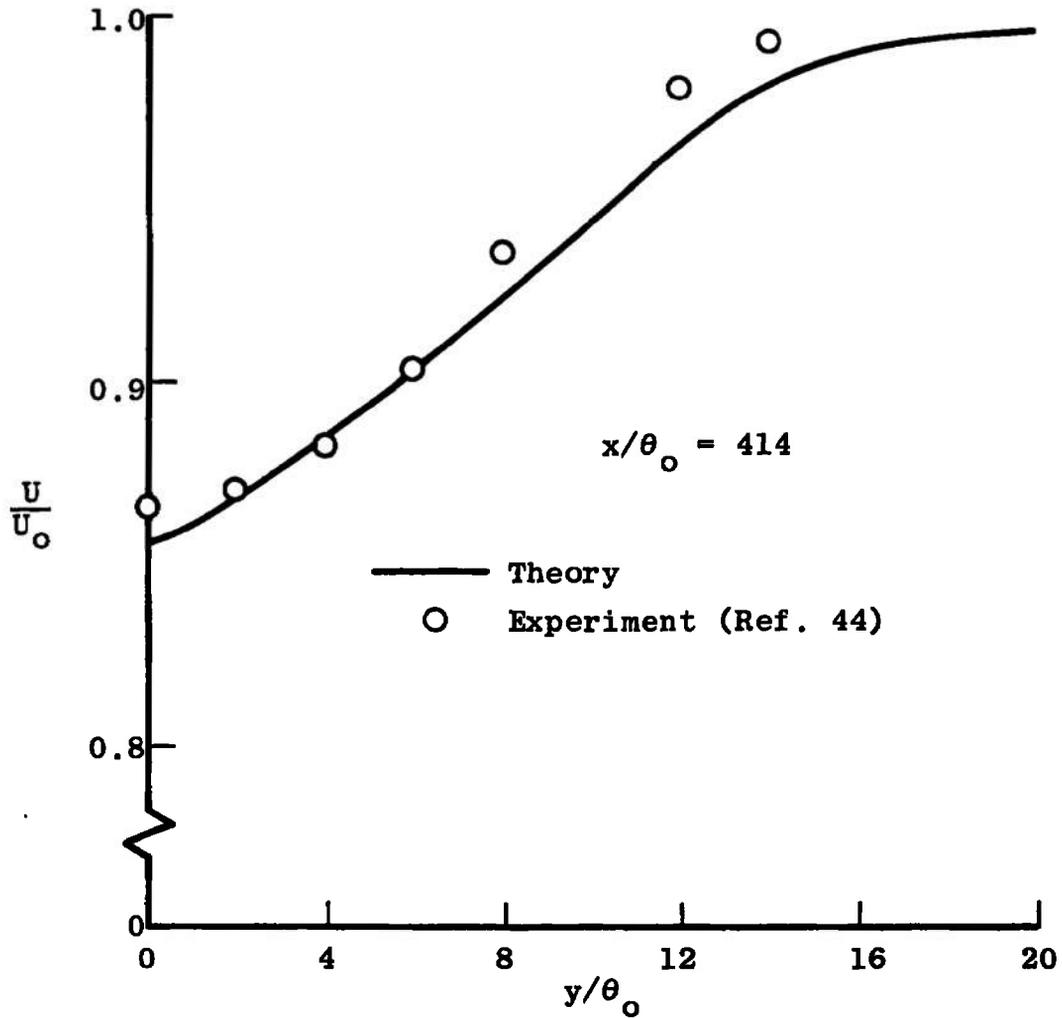
Figure 41. Velocity profile in the wake of a thin flat plate.
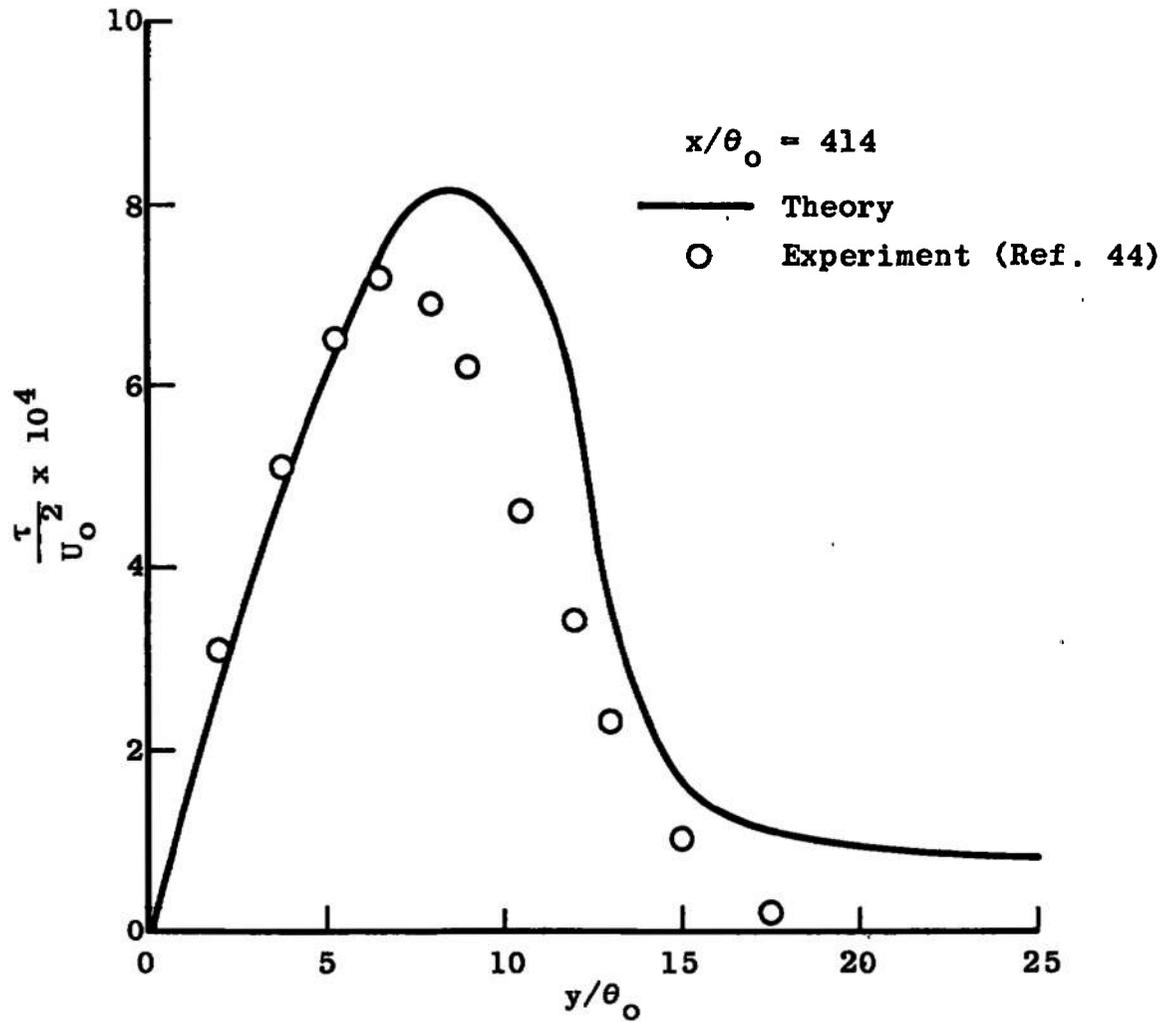
Figure 42.  Turbulent shear stress profile in the wake of a
thin flat plate.

layer momentum thickness, $\theta_o$, at the end of the flat plate calculated by Reference [44] to be 0.53 cm. The theory predicts the centerline velocity increase very well. The maximum turbulent shear stress decay is not predicted very well near the end of the flat plate but improves farther downstream. The velocity profile at 414 momentum thicknesses downstream of the flat plate is in reasonable agreement with the experimental data. The calculated shear stress profile is also in reasonable agreement with experimental data with the maximum deviation occurring in the outer mixing zone.

These results show that the theoretical method is applicable to wake calculations. However, the best functions for $a_1$, K, and f remain to be determined. Refinement of·these parameters based on experiments is necessary before completely satisfactory results can be expected.

The computer program was also modified to calculate the mixing flow field for an unsymmetric two-dimensional plane jet or plane wake. This program includes an iteration on·the vertical component of velocity to satisfy the condition required by Equation 73. So far, numerical difficulties have been encountered in trying to calculate flows where the turbulent shear changes sign, such as occurs in an unsymmetric wake behind an airfoil.

CHAPTER VIII

CONCLUDING REMARKS AND RECOMMENDATIONS

I.   CONCLUDING REMARKS

The results of the calculations presented in Chapters
VI and VII show that the turbulent kinetic energy equation
transformed into a transport equation for turbulent shear
stress is potentially useful for calculating inhomogeneous
turbulent two-stream mixing flows and wake flows.  By using
the turbulent kinetic energy equation the history of the
turbulent structure is included in the calculations.  The
eddy viscosity and Prandtl mixing length theories are in-
adequate in this respect because history is excluded.  The
key to successfully using the turbulent kinetic energy equa-
tion lies in properly modeling the diffusion and dissipation
terms and obtaining a realistic relation between the turbu-
lent shear stress and turbulent kinetic energy.  The con-
vective or flux model used in these studies for the diffusion
of turbulent kinetic energy works well.  A different diffu-
sion function is required in the first and second regimes of
axisymmetric mixing because of the basic difference in the
character of the two flow fields.  The same diffusion func-
tions work equally well for hydrogen-air and air-air mixing,
thereby suggesting that the functions are universal in their
respective regimes of application.

121

The model for the dissipation function used in this study is analogous to the dissipation expression derived for isotropic turbulence. By setting the dissipation length, L, proportional to the mixing layer width, the model chosen for the dissipation function works very well. The parameter, K, equal to 0.85 served to calculate hydrogen-air and air-air coaxial mixing flows equally well. These results imply that the parameter L used in this study exhibits a universal behavior. A value of K equal to 0.53 worked better for the two-dimensional symmetric wake.

The turbulent shear stress was assumed to be linearly proportional to the turbulent kinetic energy. The parameter $a_1$ is a variable function for axisymmetric jet mixing. On the line of symmetry its value is zero. A constant value of 0.17 for $|a_1|_m$ over the outer region of the mixing zone works well for jet mixing. In the inner mixing region $|a_1|$ ranges from zero to 0.17. A better formulation of $a_1$ in this region is desired opposed to that used in this study.

In formulating the theory the assumptions of unity Prandtl and Schmidt numbers were made. The velocity and shear stress profiles and centerline velocity and peak shear stress decay agree well with experimental data for jet mixing even though experimental results show that the Prandtl and Schmidt numbers are not unity.

The turbulent kinetic energy approach presented in this study is not yet a useful engineering tool for calculating mixing flow fields. Since the method is designed to

include flow history in the calculations initial profile data are needed to begin the calculations. Experimental data have been used in this study, but analytically derived starting profiles are needed for engineering computations. A study on the feasibility of using analytically derived starting profiles is desired.

Potentially the turbulent kinetic energy approach is a method for studying the effects of initial disturbances in turbulent flow on mixing phenomena. One can envision use of the method to study the effect of initial boundary layers on turbulent wakes and to study methods for retarding or enhancing the mixing in turbulent flows.

## II. RECOMMENDATIONS FOR FUTURE STUDY

Additional experimental confirmation of the turbulent kinetic energy approach used in this study is desired. Studies are recommended for both jets and wakes to compare the convection, diffusion, production, and dissipation of turbulent kinetic energy measured experimentally with that calculated by the analytical models used in this study. Such a study would be useful in further substantiating these analytical models and perhaps would suggest improved analytical models. In particular, a more satisfactory analytical model for the parameter $a_1$ is needed for jet mixing.

Studies should continue toward solving the transition regime between the first and second regimes in symmetric two-stream mixing. The proper analytical models for $a_1$ and

123

the diffusion are needed before success can be expected.

Including nonunity Prandtl and Schmidt numbers in the theoretical method is desired to permit proper calculation of the energy and species concentration profiles. This can be accomplished by simultaneously solving the parabolic form of the energy and species continuity equations along with the global continuity, momentum, and turbulent kinetic energy equations. A finite difference grid procedure would be required opposed to the method of characteristics because this system of equations is not hyperbolic. Another rather involved approach would be to use the transport equations, analogous to the turbulent kinetic energy equation, for the fluctuating energy and the species. These equations, however, contain six additional parameters [43] which need to be experimentally determined and appropriately modeled.

Application of the theory to supersonic mixing should be studied. Compressibility is already included in the basic flow equations. The main question is whether or not the parameter modeling can be equally applicable to incompressible and compressible flow.

Finally it is recommended that mixing flows with pressure gradient be studied using the turbulent kinetic energy approach.

# BIBLIOGRAPHY

# BIBLIOGRAPHY

1.  Forstall, W. Jr., and A. H. Shapiro. "Momentum and Mass Transfer in Coaxial Jets," Journal of Applied Mechanics, Vol. 17, No. 12, 1950, pp. 399-408.

2.  Tani, I., and Y. Kobashi. "Experimental Studies on Compound Jets," Proc. 1st Japan National Congress for Applied Mechanics, 1951, pp. 465-468.

3.  Kobashi, Y. "Experimental Studies on Compound Jets," Proc. 2nd Japan National Congress for Applied Mechanics, 1952, pp. 223-226.

4.  Corrsin, S., and A. L. Kistler. "The Free-Stream Boundaries of Turbulent Flows," NACA TN 3133, 1954.

5.  Heskestad, G. "Hot-Wire Measurements in a Plane Turbulent Jet," Journal of Applied Mechanics, Vol. 32, Series E, No. 4, December 1965, pp. 721-734.

6.  Macynski, J. F. J. "A Round Jet in an Ambient Coaxial Stream," Journal of Fluid Mechanics, Vol. 13, Part 4, August 1962, pp. 597-608.

7.  Alpinieri, L. J. "An Experimental Investigation of the Turbulent Mixing of Non-Homogeneous Coaxial Jets," Polytechnic Institute of Brooklyn, PIBAL Report 789, 1963; also "Turbulent Mixing of Coaxial Jets," AIAA Journal, Vol. 2, 1964, pp. 1560-1568.

8.  Ting, L., and P. A. Libby. "Remarks on the Eddy Viscosity in Compressible Flows," Journal of the Aerospace Sciences, Vol. 27, 1960, pp. 797-798.

9.  Mager, A. "Transformation of the Compressible Turbulent Boundary Layer," Journal of the Aerospace Sciences, Vol. 25, 1958, pp. 305-311.

10. Zakkay, V., E. Krause, and S. D. L. Woo. "Turbulent Transport Properties for Axisymmetric Heterogeneous Mixing," AIAA Journal, Vol. 2, No. 11, November, 1964, pp. 1939-1947.

11. Zakkay, V., and E. Krause. "The Radial Variation of the Eddy Viscosity in Compressible Turbulent Jet Flows," International Journal of Heat and Mass Transfer, Vol. 8, No. 7, July, 1965, pp. 1047-1050.

12. Fejer, A. A., T. P. Torda, L. I. Bochman, K. N. Ghia, and W. G. Herman. "Research on Mixing of Coaxial Streams," ARL 67-0058, March, 1967 (AD 654014).

13. Peters, C. E. "A Model for the Free Turbulent Eddy Viscosity," AEDC TR 65-209, November, 1965, (AD 473663).

14. Kleinstein, G. "Mixing in Turbulent Axially Symmetric Free Jets," Journal of Spacecraft and Rockets, Vol. 1, No. 4, July-August, 1964, pp. 403-408.

15. Warren, W. R. "An Analytical and Experimental Study of Compressible Free Jets," Princeton University Department of Aeronautical Engineering, Report No. 381.

16. Donaldson, C. du P., and K. E. Gray. "Theoretical and Experimental Investigation of the Compressible Free Mixing of Two Dissimilar Gases," AIAA Journal, Vol. 4, No. 11, November, 1966, pp. 2017-2025.

17. Peters, C. E. "Turbulent Mixing and Burning of Coaxial Streams Inside a Duct of Arbitrary Shape," AEDC TR 68-270.

18. Chriss, D. E. "Experimental Study of the Turbulent Mixing of Subsonic Axisymmetric Gas Streams," AEDC TR 68-133.

19. Paulk, R. A. "Experimental Investigation of Free Turbulent Mixing of Nearly Constant Density Coaxial Streams," Masters Thesis, University of Tennessee, June, 1969.

20. Sami, S., T. Carmody, and H. Rouse. "Jet Diffusion in the Region of Flow Establishment," Journal of Fluid Mechanics, Vol. 27, Part 2, 1967, pp. 231-252.

21. Sami, S. "Balance of Turbulent Energy in the Region of Jet-Flow Establishment," Journal of Fluid Mechanics, Vol. 29, Part 1, 1967, pp. 81-92.

22. Schlichting, H. Boundary Layer Theory, 4th ed., McGraw-Hill, New York, 1960, Chapters 19 and 23.

23. Ferri, A. "A Critical Review of Heterogeneous Mixing Problems," ARL 67-0187.

24. Bradshaw, P., D. H. Ferriss, and N. P. Atwell. "Calculation of Boundary Layer Development Using the Turbulent Energy Equation," Journal of Fluid Mechanics, Vol. 28, Part 3, 1967, pp. 593-616.

25. Bradshaw, P., and D. H. Ferriss. "Calculation of the Boundary Layer Development Using the Turbulent Energy Equation. II - Compressible Flow on Adiabatic Walls," NPL AERO Report 1217.

26. Townsend, A. A. The Structure of Turbulent Shear Flows, Cambridge University Press, London, 1956.

27. Hinze, J. O. Turbulent Flow, McGraw-Hill, New York, 1959.

28. Bradshaw, P., D. H. Ferriss, and R. F. Johnson. "Turbulence in the Noise-Producing Region of a Circular Jet," Journal of Fluid Mechanics, Vol. 19, 1964, p. 591.

29. Patankar, S. V., and D. B. Spalding. "A Finite-Difference Procedure for Solving the Equations of the Two Dimensional Boundary Layer," Journal of Heat Mass Transfer, Vol. 10, 1967, pp. 1389-1411.

30. Lee, S. C., and P. T. Harsha. "Use of Turbulent Kinetic Energy in Free Mixing Studies," Presented at the AIAA 2nd Fluid and Plasma Dynamics Conference, San Francisco, California, June, 1969.

31. Morkovin, M. V. "Effects of Compressibility on Turbulent Flows," Mechanics of Turbulence, National Science Research Center, Gordon and Breach, New York, 1961, p. 367.

32. Courant, R., and K. O. Friedrichs. Supersonic Flow and Shock Waves, Vol. 1, Interscience Publishers, Inc., New York, 1948.

33. Miles, E. R. C. Supersonic Aerodynamics, 1st ed., McGraw-Hill, New York, 1950, p. 72.

34. Mills, R. D. "Numerical and Experimental Investigations of the Shear Layer Between Two Parallel Streams," Journal of Fluid Mechanics, Vol. 33, Part 3, 1968, p. 591.

35. Klebanoff, P. S. "Characteristics of Turbulence in a Boundary Layer with Zero Pressure Gradient," NACA Report 1247.

36. Zawachi, T. S., and H. Weinstein. "Experimental Investigation of Turbulence in the Region Between Coaxial Streams," NASA CR-959, February, 1968.

37. Heskestad, G. "Hot-Wire Measurements in a Plane Turbulent Jet," Journal of Applied Mechanics, Vol. 32, 1965, pp. 721-724.

38.  Heskestad, G.  "Hot-Wire Measurements in a Radial
     Turbulent Jet,"  Journal of Applied Mechanics, Vol.
     33, 1966, pp. 417-424.

39.  Lee, S. C.  "A Study of the Two Dimensional Free
     Turbulent Mixing Between Converging Streams with
     Initial Boundary Layers,"  Ph.D. dissertation, 1966,
     University of Washington, Seattle, Washington.

40.  Harsha, P. T., and S. C. Lee.  "Correlation Between
     Turbulent Shear Stress and Turbulent Kinetic Energy,"
     Unpublished Report, ARO, Inc., October, 1969.

41.  Wygnanski, I., and H. Fiedler.  "Some Measurements in
     the Self Preserving Jet,"  Journal of Fluid Mechanics,
     Vol. 38, Part 3, 1969, p. 577.

42.  Peters, C. E., D. E. Chriss, and R. A. Paulk.
     "Turbulent Transport Properties in Subsonic Coaxial
     Free Mixing Systems,"  AIAA Paper No. 69-681,
     June, 1969.

43.  Argyropoulos, G. S., S. T. Demetriades, and K. Lackner.
     "Compressible Turbulent Magnetohydrodynamic Boundary
     Layers,"  Physics of Fluids, Vol. 11, No. 12,
     December, 1968, pp. 2559-2566.

44.  Chevray, R., and L. S. G. Kovasznay.  "Turbulence
     Measurements in the Wake of a Thin Flat Plate,"  AIAA
     Journal, Vol. 7, No. 8, August, 1969, pp. 1641-1643.

APPENDIXES

## APPENDIX A

## ORDER ANALYSIS OF THE CONTINUITY, MOMENTUM, AND TURBULENT KINETIC ENERGY EQUATIONS

To facilitate simplification of the equations of motion and the turbulent kinetic energy equation relative estimates of the derivatives and of the perturbation components are needed. If L is chosen as a length scale conforming to the variation of parameters in the X-direction and similarly $\ell$ for the Y-direction and it is assumed that $\ell/L < 1$ (Order of 0.1), then

$$\frac{\frac{\partial}{\partial x}}{\frac{\partial}{\partial y}} = \mathscr{O}\left(\frac{\ell}{L}\right) \tag{A1}$$

Also $U_s$ is chosen as a characteristic velocity such that it represents the velocity difference across the mixing zone, and $U/U_s$ is assumed to be of order unity. It is further assumed that

$$\frac{\partial \tau}{\partial y} = \mathscr{O}\left(\rho U \frac{\partial U}{\partial x}\right) \tag{A2}$$

and

$$V' = \mathscr{O}(U') \tag{A3}$$

Then

$$\tau = \mathscr{O}\left(\frac{\rho U_s^2 \ell}{L}\right) \tag{A4}$$

133

and

$$U' = \mathcal{O}(U_s \sqrt{\ell/L}) \tag{A5}$$

## I. CONTINUITY

From Equations 17 and A5

$$\frac{\rho'}{\rho} = \mathcal{O}(\sqrt{\ell/L}) \tag{A6}$$

The order of V is found from the continuity equation. First note that

$$\frac{\overline{\rho'U'}}{\rho U} = \mathcal{O}\left[\frac{\ell}{L}\right] \tag{A7}$$

then retaining the highest order terms, the continuity equation is expressed as

$$\frac{\partial \rho U}{\partial x} + \frac{\partial}{\partial y}(\rho V + \overline{\rho'V'}) = 0 \tag{A8}$$

From Equations A5 and A6

$$\frac{\partial}{\partial y}(\overline{\rho'V'}) = \mathcal{O}\left[\frac{\rho U_s}{L}\right]$$

which is of the same order as $\partial \rho U/\partial x$. This gives

$$V = \mathcal{O}\left[U_s \frac{\ell}{L}\right] \tag{A9}$$

Note that $\overline{\rho'V'}$ and $\rho V$ are of the same order which requires that both terms must be retained in the continuity equation.

## II. MOMENTUM

Assuming that the viscous stresses in the momentum equation (Equation 7, Chapter II) are small compared to the turbulent stresses, the X- and Y-components of momentum are written with the order of each term written below. The bars over the mean flow parameters have been dropped for convenience.

X-component

$$(\rho U + \overline{\rho' U'})\frac{\partial U}{\partial x} + (\rho V + \overline{\rho' V'})\frac{\partial U}{\partial y}$$

$$\left[\rho U_s, \ \rho U_s \ \frac{\ell}{L}\right]\frac{U_s}{L} \qquad \left[\rho U_s \ \frac{\ell}{L}, \ \rho U_s \ \frac{\ell}{L}\right]\frac{U_s}{L}$$

$$+ \overline{\rho' U'}\left(\frac{\partial U}{\partial x} + \frac{\partial V}{\partial y}\right) + U \ \frac{\partial \overline{\rho' U'}}{\partial x}$$

$$\rho U_s \ \frac{\ell}{L}\left(\frac{U_s}{L}, \ \frac{U_s}{L}\right) \qquad \frac{\rho U_s^2 \ell}{L^2}$$

$$+ V \ \frac{\partial \overline{\rho' U'}}{\partial y} = - \ \frac{\partial P}{\partial x} - \frac{\partial \overline{\rho' U'^2}}{\partial x}$$

$$\rho U_s^2\left(\frac{\ell}{L}\right)^2 \ \frac{1}{L} \qquad \frac{\rho U_s^2}{L}\left(\frac{\ell}{L}\right)^{3/2}$$

$$- \frac{\partial}{\partial x} (\rho \overline{U'^2}) - \frac{\partial}{\partial y} (\rho \overline{U'V'}) - \frac{\partial \overline{\rho' V' U'}}{\partial y}$$

$$\frac{\rho U_s^2 \ell}{L^2} \qquad\qquad \frac{\rho U_s^2}{L} \qquad \frac{\rho U_s^2}{L}\left(\frac{\ell}{L}\right)^{3/2}$$

Y-component

$$\left(\rho U + \overline{\rho'U'}\right)\frac{\partial V}{\partial x} + \left(\rho V + \overline{\rho'V'}\right)\frac{\partial V}{\partial y}$$

$$\left[\rho U_s, \ \rho U_s\frac{\ell}{L}\right]\left[\frac{U_s\ell}{L^2}\right] \quad \left[\rho U_s\frac{\ell}{L}, \ \rho U_s\frac{'\ell}{L}\right]\left[\frac{U_s}{L}\right]$$

$$+ \overline{\rho'V'}\left[\frac{\partial U}{\partial x} + \frac{\partial V}{\partial y}\right] + U\frac{\partial \overline{\rho'V'}}{\partial x}$$

$$\rho U_s\frac{\ell}{L}\left[\frac{U_s}{L}, \ \frac{U_s}{L}\right] \quad \frac{\rho U_s^2\ell}{L^2}$$

$$+ V\frac{\partial \overline{\rho'U'}}{\partial y} = - \frac{\partial P}{\partial y} - \frac{\partial \rho \overline{U'V'}}{\partial x}$$

$$\frac{\rho U_s^2\ell}{L^2} \qquad \frac{\rho U_s^2\ell}{L^2}$$

$$- \frac{\partial \rho\overline{V'^2}}{\partial y} - \frac{\partial \overline{\rho'U'V'}}{\partial x} - \frac{\partial \overline{\rho'V'^2}}{\partial y}$$

$$\frac{\rho U_s^2}{L} \qquad \frac{\rho U_s^2}{L}\left(\frac{\ell}{L}\right)3/2 \qquad \frac{\rho U_s^2}{\ell}\left(\frac{\ell}{L}\right)3/2$$

If all terms of an order less than $\rho U_s^2/L$ are neglected the
X- and Y-components of the momentum equation reduce to

X-component

$$\rho U\frac{\partial U}{\partial x} + \left(\rho V + \overline{\rho'V'}\right)\frac{\partial U}{\partial y} = - \frac{\partial P}{\partial x} - \frac{\partial \rho\overline{U'V'}}{\partial y} \qquad\qquad (A10)$$

Y-component

$$\frac{\partial P}{\partial y} = \frac{\partial \rho \overline{V'^2}}{\partial y} \tag{A11}$$

The latter equation can be integrated directly to give

$$P_O = P - \rho \overline{V'^2}$$

where

$$P_O = P_O(x)$$

then

$$\frac{\partial P}{\partial x} = \frac{\partial P_O}{\partial x} + \frac{\partial \rho \overline{V'^2}}{\partial x}$$

and

$$\frac{\partial \rho \overline{V'^2}}{\partial x} = \mathcal{O}\left(\frac{\rho U_s^2 \ell}{L^2}\right)$$

This term is neglected since it is an order less than the order of the terms in the X-component of momentum.

### III.  TURBULENT KINETIC ENERGY

Before an order analysis is performed on the turbulent kinetic energy equation (Equation 10, Chapter II) the convection term (I) and normal stress term (III) are combined and rearranged with the aid of the continuity equation as follows:

$$U_j \frac{\partial}{\partial x_j}\left(\frac{1}{2}\rho\overline{U_i'}^2 + \frac{1}{2}\overline{\rho'U_i'}^2\right) + \left(\frac{1}{2}\rho\overline{U_i'}^2 + \frac{1}{2}\overline{\rho'U_i'}^2\right)\frac{\partial U_j}{\partial x_j}$$

$$\equiv (\rho U_j + \overline{\rho'U_j'})\frac{\partial}{\partial x_j}\left(\frac{1}{2}\overline{U_i'}^2\right) - \frac{\partial}{\partial x_j}\left(\frac{1}{2}\overline{U_i'}^2 \cdot \overline{\rho'U_j'}\right)$$

With this rearrangement the turbulent kinetic energy equation is restated as

$$(\rho U_j + \overline{\rho'U_j'})\frac{\partial}{\partial x_j}\left(\frac{1}{2}\overline{U_i'}^2\right) - \frac{\partial}{\partial x_j}\left(\frac{1}{2}\overline{U_i'}^2 \cdot \overline{\rho'U_j'}\right)$$

$$\qquad\qquad (a) \qquad\qquad\qquad\qquad\qquad (b)$$

$$+ \overline{\rho'U_i'}\, U_j \frac{\partial U_i}{\partial x_j} + (\rho\overline{U_i'U_j'} + \overline{\rho'U_i'U_j'})\frac{\partial U_i}{\partial x_j}$$

$$\qquad\qquad (c) \qquad\qquad\qquad (d)$$

$$+ \frac{\partial}{\partial x_j}\left(\overline{P'U_j'} + \frac{1}{2}\rho\overline{U_i'^2U_j'} + \frac{1}{2}\overline{\rho'U_i'^2U_j'}\right)$$

$$(e)$$

$$- \overline{P'\frac{\partial U_j'}{\partial x_j}} + \overline{U_i'\frac{\partial \sigma_{ij}'}{\partial x_j}} = 0$$

$$\qquad (f) \qquad\qquad (g)$$

Each of the first five terms are expanded in two-dimensional Cartesian coordinates with the order of the respective terms listed.

Term (a)

$$(\rho U + \overline{\rho' U'})\frac{\partial \overline{q'^2}/2}{\partial x} + (\rho V + \overline{\rho' V'})\frac{\partial \overline{q'^2}/2}{\partial y}$$

$$\left[\rho U_s, \ \rho U_s \frac{\ell}{L}\right]\left[\frac{U_s^2 \ell}{L^2}\right] \qquad \left[\rho U_s \frac{\ell}{L}, \ \rho U_s \frac{\ell}{L}\right]\frac{U_s^2}{L}$$

Term (b)

$$\frac{\partial \overline{\rho' U'} \ \overline{q'^2}/2}{\partial x} + \frac{\partial \overline{\rho' V'} \ \overline{q'^2}/2}{\partial y}$$

$$\frac{\rho U_s^3}{L}\left(\frac{\ell}{L}\right)^2 \qquad\qquad \frac{\rho U_s^3}{L}\left(\frac{\ell}{L}\right)$$

Term (c)

$$\overline{\rho' U'}\left[U\ \frac{\partial U}{\partial x} + V\ \frac{\partial U}{\partial y}\right] + \overline{\rho' V'}\left[U\ \frac{\partial V}{\partial x} + V\ \frac{\partial V}{\partial y}\right]$$

$$\frac{\rho U_s^3}{L}\left(\frac{\ell}{L}\right) \qquad\qquad\qquad \frac{\rho U_s^3}{L}\left(\frac{\ell}{L}\right)^2$$

Term (d)

$$(\rho \overline{U'^2} + \overline{\rho' U'^2})\frac{\partial U}{\partial x} + (\rho \overline{U'V'} + \overline{\rho' U'V'})\frac{\partial U}{\partial y}$$

$$\frac{\rho U_s^3}{L}\left(\frac{\ell}{L}\right), \ \frac{\rho U_s^3}{L}\left(\frac{\ell}{L}\right)^{3/2} \qquad \frac{\rho U_s^3}{L}\left(\frac{\ell}{L}\right), \ \frac{\rho U_s^3}{L}\left(\frac{\ell}{L}\right)^{3/2}$$

$$+ (\rho \overline{U'V'} + \overline{\rho' V' U'})\frac{\partial V}{\partial x} + (\rho \overline{V'^2} + \overline{\rho' V'^2})\frac{\partial V}{\partial y}$$

$$\frac{\rho U_s^3}{L}\left(\frac{\ell}{L}\right)^2, \ \frac{\rho U_s^3}{L}\left(\frac{\ell}{L}\right)^{5/2} \qquad \frac{\rho U_s^3}{L}\left(\frac{\ell}{L}\right), \ \frac{\rho U_s^3}{L}\left(\frac{\ell}{L}\right)^{3/2}$$

Term (e)

$$\frac{\partial}{\partial x}\left[\overline{P'U'} + \frac{1}{2}\rho\overline{q'^2U'} + \frac{1}{2}\overline{\rho'q'^2U'}\right]$$

$$\frac{1}{L}\left[\rho U_s^3\left(\frac{\ell}{L}\right)^2, \quad \rho U_s^3\left(\frac{\ell}{L}\right)^{3/2}, \quad \rho U_s^3\left(\frac{\ell}{L}\right)^2\right]$$

$$\frac{\partial}{\partial y}\left[\overline{P'V'} + \frac{1}{2}\rho\overline{q'^2V'} + \frac{1}{2}\overline{\rho'q'^2V'}\right]$$

$$\frac{1}{\ell}\left[\rho U_s^3\left(\frac{\ell}{L}\right)^2, \quad \rho U_s^3\left(\frac{\ell}{L}\right)^{3/2}, \quad \rho U_s^3\left(\frac{\ell}{L}\right)^2\right]$$

Term (f)

$$\overline{P'\frac{\partial U'}{\partial x}} + \overline{P'\frac{\partial V'}{\partial y}}$$

$$\frac{\rho U_s^3}{L}\left(\frac{\ell}{L}\right)^2, \quad \frac{\rho U_s^3}{L}\left(\frac{\ell}{L}\right)$$

Term (g)

In reviewing the order of each of the preceding terms, the highest order term occurs only in term d. Therefore, the viscous dissipation must be of the same order and should be retained.

Retaining all terms of the order of $\rho U_s^3\ell/L^2$ or higher reduces the turbulent kinetic energy equation to

$$\frac{\rho U}{2}\frac{\partial \overline{q'^2}}{\partial x} + \frac{(\rho V + \overline{\rho'V'})}{2}\frac{\partial \overline{q'^2}}{\partial y} - \frac{\partial \overline{\rho'V'}\,\overline{q'^2}/2}{\partial y}$$

$$+ \overline{\rho'U'}\left[U\frac{\partial U}{\partial x} + V\frac{\partial U}{\partial y}\right] + \rho\overline{U'^2}\frac{\partial U}{\partial x} + (\rho\overline{U'V'} + \overline{\rho'U'V'})\frac{\partial U}{\partial y}$$

$$+ \rho\overline{V'}^2 \frac{\partial V}{\partial y} + \frac{\partial}{\partial y}\left[\overline{P'V'} + \frac{1}{2} \rho\overline{q'^2V'} + \frac{1}{2} \overline{\rho'q'^2V'}\right]$$

$$+ \overline{P' \frac{\partial V'}{\partial y}} + \overline{U'_i \frac{\partial \sigma'_{ij}}{\partial x_j}} = 0 \qquad\qquad (A12)$$

If only terms of the order of $(\rho U_s^2/L)(\sqrt{\ell/L})$ or higher are retained the turbulent kinetic equation reduces to

$$(\rho\overline{U'V'} + \overline{\rho'U'V'})\frac{\partial U}{\partial y} + \frac{\partial}{\partial y}\left(\frac{1}{2} \rho\overline{q'^2V'}\right) + \overline{U'_i \frac{\partial \sigma'_{ij}}{\partial x_j}} = 0 \quad (A13)$$

These three terms remaining are the production, diffusion, and dissipation of turbulent kinetic energy. The convection term is at least half of an order of magnitude smaller than the diffusion which itself is half an order of magnitude smaller than production and dissipation. The $\overline{\rho'U'V'}$ term is included in the production term because it is of the same order as the diffusion. This causes no problem with the solution to the equations because $(\rho\overline{U'V'} + \overline{\rho'U'V'})$ can be treated as one variable.

Since the ensuing objective of this study will be to include as much physics as practical into the solution of the turbulent jet, the form of the turbulent kinetic energy equation given in Equation A12 will be used as the starting point. The normal stresses in term (d) and term (f) will be neglected. Terms (b) and (c) will be defined as

$$\rho D \equiv \overline{\rho'U'}\left[U \frac{\partial U}{\partial x} + V \frac{\partial U}{\partial y}\right] - \frac{\frac{1}{2} \partial\overline{\rho'V'}\ \overline{q'^2}}{\partial y} \qquad\qquad (A14)$$

141

The form of the turbulent kinetic energy equation remaining is

$$\frac{1}{2} \rho U \frac{\partial \overline{q'^2}}{\partial x} + \frac{1}{2}(\rho V + \overline{\rho' V'})\frac{\partial \overline{q'^2}}{\partial y} + (\rho \overline{U'V'} + \overline{\rho'U'V'})\frac{\partial U}{\partial y}$$

$$+ \frac{\partial}{\partial y}\left[\overline{P'V'} + \frac{1}{2} \rho \overline{q'^2V'} + \frac{1}{2} \overline{\rho'q'^2V'}\right]$$

$$+ \overline{U'_i \frac{\partial \sigma'_{ij}}{\partial x_j}} + \rho D = 0 \qquad\qquad (A15)$$

This form of the turbulent kinetic energy equation is used in this study of the inhomogeneous two-stream jet mixing problem.

$$\left| A - \frac{\partial x}{\partial \gamma} B \right| = 0$$

## APPENDIX B

## DEVELOPMENT OF THE CHARACTERISTIC AND

## COMPATIBILITY EQUATIONS

Using vector notation and subscript notation for the differentials, consider the quasilinear hyperbolic differential equation

$$AW_x + BW_r + C = 0 \tag{B1}$$

where A and B are square matrix coefficients and W and C are vectors. By definition of the differential

$$dW = W_x dx + W_r dr \tag{B2}$$

Define $\lambda$ to be a characteristic direction of the system of equations, (Equation B1), such that

$$\lambda = \frac{dx}{dr}$$

Then

$$|A - \lambda B| = 0 \tag{B3}$$

is the equation of the characteristic directions. The compatibility equations are found by combining Equations B1 and B2 to give

$$B \frac{dW}{dr} + C = (B\lambda - A) W_x \tag{B4}$$

Let D be a vector (yet to be defined), and form the inner

product of both sides of Equation B4 with D,

$$(B \frac{dW}{dr} + C) \cdot D = (B\lambda - A) W_x \cdot D$$

$$= W_x \cdot (B\lambda - A)^T D \tag{B5}$$

where $(B\lambda - A)^T$ is the transpose of $(B\lambda - A)$. If D can be chosen such that the right-hand side of Equation B5 is identically zero with respect to $W_x$, then Equation B5 will contain derivatives only in the characteristic direction, $\lambda$, and therefore, will be the compatibility equation in that direction. Such a D does indeed exist, and is obtained as a non-trivial solution of the linear algebraic system,

$$(B\lambda - A)^T D = 0 \tag{B6}$$

Non-trivial solutions of Equation B6 are guaranteed as a result of Equation B3. The technique outlined is used to derive the characteristic directions and compatibility equations from the continuity, momentum, and turbulent kinetic energy equations. Denote the unknown vector, W, as

$$W = \begin{pmatrix} U \\ V \\ \tau \end{pmatrix} \tag{B7}$$

From the partial differential equations (Equations 54, 55, and 56), the matrices A and B and vector C are

$$A = \begin{pmatrix} 1 + U(F_1 - F_2) & 0 & 0 \\ U & 0 & 0 \\ 0 & 0 & \frac{U}{2a_1} \end{pmatrix}$$

144

$$
B = \begin{Bmatrix} V(F_1 - F_2) & 1 & 0 \\[2em] V - \tau(F_1 - F_2) & 0 & -1 \\[2em] \begin{bmatrix} \tau\left[\dfrac{V_d}{2a_1}(F_1 - F_2) - 1\right] \\[1.5em] -\tau\left(\dfrac{\tau}{2a_1}\right)\left(\dfrac{1 - F_2 U}{h}\right) \end{bmatrix} & 0 & \left(\dfrac{V + V_d}{2a_1} - \dfrac{\tau U}{2a_1 h}\right) \end{Bmatrix}
$$

$$
C = \begin{Bmatrix} \dfrac{V}{r}k + \dfrac{U}{P}\dfrac{dP}{dx} \\[1.5em] -\dfrac{\tau}{r}k + \left(\dfrac{\gamma - 1}{\gamma}\right)\dfrac{h}{P}\dfrac{dP}{dx} \\[1.5em] G \end{Bmatrix}
$$

Substituting A, B, and C into Equation B3 gives

$$
\lambda\{U - \lambda[V - \tau(F_1 - F_2)]\}\left\{\dfrac{U}{2a_1} - \lambda\left[\dfrac{V + V_d}{2a_1} - \dfrac{\tau U}{2a_1 h}\right]\right\}
$$
$$
+ \lambda^2\left\{\tau\left[\dfrac{V_d}{2a_1}(F_1 - F_2) - 1\right] - \tau\left(\dfrac{\tau}{2a_1}\right)\left(\dfrac{1 - F_2 U}{h}\right)\right\} = 0 \quad (B8)
$$

One solution of Equation B8 is

$$
\lambda = 0 \tag{B9}
$$

or

$$
\frac{dr}{dx} = \infty \tag{B9a}
$$

Corresponding to this solution the unknown vector D is

$$\begin{pmatrix} 1 + U(F_1 - F_2) & U & 0 \\ 0 \cdot & 0 & 0 \\ 0 & 0 & \dfrac{U}{2a_1} \end{pmatrix} \begin{pmatrix} D_1 \\ D_2 \\ D_3 \end{pmatrix} = 0$$

or

$$D_1[1 + U(F_1 - F_2)] + D_2U = 0$$

$$\frac{U}{2a_1} D_3 = 0$$

A non-trivial solution is

$$D_1 = -U/[1 + U(F_1 - F_2)]$$

$$D_2 = 1$$

$$D_3 = 0 \tag{B10}$$

Substituting this solution into

$$\left[ B \frac{dW}{dr} + C \right] \cdot D = 0 \tag{B11}$$

gives the vertical compatibility equation. To illustrate

$$B \frac{dW}{dr} = \begin{pmatrix} V(F_1 - F_2) & 1 & 0 \\ V - \tau(F_1 - F_2) & 0 & -1 \\ \left[ \tau\left[ \dfrac{V_d}{2a_1}(F_1 - F_2) - 1 \right] \right. & 0 & \left[ \dfrac{V + V_d}{2a_1} - \dfrac{\tau U}{2a_1 h} \right] \\ \left. - \tau\left( \dfrac{\tau}{2a_1} \right)\left( \dfrac{1 - F_2 U}{h} \right) \right] & & \end{pmatrix} \begin{pmatrix} \dfrac{dU}{dr} \\ \dfrac{dV}{dr} \\ \dfrac{d\tau}{dr} \end{pmatrix}$$

146

Then

$$
B \frac{dW}{dr} + C = \left\{
\begin{array}{l}
\left[ V(F_1 - F_2)\frac{dU}{dr} + \frac{dV}{dr} + \frac{V}{r} k + \frac{U}{P} \frac{dP}{dx} \right] \\[2ex]
\left\{ [V - \tau(F_1 - F_2)]\frac{dU}{dr} - \frac{d\tau}{dr} - \frac{\tau}{r} k \right. \\[2ex]
\left. + \left(\frac{\gamma - 1}{\gamma}\right) \frac{h}{P} \frac{dP}{dx} \right\} \\[2ex]
\left\{ \tau \left[ \frac{V_d}{2a_1}(F_1 - F_2) - 1 \right] - \tau\left(\frac{\tau}{2a_1}\right) \left(\frac{1 - F_2 U}{h}\right)\frac{dU}{dr} \right. \\[2ex]
\left. - \tau\left(\frac{\tau}{2a_1}\right) \left(\frac{1 - F_2 U}{h}\right) \frac{d\tau}{dr} + G \right\}
\end{array}
\right\}
$$

Thus

$$
\left[ B \frac{dW}{dr} + C \right] \cdot D
$$

$$
= - \frac{U}{[1 + U(F_1 - F_2)]} \left[ V(F_1 - F_2)\frac{dU}{dr} + \frac{dV}{dr} + \frac{V}{r} k + \frac{U}{P} \frac{dP}{dx} \right]
$$

$$
+ [V - \tau(F_1 - F_2)]\frac{dU}{dr} - \frac{d\tau}{dr} - \frac{\tau}{r} k + \left(\frac{\gamma - 1}{\gamma}\right)\frac{h}{P} \frac{dP}{dx}
$$

$$
= 0 \tag{B12}
$$

which reduces to Equation 61.

The compatibility relations, Equations 62, corresponding to nonzero λ are obtained in a similar manner.

## APPENDIX C

### CONSERVATION OF MASS AND MOMENTUM

Conservation of mass and momentum are checked to determine the accuracy of the method of characteristics used in the calculation of the mixing flow field. The check method uses the integral form of the continuity and momentum equations. First, consider the mass continuity check.

### I. MASS CONTINUITY

The mass continuity equation is integrated between the inner and outer boundaries

$$\int_{r_i}^{r_o} \left( \frac{\partial \rho U r^k}{\partial x} + \frac{\partial \rho V r^k}{\partial r} \right) dr = 0 \tag{C1}$$

The second term is integrated directly to give

$$\int_{r_i}^{r_o} \frac{\partial \rho U r^k}{\partial x} dr + \rho_o V_o r_o^k - \rho_i V_i r_i^k = 0 \tag{C2}$$

Using Leibnitz's rule the first term is rearranged as

$$\int_{r_i}^{r_o} \frac{\partial \rho U r^k}{\partial x} dr = \frac{d}{dx} \int_{r_i}^{r_o} \rho U r^k dr$$

$$- \left( \rho_o U_o r_o^k \frac{dr_o}{dx} - \rho_i U_i r_i^k \frac{dr_i}{dx} \right) \tag{C3}$$

Combining Equations C2 and C3

$$\frac{d}{dx} \int_{r_i}^{r_o} \rho U r^k dr = \left( \rho_o U_o r_o^k \frac{dr_o}{dx} - \rho_i U_i r_i^k \frac{dr_i}{dx} \right)$$

$$- (\rho_o V_o r_c^k - \rho_i V_i r_i^k) \qquad (C4)$$

Equation C4 is integrated with respect to x, giving

$$\int_{r_i}^{r_o} \rho U r^k dr \bigg|_x - \int_{r_i}^{r_o} \rho U r^k dr \bigg|_{x_s}$$

$$= \int_{x_s}^{x} \left( \rho_o U_o r_o^k \frac{dr_o}{dx} - \rho_i U_i r_i^k \frac{dr_i}{dx} \right) dx$$

$$- \int_{x_j}^{x} (\rho_o V_o r_o^k - \rho_i V_i r_i^k) dx \qquad (C5)$$

where $x_s$ is the position of the initial profile. Letting $R_q$ be defined as

$$R_q \equiv \int_{r_i}^{r_o} \rho U r^k dr \bigg|_x$$

$$\div \left( \int_{r_i}^{r_o} \rho U r^k dr \bigg|_{x_o} + \int_{x_s}^{x} \left( \rho_o U_o r_o^k \frac{dr_o}{dx} - \rho_i U_i r_i^k \frac{dr_i}{dx} \right) dx \right.$$

$$- \int_{x_s}^{x} (\rho_o V_o r_o^k - \rho_i V_i r_i^k) \, dx \Bigg) \tag{C6}$$

$R_q$ is evaluated at each axial station by substituting into the integrals the values of the parameters calculated by the method of characteristics. By letting $x_s$ always be the position of the initial profile, the variation of $R_q$ from unity will indicate the error accumulated by the method of characteristics.

## II. MOMENTUM

The differential forms of the mass continuity and momentum equations (Equations 33 and 34) are combined to give

$$\frac{\partial \rho U^2 r^k}{\partial x} + \frac{\partial \rho V U r^k}{\partial r} = \frac{\partial r^k \tau}{\partial r} - \frac{dP}{dx} \tag{C7}$$

By integrating across the mixing zone

$$\int_{r_i}^{r_o} \frac{\partial \rho U^2 r^k}{\partial x} \, dr + \rho_o V_o U_o r_o^k - \rho_i V_i U_i r_i^k$$

$$= r_o^k \tau_o - r_i^k \tau_i - (r_o - r_i) \frac{dP}{dx} \tag{C8}$$

The first term is integrated by Leibnitz's rule.

$$\int_{r_i}^{r_o} \frac{\partial \rho U^2 r^k}{\partial x} \, dr = \frac{d}{dx} \int_{r_i}^{r_o} \rho U^2 r^k dr - \left( \rho_o U_o r_o^k \frac{dr_o}{dx} \right)$$

$$+ \left( \rho_i U_i^2 r_i^k \frac{dr_i}{dx} \right) \tag{C9}$$

By combining Equations C8 and C9,

$$\frac{d}{dx} \int_{r_i}^{r_o} \rho U^2 r^k dr = \left( \rho_o U_o^2 r_o^k \frac{dr_o}{dx} - \rho_i U_i^2 r_i^k \frac{dr_i}{dx} \right)$$

$$+ r_o^k \tau_o - r_i^k \tau_i - \frac{dP}{dx}(r_o - r_i)$$

$$- \rho_o V_o U_o r_o^k + \rho_i V_i U_i r_i^k \tag{C10}$$

and integrating with respect to x gives

$$\int_{r_i}^{r_o} \rho U^2 r^k dr \Big|_x - \int_{r_i}^{r} \rho U^2 r^k dr \Big|_{x_s}$$

$$= \int_{x_s}^{x} \left( \rho_o U_o^2 r_o^k \frac{dr_o}{dx} - \rho_i U_i^2 r_i^k \frac{dr_i}{dx} \right) dx$$

$$+ \int_{x_s}^{x} (r_o^k \tau_o - r_i \tau_i^k)dx - \int_{x_s}^{x} (r_o - r_i) \frac{dP}{dx} dx$$

$$- \int_{x_s}^{x} \rho_o U_o V_o r_o^k dx + \int_{x_s}^{x} \rho_i U_i V_i r_i^k dx \tag{C11}$$

By definition let

$$R_m = \int_{r_i}^{r_o} \rho U^2 r^k dr \bigg|_x$$

$$\div \left[ \int_{r_i}^{r_o} \rho U^2 r^k dr \bigg|_{x_s} + \int_{x_s}^{x} \left( \rho_o U_o^2 r_o^k \frac{dr_o}{dx} - \rho_i U_i^2 r_i^k \frac{dr_i}{dx} \right) dx \right.$$

$$+ \int_{x_s}^{x} (r_o^k \tau_o - r_i^k \tau_i) dx - \int_{x_s}^{x} \rho_o U_o V_o r^k dx$$

$$\left. + \int_{x_s}^{x} \rho_i U_i V_i r^k dx - \int_{x_s}^{x} (r_o - r_i) \frac{dP}{dx} dx \right] \qquad (C12)$$

Again, the integrals at each of the appropriate x stations are evaluated. The accumulated error in momentum calculated by the method of characteristics is determined by comparing $R_m$ to unity.

In the computer program $R_\sigma$ and $R_m$ are calculated at each x station so that the loss or gain in mass or momentum can be observed.

152

## DOCUMENT CONTROL DATA - R & D

*(Security classification of title, body of abstract and indexing annotation must be entered when the overall report is classified)*

| 1. ORIGINATING ACTIVITY *(Corporate author)* | 2a. REPORT SECURITY CLASSIFICATION |
|---|---|
| Arnold Engineering Development Center<br>Directorate of Plans and Technology<br>Research Division | UNCLASSIFIED |
| | 2b. GROUP<br>N/A |

**3. REPORT TITLE**

INHOMOGENEOUS TWO-STREAM TURBULENT MIXING USING THE TURBULENT
KINETIC ENERGY EQUATION

**4. DESCRIPTIVE NOTES** *(Type of report and inclusive dates)*

Final Report

**5. AUTHOR(S)** *(First name, middle initial, last name)*

M. L. Laster

| 6. REPORT DATE | 7a. TOTAL NO. OF PAGES | 7b. NO. OF REFS |
|---|---|---|
| May 1970 | 165 | 44 |

| 8a. CONTRACT OR GRANT NO. | 9a. ORIGINATOR'S REPORT NUMBER(S) |
|---|---|
| b. PROJECT NO. 6952 | AEDC-TR-70-134 |
| c. Program Elements 64719F, 61102F | 9b. OTHER REPORT NO(S) *(Any other numbers that may be assigned this report)* |
| d. | N/A |

**10. DISTRIBUTION STATEMENT**

This document has been approved for public release and sale;
its distribution is unlimited.

| 11. SUPPLEMENTARY NOTES | 12. SPONSORING MILITARY ACTIVITY |
|---|---|
| Available in DDC | AFOAR/AEDC |

**13. ABSTRACT** A study is made on applying the turbulent kinetic energy approach to inhomogeneous two-stream turbulent mixing calculations and to calculations of a two-dimensional symmetric wake. Mixing calculations are made and compared with experimental data for coaxial hydrogen-air and air-air mixing flows. The turbulent kinetic energy equation is transformed into a transport equation for the turbulent shear stress by assuming that the turbulent shear stress is directly proportional to the turbulent kinetic energy. A flux model is assumed for the lateral diffusion of turbulent kinetic energy. The energy dissipation is modeled to a form similar to that derived for isotropic turbulence. Mass and energy transport are incorporated in the analysis by assuming the Prandtl and Lewis numbers to be unity. The resulting set of partial differential equations is hyperbolic and the method of characteristics are chosen for their solution. The theoretical method inherently incorporates history of the turbulent structure in the calcuations which is physically more acceptable than turbulent structure models based on local flow properties. The results show that the turbulent kinetic energy approach is quite applicable to two-stream mixing problems, although the method requires further development before it is useful for routine engineering calculations. Calculations for a wake behind a flat plate are made and found to compare well with experimental data. The flux model for the diffusion of turbulent kinetic energy and the energy dissipation model were found to produce results which agree well with experimental data for both the mixing jet and the wake.

DD FORM 1473
1 NOV 65

| 14. KEY WORDS | LINK A | | LINK B | | LINK C | |
|---|---|---|---|---|---|---|
| | ROLE | WT | ROLE | WT | ROLE | WT |
| turbulent jets | | | | | | |
| turbulent wakes | | | | | | |

AFSC
Arnold AFB Tenn.